

**IZMIR KATIP CELEBI UNIVERSITY
GRADUATE SCHOOL OF NATURAL AND APPLIED SCIENCES**

**SIMULATION OF IMMISCIBLE DISPLACEMENT OF PETROLEUM VIA
SECOND AND THIRD ORDER FINITE DIFFERENCING TECHNIQUES**

M.Sc. THESIS

Osman ÜNAL

Department of Energy Engineering

DECEMBER 2019

IZMIR KATIP CELEBI UNIVERSITY
GRADUATE SCHOOL OF NATURAL AND APPLIED SCIENCES

**SIMULATION OF IMMISCIBLE DISPLACEMENT OF PETROLEUM VIA
SECOND AND THIRD ORDER FINITE DIFFERENCING TECHNIQUES**

M.Sc. THESIS

Osman ÜNAL
(Y170208004)

Department of Energy Engineering

Thesis Advisor: Prof. Dr. İbrahim KOCABAŞ

DECEMBER 2019

İZMİR KATİP ÇELEBİ ÜNİVERSİTESİ
FEN BİLİMLERİ ENSTİTÜSÜ

İKİNCİ VE ÜÇÜNCÜ DERECEDEDEN SONLU FARKLILAŞTIRMA
YÖNTEMLERİYLE PETROLÜN KARIŞMADAN ÖTELENMESİNİN
SAYISAL BENZETİMİ

YÜKSEK LİSANS TEZİ

Osman ÜNAL
(Y170208004)

Enerji Mühendisliği Ana Bilim Dalı

Tez Danışmanı: Prof. Dr. İbrahim KOCABAŞ

ARALIK 2019

Osman ÜNAL, a **M.Sc.** student of **IKCU Graduate School Of Natural And Applied Sciences**, successfully defended the thesis entitled “**SIMULATION OF IMMISCIBLE DISPLACEMENT OF PETROLEUM VIA SECOND AND THIRD ORDER FINITE DIFFERENCING TECHNIQUES**”, which he prepared after fulfilling the requirements specified in the associated legislations, before the jury whose signatures are below.

Thesis Advisor :

Prof. Dr. İbrahim KOCABAŞ
İzmir Katip Çelebi University

Jury Members :

Asst. Prof. Dr. Sercan ACARER
İzmir Katip Çelebi University

Asst. Prof. Dr. İhsan Burak KULGA
İstanbul Technical University

Date of Submission : 16.12.2019

Date of Defense : 23.12.2019

To my family

FOREWORD

First and foremost, I would like to thank my advisor, Prof. Dr. İbrahim KOCABAŞ for his support in this study. I would also like to thank him for providing me sincere and friendly work environment.

I would like to thank my family for their support in my entire life. I owe them for all my accomplishments.

I would like to thank the İzmir Katip Çelebi University for providing Matlab Software to the laboratory computer in our department.

December 2019

Osman ÜNAL

TABLE OF CONTENTS

	<u>Page</u>
FOREWORD	v
TABLE OF CONTENTS	vi
ABBREVIATIONS	viii
LIST OF TABLES	ix
LIST OF FIGURES	x
ABSTRACT	xii
ÖZET	xiv
1. INTRODUCTION	1
2. LITERATURE REVIEW	4
2.1 Convection-Dispersion Equations.....	4
2.2 Discretization Methods of Flow and Transport Equations.....	11
2.2.1 Conventional Mathematical Approach	12
2.2.2 Engineering Approach	13
2.3 Problems in Convective Term Discretization	15
3. MATHEMATICAL DEVELOPMENTS FOR MISCIBLE DISPLACEMENT SIMULATIONS	21
3.1 Miscible Displacement Simulations Using Elementary Difference Schemes .	21
3.2 Feedback Sensitivity and Improved Discretization Techniques	23
3.2.1 In Depth Investigation of the Explicit Numerical Schemes.....	25
3.2.2 In Depth Investigation of the Implicit schemes	29
3.2.3 In Depth Investigation of Semi-implicit schemes.....	32
4. CONVECTIVE DISPERSIVE NATURE OF IMMISCIBLE DISPLACEMENT SIMULATIONS	37
4.1 In depth Investigation of IMPES First Order Space and Time Solutions	40
4.1.1 First order pressure solution.....	40
4.1.2 First order saturation solution	42
4.2 Impes Second Order (TVD) Space and Time Solutions	47
4.2.1 TVD pressure solution	47
4.2.2 TVD saturation solution.....	49
4.3 Impes Third Order (TVD- Leonard) Space and Time Solutions.....	51
4.3.1 TVD- Leonard pressure solution.....	53
4.3.2 TVD-Leonard saturation solution	55
4.4 Fully Implicit First Order Space and First Order Time Solution	59
4.5 TVD Implemented Fully Implicit First Order Method	63
4.6 Fully Implicit Third Order Space (TVD-L) and First Order Time Solution	67
4.7 Fully Implicit Third Order Space (TCDF) and First Order Time Solution.....	71
4.8 First Order Space and Semi Implicit Second Order Time (Crank-Nicolson) Solution	73
5. TCDF-LEONARD WITH CRANK NICOLSON SCHEME	76
6. FLEXIBLE FLUX LIMITER APPLICATIONS	79

7. APPLICATIONS OF THE METHODS TO DIFFERENT RESERVOIRS ..	83
7.1 Oil Wet Reservoirs	83
7.2 Intermediate Wettability Reservoirs	86
8. CONCLUSION.....	92
REFERENCES	94
APPENDICES	97
APPENDIX A	97
APPENDIX B	98
APPENDIX C	101
APPENDIX D	107
APPENDIX E.....	110
CURRICULUM VITAE.....	113

ABBREVIATIONS

1 D	: One Dimension
2 D	: Two Dimension
CN	: Crank Nicolson
FO	: First Order
SO	: Second Order
TO	: Third Order
TVD	: Total Variation Diminishing
TCDF	: Third-order Continuous Diferentiable Function

LIST OF TABLES

	<u>Page</u>
Table 2.1: Stability table.	6
Table 4.1: Input data for one and two dimensional simulations.	37

LIST OF FIGURES

	<u>Page</u>
Figure 2.1: Fig. 12C in Peaceman's book.....	9
Figure 2.2: Fig. 13A2 in Peaceman's book.....	9
Figure 2.3: Summary of Miscible Displacement Simulations $dx=0.1$ $dt=0.05$	10
Figure 2.4: Engineering and classical approaches [8].	15
Figure 2.5: Comparison of higher and first order techniques.	17
Figure 2.6: Breakthrough times of higher and first order methods.....	18
Figure 2.7: Breakthrough times of higher and first order methods in detail.....	18
Figure 2.8: 1D five grid blocks.	20
Figure 3.1: 1st order space and 2nd order time (using Matlab code).....	23
Figure 3.2: 3rd order space and 2nd order time (using Matlab code).....	25
Figure 3.3: Improved method $n=440$ $dx=0.025$ $Nc=0.1$ (Explicit).....	26
Figure 3.4: Improved method $n=80$ $dx=0.025$ $Nc=0.55$ (Explicit).....	26
Figure 3.5: Improved method $n=40$ $dx=0.025$ $Nc=1.1$ (Explicit).....	27
Figure 3.6: Improved method $n=110$ $dx=0.1$ $Nc=0.1$ (Explicit).....	27
Figure 3.7: Improved method $n=20$ $dx=0.1$ $Nc=0.55$ (Explicit).....	28
Figure 3.8: Improved method $n=10$ $dx=0.1$ $Nc=1.1$ (Explicit).....	28
Figure 3.9: Improved method $n=440$ $dx=0.025$ $Nc=0.1$ (Implicit).....	30
Figure 3.10: Improved method $n=80$ $dx=0.025$ $Nc=0.55$ (Implicit).....	30
Figure 3.11: Improved method $n=40$ $dx=0.025$ $Nc=1.1$ (Implicit).....	31
Figure 3.12: Improved method $n=110$ $dx=0.1$ $Nc=0.1$ (Implicit).....	31
Figure 3.13: Improved method $n=20$ $dx=0.1$ $Nc=0.55$ (Implicit).....	32
Figure 3.14: Improved method $n=10$ $dx=0.1$ $Nc=1.1$ (Implicit).....	32
Figure 3.15: Improved method $n=440$ $dx=0.025$ $Nc=0.1$ (C-N).....	33
Figure 3.16: Improved method $n=80$ $dx=0.025$ $Nc=0.55$ (C-N).....	33
Figure 3.17: Improved method $n=40$ $dx=0.025$ $Nc=1.1$ (C-N).....	34
Figure 3.18: Improved method $n=110$ $dx=0.1$ $Nc=0.1$ (C-N).....	34
Figure 3.19: Improved method $n=20$ $dx=0.1$ $Nc=0.55$ (C-N).....	35
Figure 3.20: Improved method $n=10$ $dx=0.1$ $Nc=1.1$ (C-N).....	35
Figure 4.1: Relative permeability curves.	38
Figure 4.2: Determination of flood front water saturation (0.7131).	39
Figure 4.3 : Impes first order Matlab result.	44
Figure 4.4: First order method for large Δx	45
Figure 4.5: First order method for intermediate simulation time.....	45
Figure 4.6: First order method for intermediate simulation time.....	46
Figure 4.7 : 2D Impes first order Matlab result.	46
Figure 4.8 : Impes second order (TVD) result.	50
Figure 4.9: IMPES TVD with large Δx	50
Figure 4.10 : 2D Impes second order (TVD) Matlab result.....	51
Figure 4.11: TVD region.....	52
Figure 4.12 : IMPES TVD-Leonard for small Δx	57

Figure 4.13: IMPES TVD-Leonard for large Δx .	57
Figure 4.14 : 2D Impes third order (TVD-L) Matlab result.	58
Figure 4.15: Unstability of IMPES.	58
Figure 4.16 : Fully implicit first order Matlab result.	61
Figure 4.17: Fully implicit first order for large Δx .	61
Figure 4.18: Fully implicit first order for large Δt .	62
Figure 4.19 : 2D Fully implicit first order Matlab result.	62
Figure 4.20 : Fully implicit second order space first order time Matlab result.	65
Figure 4.21: Fully implicit TVD for large Δx .	65
Figure 4.22: Fully implicit TVD for large Δt .	66
Figure 4.23: 2D Fully implicit second order space first order time Matlab result.	67
Figure 4.24 : Fully implicit third order space first order time Matlab result.	69
Figure 4.25: Fully implicit TVD for large Δx .	70
Figure 4.26: Fully implicit TVD-L for large Δt .	70
Figure 4.27 : 2D Fully implicit (TVD-L) result.	71
Figure 4.28 : TCDF and TVD-L methods.	72
Figure 4.29 : 2D Fully implicit third order space (TCDF) first order time Matlab result.	72
Figure 4.30 : 1D Fully implicit first order space and second order time Matlab result.	74
Figure 4.31: Crank-Nicholson with large time step.	75
Figure 4.32 : 2D Fully implicit first order space and second order time Matlab result.	75
Figure 5.1: 1D Fully implicit third order space and second order time Matlab result.	77
Figure 5.2: 2D Fully implicit third order space and second order time Matlab result.	78
Figure 6.1: Matlab result of flexible flux limiter $N_c=1.8515$.	80
Figure 6.2: Matlab result of flexible flux limiter $N_c=0.4115$.	80
Figure 6.3: 2D Matlab result of flexible flux limiter (before breakthrough time).	81
Figure 6.4: 2D Matlab result of flexible flux limiter (after breakthrough time).	82
Figure 7.1: Relative permeability curves for case 2.	83
Figure 7.2: $dx=100ft$ and $dt=100days$ for oil wet reservoir.	84
Figure 7.3: $dx=50ft$ and $dt=50days$ oil wet reservoir.	84
Figure 7.4: $dx=25ft$ and $dt=25days$ for oil wet reservoir.	85
Figure 7.5: $dx=10ft$ and $dt=10days$ for oil wet reservoir.	85
Figure 7.6: Relative permeability curves for intermediate wettability reservoir.	86
Figure 7.7: Fractional flow curves for intermediate wettability reservoir ($S_{wf}=0.7041$).	87
Figure 7.8: $dx=100ft$ and $dt=100days$ for case 3.	87
Figure 7.9: $dx=50ft$ and $dt=50days$ for intermediate wettability reservoir.	88
Figure 7.10: $dx=25ft$ and $dt=25days$ for intermediate wettability reservoir.	88
Figure 7.11: $dx=10ft$ and $dt=10days$ for intermediate wettability reservoir.	89
Figure 7.12: $dx=1ft$ and $dt=1days$ for intermediate wettability reservoir.	89
Figure 7.13: Water breakthrough time for intermediate wettability reservoir.	90
Figure 7.14: Water breakthrough time for intermediate wettability reservoir in detail.	91

SIMULATION OF IMMISCIBLE DISPLACEMENT OF PETROLEUM VIA SECOND AND THIRD ORDER FINITE DIFFERENCING TECHNIQUES

ABSTRACT

Finite difference simulation of convection dominated flow and transport in porous media suffers significant numerical dispersion and unphysical oscillations problems. Leonard has extensively investigated differencing of the convection term in terms of feedback sensitivity. According to feedback sensitivity concept, we have to obtain negative feedback sensitivity in order to suppress the unphysical oscillations. He stated that the greater the magnitude of feedback sensitivity coefficient, the more capable the scheme suppressing the oscillations. Note that, the second order accurate central differencing of convection term has a neutral feedback sensitivity, which potentially cause unstable numerical solutions. Therefore, in order to suppress unphysical oscillations, Leonard suggests using a high odd order upstream differencing of convection term instead of using the second order central differencing of convection term. Using the first order accurate single point upstream method can suppress the oscillation but leads to a excessive numerical dispersion. Therefore, Leonard proposed the third order upstream method for both higher accuracy and better feedback sensitivity. Thus, employing the third order upstream method yields sharper flood fronts with small numerical dispersion compared to both single point upstream method and central differencing, and negligible unphysical oscillations compared to central differencing. In this study, we combined Leonard's third order upstream differencing and Crank-Nicolson time discretization methods with a flexible flux limiter to mitigate both numerical dispersion and unphysical oscillations.

Despite the superiority of Leonard's method it did not completely eliminate neither the numerical dispersion nor the unphysical oscillations. In 1984, Harten has introduced the Total Variation Diminishing (TVD) scheme which aims eliminating the unphysical oscillations that violate the entropy condition. In the same year, Sweby has published a classical work which specified the stability region for the TVD schemes. Later, Leonard's third order method and the TVD algorithm have been employed in petroleum engineering by a number of investigators, including Liu, Gupta et al., Pinto et al., Chen et.al., Wollcot et.al, and Jiang et.al. In 1992 Pinto et al, referring to Liu, pointed out that the TVD method can be applied to Leonard's third order differencing. In 1993, Chen et. al. applied TVD method to single point upstream differencing of convection term. The TVD method has practically lead to second order differencing, and hence, sharper flood fronts have been observed compared with pure single point upstream method. In 1991, Gupta et al, and in 1994-1995 Liu et. al. and in 1996 Wollcot et. al. applied third order upstream Leonard method to TVD schemes and they obtained better results compared to single point TVD method. Later, this method has been widely employed in various simulation studies specially by reseachers in UT Texas at Austin upto present. In

2017, Jiang et. al. applied the TCDF (third-order continuously differentiable function) method for discretization of convection term for the purpose of reducing the computational iterations of TVD schemes. The TCDF method reduced total number of iterations only slightly for small Courant number simulations compared to the TVD-L method, however, it becomes superior when the Courant numbers are increased to values close to 2.

This thesis undertakes, a extensive investigation of performances of the above mentioned methods in both miscible and immiscible displacement, and the application of the TCDF method to waterflooding problems by closely following the procedures presented by Chen et. al., Wollcot et.al., and Jiang et.al.. All the simulators used in this work developed in MATLAB environment which makes them easily accessible to researchers in this area. Application of the flexible TCDF method for simulating immiscible displacement of petroleum is great importance as the incompressible immiscible displacement is a type of convection dominated flow in porous media. Also in this study, we improved third order TCDF method by combining it with second order time accurate Crank-Nicolson scheme.

Finally, we further improved the TCDF method by developing flexible flux limiter increase the stability region of the pure TCDF method. The novel flexible flux limiter gave better results than previously developed methods even for Courant numbers as high as 1.85 while the pure TCDF worked without unphysical oscillation for Courant numbers up to 1.5.

İKİNCİ VE ÜÇÜNCÜ DERECEDEDEN SONLU FARKLILAŞTIRMA YÖNTEMLERİYLE PETROLÜN KARIŞMADAN ÖTELENMESİNİN SAYISAL BENZETİMİ

ÖZET

Konveksiyonun egemen olduğu akışların sonlu fark yöntemi ile simülasyonu ve gözenekli ortamlarda taşınım, önemli sayısal dağılım ve fiziksel olmayan salınım problemlerine sahiptir. Leonard, taşınım teriminin geri besleme duyarlılığı açısından farklılıklarını kapsamlı bir şekilde araştırmıştır. Geri besleme duyarlılığına göre, kararlı sayısal çözümler alabilmek için negatif geri besleme duyarlılığı elde edilmesi gerekmektedir. Geri besleme hassasiyet katsayısı ne kadar büyük olursa, salınımları baskılayan şema o kadar etkindir. Konveksiyon teriminin ikinci dereceden merkezi farkı, potansiyel olarak kararsız sayısal çözümlere neden olan nötr bir geri besleme hassasiyetine sahiptir. Bu nedenle, fiziksel olmayan salınımları bastırmak için Leonard, konveksiyon teriminin merkezi farkını kullanmak yerine konveksiyon teriminin yukarı yelpaze farkının kullanılmasını önerir. Birinci dereceden yukarı yelpaze yöntemi kullanılarak salınım baskılanabilir, ancak büyük bir sayısal dağılmaya yol açar. Bu nedenle Leonard, hem daha yüksek doğruluk hem de daha iyi geri besleme hassasiyeti için üçüncü dereceden yukarı yelpaze yöntemini önerdi. Böylece, üçüncü dereceden yukarı yelpaze yönteminin kullanılması, hem tek nokta yukarı yelpaze yöntemine hem de merkezi farklılaşmaya kıyasla daha küçük sayısal dağılım ile daha doğru sonuçlar ayrıca merkezi farklılıklara kıyasla ihmal edilebilir fiziksel salınımlar sağladı. Bu çalışmada, hem sayısal dağılımı hem de fiziksel olmayan salınımları azaltmak için, Leonard'ın üçüncü dereceden yukarı yelpaze tekniğini ve Crank-Nicolson zaman ayrıklaştırma yöntemini, değişken bir sınırlayıcı fonksiyon ile birleştirdik.

Leonard'ın yöntemi büyük avantajlara sahip olmasına rağmen ne sayısal dağılımı ne de fiziksel olmayan salınımları tamamen ortadan kaldıramadı. 1984 yılında Harten, entropi durumunu aşan fiziksel olmayan salınımları ortadan kaldırmayı amaçlayan Total Variation Diminishing (TVD) şemasını geliştirdi. Aynı yıl, Sweby, TVD şemaları için stabilite bölgesini belirten klasik bir çalışma yayınladı. Daha sonra, Leonard'ın üçüncü dereceden yöntemi ve TVD algoritması, petrol mühendisliğinde Liu, Gupta ve arkadaşları, Pinto ve arkadaşları, Chen ve arkadaşları, Wollcot ve arkadaşları ve Jiang ve arkadaşları dahil olmak üzere bir dizi araştırmacı tarafından kullanıldı. 1992'de Pinto ve arkadaşları, Liu'ya atıfta bulunarak, TVD yönteminin Leonard'ın üçüncü dereceden farkına uygulanabileceğini belirtti. 1993 yılında Chen ve arkadaşları konveksiyon teriminin tek nokta yukarı yelpaze farkına, TVD yöntemini uyguladı. TVD yöntemi pratik olarak ikinci dereceden farklılığa yol açmıştır ve bu nedenle tek nokta yukarı yelpaze yöntemine kıyasla daha doğru sonuçlar gözlenmiştir. 1991'de Gupta ve arkadaşları, 1994-1995'te Liu ve arkadaşları ve 1996'da Wollcot ve arkadaşları TVD şemalarına üçüncü derece Leonard yöntemini uyguladılar ve tek noktalı TVD yöntemine kıyasla daha iyi sonuçlar elde ettiler. Bu yöntem şimdiye kadar UT Texas'ta araştırmacılar tarafından çeşitli simülasyon çalışmalarında yaygın olarak kullanılmıştır. 2017 yılında Jiang ve arkadaşları iterasyon sayısını azaltmak amacıyla konveksiyon teriminin ayrıklaştırılması için TCDF (üçüncü dereceden sürekli farklılaştırılabilir fonksiyon) yöntemini uyguladılar. TCDF yöntemi, TVD-L yöntemine kıyasla küçük Courant sayısı simülasyonları için toplam iterasyon sayısını biraz azaltmaktadır, ancak

Courant sayıları 2'ye yakın deęerlere yükseltildiğinde TCDF yöntemi daha üstün hale gelmektedir.

Bu tez, yukarıda bahsedilen yöntemlerin, petrolün karışarak ve karışmadan ötelenmesinde uygulanmasını kapsar. Aynı zamanda bu çalışma; TCDF yönteminin su enjeksiyon problemlerine uygulanmasını, Chen ve arkadaşları, Wollcot ve arkadaşları ve Jiang ve arkadaşları tarafından yapılan çalışmalarını takip ederek içerir. Bu çalışmada kullanılan tüm simülatörler, bu alandaki araştırmacılar tarafından kolayca erişilebilir olmasını sağlayan MATLAB programı ile geliştirilmiştir. Petrolün karışmayan yer deęiştirmesini simüle etmek için uygulanan deęişken TCDF yöntemi, gözenekli ortamdaki konveksiyonel akışlar için büyük önem taşımaktadır. Ayrıca bu çalışma; üçüncü derece TCDF yönteminin, ikinci derece Crank-Nicolson şeması ile birleştirilerek geliştirilmesini de içermektedir.

Son olarak, deęişken sınırlayıcı fonksiyonunu uygulayarak, TCDF yönteminin stabilite bölgesini arttırıp TCDF yöntemini bir adım daha geliştirdik. TCDF yöntemi, 1.5'e kadar olan Courant sayıları için fiziksel salınım olmadan çalışırken, yeni bulunan deęişken sınırlayıcı fonksiyonu, 1.85'e kadar olan yüksek Courant sayıları için bile daha önce geliştirilmiş yöntemlerden daha iyi sonuçlar vermektedir.

1. INTRODUCTION

Flow and transport through porous media is of profound importance for many engineering fields, particularly for petroleum engineering. While the single-phase flow of reservoir fluids in porous media can be accurately modeled by heat equation, most transport processes such as immiscible displacement, miscible displacement, chemical and thermal EOR methods and tracer tests are of convective-dispersive nature.

In addition the natural state of oil and gas reservoirs are far from being homogeneous and isotropic with ideal geometrical shapes, most governing flow and transport equations has to be solved numerically. The numerical modeling of flow and transport in porous media are generally known as reservoir simulation and the models are called numerical simulators.

Over the last 100 years, which deserved to be called as oil century, the recovery fraction of oil reservoirs has been between 20 to 30 percent worldwide. That means 70 to 80 percent of the total discovered oil resources still remains unproducable in the reservoirs. Therefore, enhancing recovery and accelerating the production rate is the primary objective of the reservoir management practices. Reservoir simulation/modeling plays a central role in all reservoir management schemes. In fact, reservoir simulators are the most widely used tools for determining the present flow conditions, estimating the future conditions and designating the operations to control the fluid flow and transport in reservoirs. Reservoir simulations studies are the most useful tools of identifying the necessary steps to improve reservoir performance and enhance ultimate recovery rates. On the other hand, the heterogeneous and usually anisotropic nature of reservoirs and presence of strong capillary forces in multiphase flow in porous media pose great challenges to the development accurate numerical models in reservoir simulation studies. For instance, modelling convective-dispersive transport involves many problems such as numerical dispersion, unphysical oscillations and grid orientation effects. Such problems are especially more pronounced in convection-dominated flow and

transport in both miscible displacement and immiscible displacement. The main objective of this study is to mitigate of the numerical dispersion and unphysical oscillations problems.

The problem of numerical dispersion and unphysical oscillations for some elementary finite difference schemes of convection-dominated transport models have been thoroughly investigated by, Peaceman, in 1977, in his classical book titled *Fundamentals of Numerical Reservoir Simulation*. Peaceman has used three elementary space discretization of the convection term, namely upstream (backward), downstream (forward) and midpoint(central) differencing methods. He has also employed three time schemes of time treatment of the discrete governing equations namely, explicit, implicit and Crank Nicholson methods. For all differencing schemes, he has developed and presented the stability limits and numerical dispersion expressions. Indeed these two mathematical expressions serves as an excellent tool for interpreting the concentration profiles and quantifying the numerical errors involved for each scheme. Unfortunately, none of the methods he has used yielded satisfactory results for convection dominated transport especially limiting the schemes for small Courant Numbers (less than one) for acceptable results. In summary, Peaceman has found that first order upstream space discretization schemes can avoid unphysical oscillations but a cost of considerable numerical dispersion. In 1979, Leonard presented a third order finite differencing technique for the convective term with a novel concept of feedback sensitivity to suppress unphysical oscillations. Leonard has his method as QUICK method with an explicit time treatment and has showed that the third order upstream (upstream) space discretization methods exhibit a negative feedback sensitivity, which is a necessary condition to suppress oscillations. Thus, Leonard has observed QUICK method yields numerical results that are more accurate and highly stable compared to those of first order upstream differencing. Although Leonard's third order upstream method yields sharper flood front and lesser numerical dispersion, it suffered from stability limitation. In 1997, Kocabas and Margoub employed the QUICK method combined with a Crank Nicholson scheme which has significantly increased the accuracy and stability of the numerical solutions. Nevertheless, neither Leonard's method nor Kocabas and Margoub modification of it could totally eliminate the arising of the profiles violating the second law of thermodynamics or entropy

generation rule specially for large Courant Numbers. Especially, for the sharp flood fronts, some of the grid blocks near the front had higher concentrations than their upstream neighbors. The second law of thermodynamics prohibits any block to have a higher concentration than those of its upstream location as the transport must spontaneously and naturally take place from higher concentrations to lower concentrations via dispersion. The remedy to entropy violation again came from computational fluid dynamics community. In 1984, Harten has introduced the (Total Variation Diminishing) TVD concept which practically imposes a limited antidiffusive term called as flux limiter, and later in the same year Sweby has determined the stability limits for various TVD flux limiters. In 1991, Liu and Gupta et al published the third order flux limiter function for Leonard's scheme. In 1993, Chen used a second order TVD space discretization method. Later in 1992 Pinto et al, 1994 Liu et al and in 1996 Wollcot et al employed combination of Leonard's third order method and TVD limiter function. This TVD-Leonard method has given to us third order space accurate profiles and a sharper flood front compared with that of Chen's second order TVD method. In 2017, Jiang used third order space TCDF (third-order continuously differentiable function) method instead of using TVD-Leonard method. The advantage of TCDF (also third order Leonard's method is used in TCDF method only difference is the limiter function) method over TVD-Leonard method is that it yields obtain numerical solutions with only slightly lesser total iterations for small Courant number simulations, however, it becomes superior when the Courant numbers are increased to values close to 2.

The objective of this thesis is threefold. First, we will develop 1D and 2D MATLAB codes for both widely used elementary and promising advanced schemes used in both miscible and immiscible displacement processes. The second objective is to search for a technique which will combine third order space TCDF method and second order Crank-Nicolson method as a remedy to violation of entropy destruction law, and still preserving the accurate (minimal numerical dispersion) nature of numerical solutions. The final objective is to present a novel flexible flux limiter function, which works at very large Courant number without any unphysical oscillation compared with the previously developed techniques.

2. LITERATURE REVIEW

This section, we presents a review of the literature related to finite difference schemes employed to solve the classical convection-dispersion equation. The focus is on the large number of discretization techniques of the convective term.

2.1 Convection-Dispersion Equations

Convection-dispersion equation has been widely employed in simulation of fluid flow and solute transport in petroleum reservoir simulations as well as in many other engineering disciplines including chemical, mechanical, environmental and hydrogeological engineering. The behavior of many variables such as concentration and temperature related to heat and mass transport especially in flow through porous media are governed by the convection-dispersion equation.

Specific areas where the convection-diffusion equation is used to describe the transport process are vast in numbers including the solute/contaminant/sediment transport in the atmosphere, oceans, lakes, rivers or groundwater, tracer transport in oil gas and geothermal reservoirs and groundwater aquifers. Another important area of employment for convection dispersion equation is flow and transport through packed beds in chemical engineering [1]. In addition, convection–diffusion equations are particularly important for modeling flow and transport in geothermal, oil and gas reservoirs in two phase flow in oil reservoirs [2].

In particular, convection–diffusion equation is an indispensable tool modeling for various secondary and enhanced oil recovery processes such as miscible displacement, chemical displacement (polymer, alkaline and surfactant flooding), immiscible displacement, nonisothermal injection methods and also in immiscible displacement saturation propagation [3]. In other words, convective dispersive transport is involved in chemical flooding, miscible displacement, tracer flow, solute-contaminant transport and heat transport in porous energy fluids bearing reservoirs.

The classical governing partial differential equation of convective dispersive transport is presented by many authors including Peaceman (1977) as follows:

$$D\nabla^2 C - v \cdot \nabla C = \frac{\partial C}{\partial t} \quad (2.1)$$

In Eq. 2.1, the dependent variable, C , represents concentration. The first term of eq. 2.1 is the diffusion term and, when it dominates, eq. 2.1 behaves like the parabolic heat conduction equation. On the other hand, for the negligible the diffusion (dispersion) term is negligible the convection term dominates and eq. 2.1 approaches the first-order hyperbolic equation (eq. 2.2) [4].

$$-v \cdot \nabla C = \frac{\partial C}{\partial t} \quad (2.2)$$

Equation 2.1 may be simplified assuming one-dimensional and horizontal flow as equation 2.3. [4].

$$D \frac{\partial^2 C}{\partial x^2} - v \frac{\partial C}{\partial x} = \frac{\partial C}{\partial t} \quad (2.3)$$

The velocity, v , is assumed to be positive, corresponding to flow in the direction of increasing x . In this form equation 2.3 serves as the model of miscible displacement, tracer testing or chemical displacement in single phase reservoir flow conditions.

A thorough treatment of some elementary finite difference schemes of equation 2.3 has been presented by Peaceman. Particularly valuable is the part of his work that corresponds to development of stability criteria and numerical dispersion expressions for the finite difference solutions of equation 2.2. A general form of finite difference equation of equation 2.2 is presented by Peaceman as follows:

$$\begin{aligned}
& \frac{D\Delta t}{2\Delta x^2} (C_{i+1,n+1} - 2C_{i,n+1} + C_{i-1,n+1} + C_{i+1,n} - 2C_{i,n} + C_{i-1,n}) \\
& - \frac{vf'\Delta t}{\Delta x} [Q\{(1-W)C_{i+1,n+1} + (2W-1)C_{i,n+1} \\
& - (W)C_{i-1,n+1}\} \\
& + (1-Q)\{(1-W)C_{i+1,n} + (2W-1)C_{i,n} \\
& - (W)C_{i-1,n}\}] = C_{i,n+1} - C_{i,n}
\end{aligned} \tag{2.4}$$

In this general difference scheme (eq. 2.4) while W specifies the spatial weighting and θ specifies temporal weighting. For backward differencing $W=1$, for central differencing $W=1/2$ and for forward differencing $W=0$, and for explicit solutions $\theta=0$, for implicit solutions $\theta=1$ and for Crank Nickolson schemes $\theta=1/2$.

Peaceman has also presented a comprehensive table for stability and numerical dispersion corresponding to each scheme reproduced here as table 2.1.

Table 2.1: Stability table.

	W=1	W=0.5	W=0
Q=1	always stable $D_{num} = 0.5vf\Delta x(N_c + 1)$	always stable $D_{num} = -0.5vf\Delta x(N_c)$	stable if $N_c \geq 1$ $D_{num} = 0.5vf\Delta x(N_c - 1)$
Q=0.5	always stable $D_{num} = 0.5vf\Delta x$	neutrally stable $D_{num} = 0.5$	always unstable $D_{num} = -0.5vf\Delta x(N_c)$
Q=0	stable if $N_c \leq 1$ $D_{num} = 0.5vf\Delta x(1 - N_c)$	always unstable $D_{num} = -0.5vf\Delta x(N_c)$	always unstable $D_{num} = -0.5vf\Delta x(N_c + 1)$

In table 2.1, the stability limit has been presented as a function of Courant Number, N_c , (note that Peaceman has used the symbol λ for Courant Number). The Courant Number (equation 2.5) is defined as

$$N_c = \frac{v\Delta x}{\Delta t} \tag{2.5}$$

The general numerical dispersion expression (equation 2.6a) is also provided as

$$D_{num} = v\Delta x((W - 1/2) + N_c(Q - 1/2)) \tag{2.6a}$$

Among these elementary schemes Peaceman has found that backward in space implicit in time solution is always stable but has always have a positive numerical

dispersion. In addition, he observed that the backward in time and Crank Nicholson in time scheme is also always stable and yields a positive but smaller than that of implicit scheme numerical dispersion. The other elementary schemes suffered from at least one of the following disabilities being conditionally stable, neutrally stable or unstable, and having either always-positive numerical dispersion or sometimes having a negative numerical dispersion violating the second law of thermodynamics. In 1979, Leonard has presented a third order upstream space discretization scheme which he demonstrated by using feedback sensitivity that the scheme eliminates majority of nonphysical oscillations. He treated the time derivative explicitly and called his scheme as QUICK method. The numerical dispersion of QUICK method (equation 2.6b) may be provided as

$$D_{num-Leonard} = v\Delta x(Q - 1/2) \quad (2.6b)$$

Nevertheless, this third order upstream method had exhibited significant oscillations violating the entropy restriction especially for large Courant numbers. In 1984, Harten has introduced the Total Variation Diminishing (TVD) scheme that aims eliminating the unphysical oscillations that violate the entropy condition. In the same year, Sweby has published a classical work which specified the stability region for the TVD schemes. Later, Leonard's third order method and the TVD algorithm have been employed in petroleum engineering by a number of investigators, including Liu, Gupta et al., Pinto et al., Chen et.al., Wollcot et.al, and Jiang et.al. In 1992 Pinto et al, referring to Liu, pointed out that the TVD method can be applied to Leonard's third order differencing. In 1993, Chen et. al. applied TVD method to single point upstream differencing of convection term. The TVD method has practically lead to second order differencing, and hence, sharper flood fronts have been observed compared with pure single point upstream method. In 1991, Gupta et al, and in 1994-1995 Liu et. al. and in 1996 Wollcot et. al. applied third order upwinding Leonard method to TVD schemes and they obtained better results compared to single point TVD method. Later, this method has been widely employed in various simulation studies specially by reseachers in UT Texas at Austin upto present.

In numerical simulations of convection-diffusion equation, not only space discretization but also time discretization has great importance. Therefore, Kocabas and Margoup [5] improved Leonard space discretization employing the second order (Crank-Nicolson) time discretization method. Kocabas and Margoup obtained superior results compared to those of all elementary schemes and purely explicit or implicit methods applied to Leonard's third order space differencing scheme.

In 2017, Jiang et. al. applied the TCDF (third-order continuously differentiable function) method for discretization of convection term for the purpose of reducing the computational iterations of TVD schemes. The TCDF method reduced total number of iterations only slightly for small Courant number simulations compared to the TVD-L method, however, it becomes superior when the Courant numbers are increased to values close to 2.

At this point we rewrite the numerical dispersion equations (eq. 2.7) in terms of cell Peclet and Courant numbers as follows:

$$\frac{D_{num}}{D_{real}} = P_e((W - 1/2) + N_c(Q - 1/2)) \quad (2.7)$$

Figure 2.1, 2.2 and 2.3 shows some of the profiles reproduced from Peaceman and the scheme used by Kocabas and Margoub, namely first order space and second order (Crank-Nicolson) time numerical solution, third order space (Leonard) and second order (Crank-Nicolson) time numerical solution and exact solution of equation 2.3.

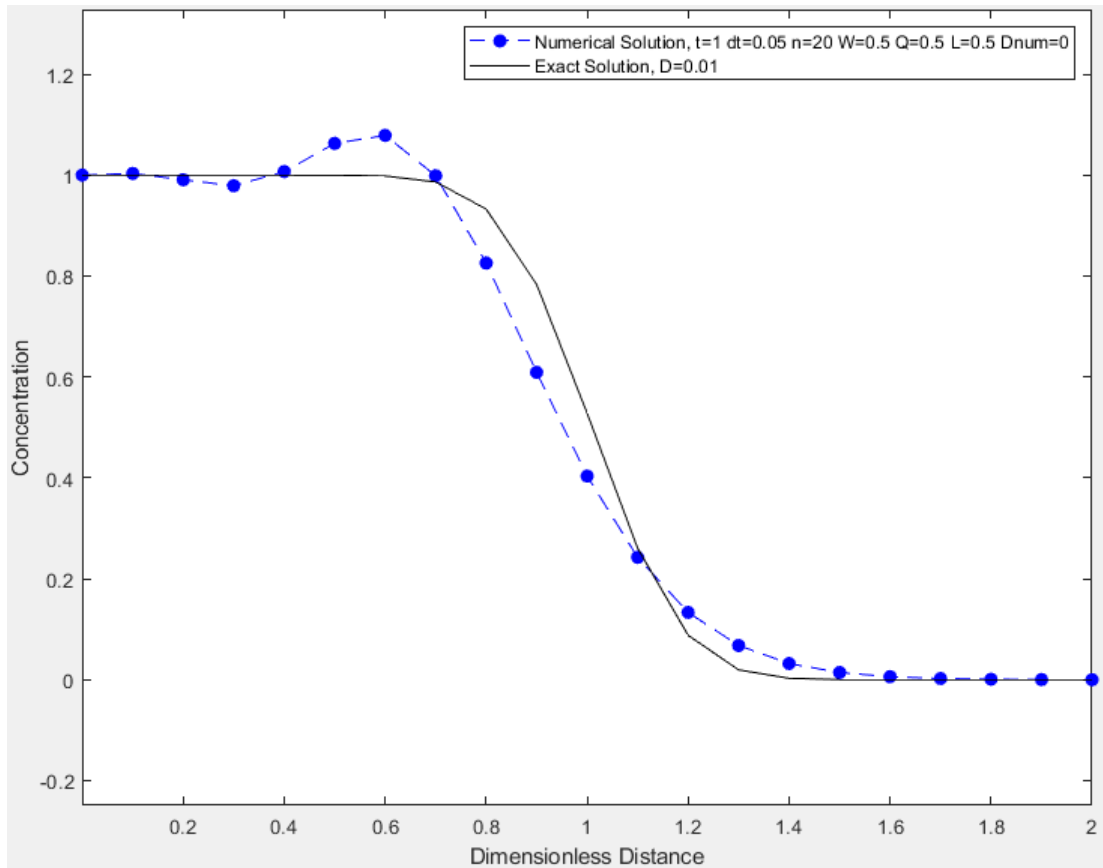


Figure 2.1: Fig. 12C in Peaceman's book.

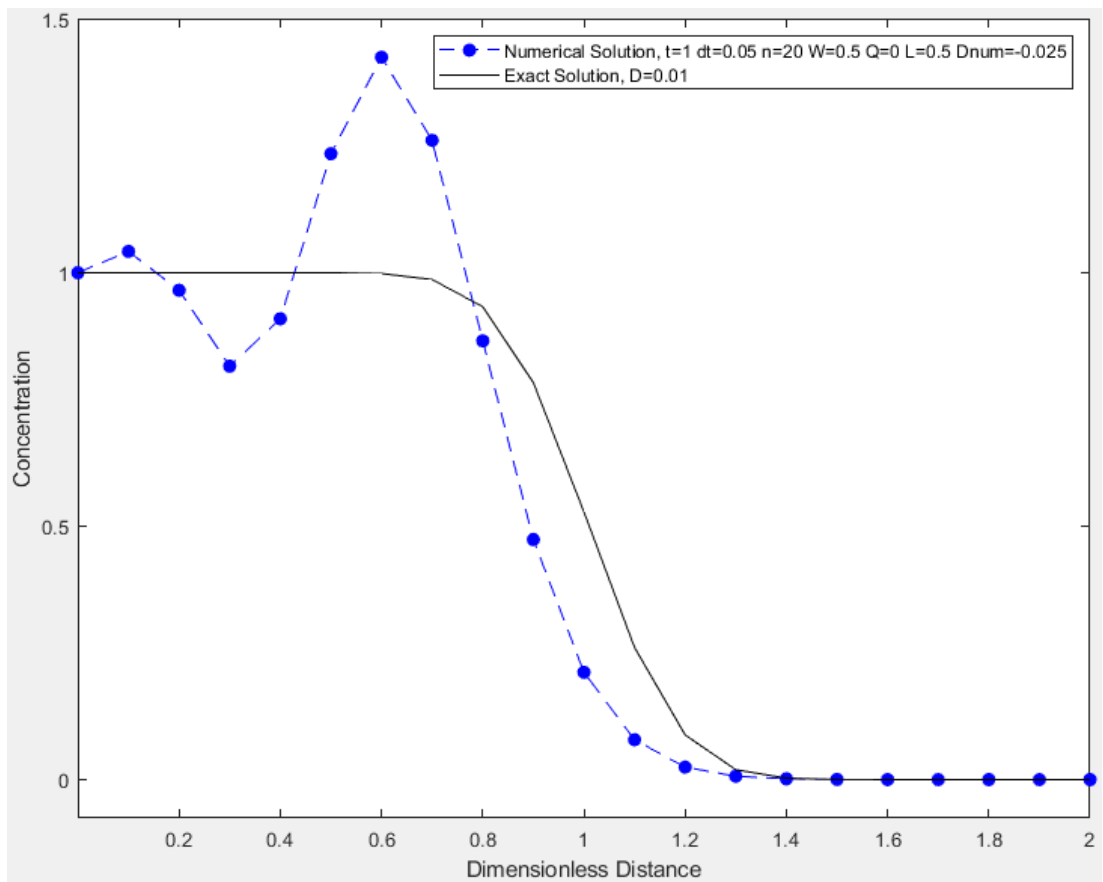


Figure 2.2: Fig. 13A2 in Peaceman's book.

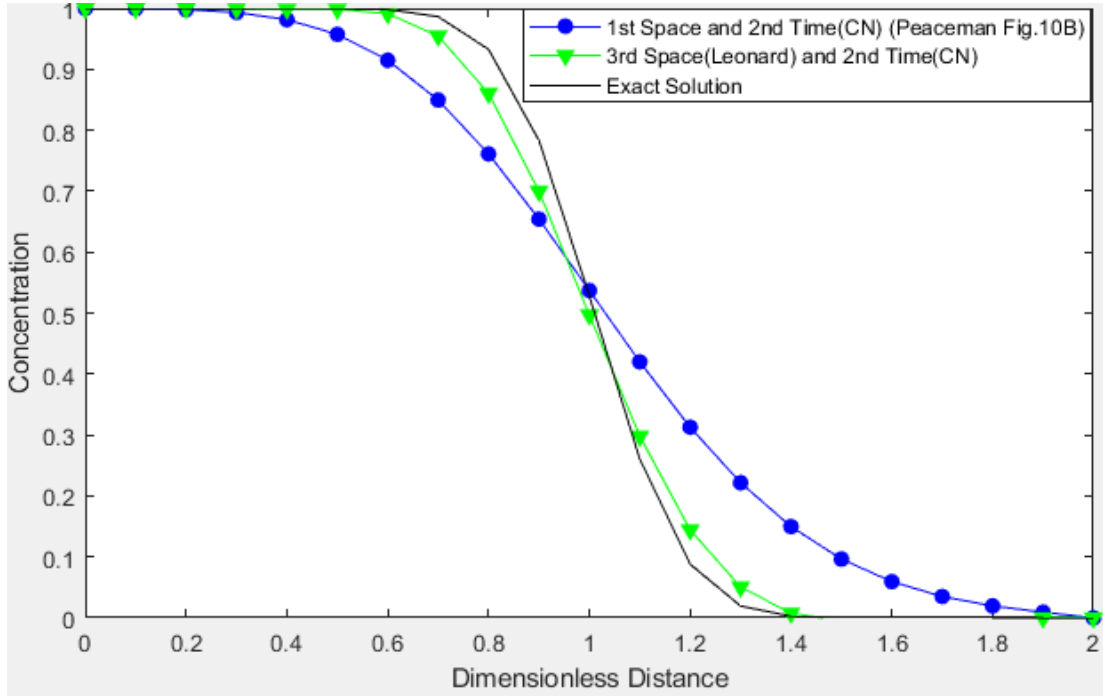


Figure 2.3: Summary of Miscible Displacement Simulations $dx=0.1$ $dt=0.05$.

Reservoir simulation has mostly focused on the solution multiphase flow oil, water and gas. Waterflooding or water influx modeling in oil reservoirs involve immiscible displacement of oil by water. Immiscible displacement of oil water is an unsteady state two phase flow process which invariably requires use of multiphase numerical simulator. In two-phase, unsteady state reservoir simulation models, saturations and velocities vary with time and space. The Darcy velocity is a function of relative permeability values and relative permeability values depend on water saturations. The following oil and water equations (equations 2.8a and 2.8b) [7] govern the one dimensional immiscible displacement processes oil reservoirs.

$$\frac{\partial}{\partial x} \left[\beta_c k_x A_x \frac{k_{ro}}{\mu_o B_o} \left(\frac{\partial p}{\partial x} \right) \right] \Delta x = \frac{V_b}{a_c} \frac{\partial}{\partial t} \left(\frac{\phi(1 - S_w)}{B_o} \right) - q_{osc} \quad (2.8a)$$

$$\frac{\partial}{\partial x} \left[\beta_c k_x A_x \frac{k_{rw}}{\mu_w B_w} \left(\frac{\partial p}{\partial x} \right) \right] \Delta x = \frac{V_b}{a_c} \frac{\partial}{\partial t} \left(\frac{\phi(S_w)}{B_w} \right) - q_{wsc} \quad (2.8b)$$

The saturations equation does in fact take the form of a nonlinear convection dispersion equation as demonstrated by Peaceman as follows (equation 2.9a-2.9f).

$$(1/\alpha)\nabla \cdot (\alpha h_w \nabla S_w) - \frac{df_w}{dS_w} \vec{v}_t \cdot \nabla S_w = \phi \frac{\partial S_w}{\partial t} + (1/\alpha)\nabla \cdot (\alpha G_w \nabla D) \quad (2.9a)$$

If the viscous forces dominates the capillary forces, that is velocities are large and h_w is much smaller, Equation 2.9a reduces to a purely convective transport equation.

$$h_w = -\frac{\lambda_n \lambda_w}{\lambda_n + \lambda_w} \frac{dp_c}{dS_w} \quad (2.9b)$$

$$-\frac{df_w}{dS_w} \vec{v}_t \cdot \nabla S_w = \phi \frac{\partial S_w}{\partial t} + (1/\alpha)\nabla \cdot (\alpha G_w \nabla D) \quad (2.9c)$$

$$\nabla D = \frac{\partial D}{\partial x} - \sin(\alpha_d) \quad (2.9d)$$

$$-\frac{df_w}{dS_w} v_{tx} \frac{\partial S_w}{\partial x} = \phi \frac{\partial S_w}{\partial t} - \sin(\alpha_d) \frac{dG_w}{dS_w} \frac{\partial S_w}{\partial x} \quad (2.9e)$$

Assuming that the flow is horizontal Equation 2.9e reduces to the well known transport equation that can be most conveniently solved by the method of characteristics.

$$v_{tx} \frac{dF_w}{dS_w} \frac{\partial S_w}{\partial x} = -\phi \frac{\partial S_w}{\partial t} \quad (2.9f)$$

2.2 Discretization Methods of Flow and Transport Equations

In developing numerical solutions of fluid flow equations in oil reservoirs, historically two different approached are followed. The first discretization method is called as Conventional Mathematical Approach and the second method is called as Engineering Approach [8]. In classical mathematical approach, PDEs formulations are developed using a finite control volume material balance of mass transport. Then each partial differential term in the PDE is discretized back on a finite grid system. In the engineering approach the discrete equations are derived directly from finite grid systems. The engineering approach has two distinct advantages, namely it first shortens the process of obtaining discretized equations, second it bears a higher order

accuracy for the finite volume. These two advantages constitute the main strength of the engineering approach.

2.2.1 Conventional Mathematical Approach

Conventional mathematical approach consists of several steps. Firstly, material balance equations are written for a control volume. Then, resultant equations are converted into partial differential equations, by taking limit of the control volume as it reduces to zero. The finite difference equations are redeveloped by discretizing the continuous derivatives of the PDEs, resulting in a set of algebraic equation written for each grid block.

As multiphase flow equations in oil reservoirs such as eq. 2.8 and eq.2.9 are strongly nonlinear PDE's, they are almost impossible to solve analytically without substantial idealizations. Therefore, reservoir engineers turn to numerical methods to obtain solutions to the multiphase unsteady flow problems [7].

Over the last hundred years almost all numerical reservoir simulators, were based finite-difference equations. For instance, eq. 2.10 may be obtained by discretization of flow equations using finite difference approximations of the second-order central derivatives of pressure with respect to space and first-order forward (explicit) derivative of pressure with respect to time [8, 9].

$$\begin{aligned} & \left(\beta_c \frac{k_x A_x k_{rp}}{\mu_p B_p \Delta x} \right)_{x+\Delta x_j}^n (p_{j+1}^n - p_j^n) + \left(\beta_c \frac{k_x A_x k_{rp}}{\mu_p B_p \Delta x} \right)_x^n (p_{j-1}^n - p_j^n) \\ & + q_{psc_j}^n = \frac{V_{bj}}{a_c \Delta t} \left\{ \left(\frac{\phi(S_p)}{B_p} \right)_j^{n+1} - \left(\frac{\phi(S_p)}{B_p} \right)_j^n \right\} \end{aligned} \quad (2.10)$$

On the other hand, eq. 2.11 is obtained by discretization of flow equation as finite difference approximations of the second-order central derivatives with respect to space and first-order backward (implicit) derivatives with respect to time.

$$\begin{aligned}
& \left(\beta_c \frac{k_x A_x k_{rp}}{\mu_p B_p \Delta X} \right)_{x+\Delta x_j}^{n+1} (p_{j+1}^{n+1} - p_j^{n+1}) \\
& + \left(\beta_c \frac{k_x A_x k_{rp}}{\mu_p B_p \Delta X} \right)_x^{n+1} (p_{j-1}^{n+1} - p_j^{n+1}) + q_{psc_j}^{n+1} \\
& = \frac{V_{bj}}{a_c \Delta t} \left\{ \left(\frac{\Phi(S_p)}{B_p} \right)_j^{n+1} - \left(\frac{\Phi(S_p)}{B_p} \right)_j^n \right\}
\end{aligned} \tag{2.11}$$

Equation 2.12 was obtained by discretization of flow equation as finite difference approximations of the second-order central derivatives with respect to space and second-order central (Crank-Nicholson) derivatives with respect to time [8,9].

$$\begin{aligned}
& \frac{1}{2} \left\{ \left(\beta_c \frac{k_x A_x k_{rp}}{\mu_p B_p \Delta X} \right)_{x+\Delta x_j}^n (p_{j+1}^n - p_j^n) + \left(\beta_c \frac{k_x A_x k_{rp}}{\mu_p B_p \Delta X} \right)_x^n (p_{j-1}^n - p_j^n) \right\} \\
& + \frac{1}{2} \left\{ \left(\beta_c \frac{k_x A_x k_{rp}}{\mu_p B_p \Delta X} \right)_{x+\Delta x_j}^{n+1} (p_{j+1}^{n+1} - p_j^{n+1}) \right. \\
& \left. + \left(\beta_c \frac{k_x A_x k_{rp}}{\mu_p B_p \Delta X} \right)_x^{n+1} (p_{j-1}^{n+1} - p_j^{n+1}) \right\} \\
& + \frac{1}{2} \{ q_{psc_j}^n + q_{psc_j}^{n+1} \} \\
& = \frac{V_{bj}}{a_c \Delta t} \left\{ \left(\frac{\Phi(S_p)}{B_p} \right)_j^{n+1} - \left(\frac{\Phi(S_p)}{B_p} \right)_j^n \right\}
\end{aligned} \tag{2.12}$$

In the equations above, subscript p refers phase, and hence for writing out water equation, p subscription will be replaced with w and thus the variable S_p will mean S_w .

2.2.2 Engineering Approach

In engineering approach, as there is no need to obtain continuous medium PDEs formulation, understanding the engineering approach is easier than conventional mathematical approach. Farouq Ali (1986) looked extensively into the nonlinear algebraic flow equations developed using the classical mathematical approach and

found that the flow terms of the discretized equations are fundamentally Darcy's law, which defines the volumetric flow rate of fluid between the block (control volume) and its neighbouring blocks at standard conditions. Forward-central-difference (forward difference in time and central difference in space) equations and backward-central-difference (backward difference in time and central difference in space) equations were developed by him based on his observation and assumption associated to the time level of evaluating the flow terms, without formulation of PDEs and PDE discretization. Farouq Ali's observation was certainly a revolution in simulation studies. 15 years later, Ertekin et al. (2001) represented control volume by a point at its center, which is pretty much closer to the engineer's view about the blocks of petroleum reservoir. Development of engineering approach thus started by mainly Farouq Ali and later by Ertekin et al. [8]. Equation 2.9 [8, 9] shows engineering approach for discretization of fluid flow equations. Note that a similar approach has also been employed by Leonard for discretizing the convection dispersion equation. Again it is important note that, subscription p means phases. For example, if equation is oil equation, p subscription will be o and S_p will be S_o .

$$\begin{aligned}
& \int_n^{n+1} \left(\beta_c \frac{k_x A_x k_{rp}}{\mu_p B_p \Delta x} \right)_x (p_{j-1} - p_j) dt \\
& - \int_n^{n+1} \left(\beta_c \frac{k_x A_x k_{rp}}{\mu_p B_p \Delta x} \right)_{x+\Delta x_j} (p_j - p_{j+1}) dt \\
& + \int_n^{n+1} q_{psc_j} dt = \frac{V_{bj}}{a_c} \left\{ \left(\frac{\phi(S_p)}{B_p} \right)_j^{n+1} - \left(\frac{\phi(S_p)}{B_p} \right)_j^n \right\}
\end{aligned} \tag{2.13}$$

Figure 2.4a shows graphical representation of the integral of equation 2.9. Nevertheless, in numerical solutions, perfectly obtaining of figure 2.4a is impossible. Argument F will be used to clarify integration of equation 2.9. It is assumed that F represents $\left(\beta_c \frac{k_x A_x k_{rp}}{\mu_p B_p \Delta x} \right)_x (p_{j-1} - p_j) dt$, $\int_n^{n+1} \left(\beta_c \frac{k_x A_x k_{rp}}{\mu_p B_p \Delta x} \right)_{x+\Delta x_j} (p_j - p_{j+1}) dt$ and q_{psc_j} . In figure 2.4b, t^z is constant over the time step Δt [8]. In that case, shaded area in figure 2.4b can be found nearly same as shaded area in figure 2.4a. Figure 2.4c shows equation 2.6 (finite difference approximations of the second-order central derivatives with respect to space and first-order forward (explicit) derivatives with respect to time). Figure 2.4d shows equation 2.7 (finite difference approximations of

the second-order central derivatives with respect to space and first-order backward (implicit) derivatives with respect to time). Figure 2.4e shows equation 2.8 (finite difference approximations of the second-order central derivatives with respect to space and second-order central (Crank-Nicholson) derivatives with respect to time).

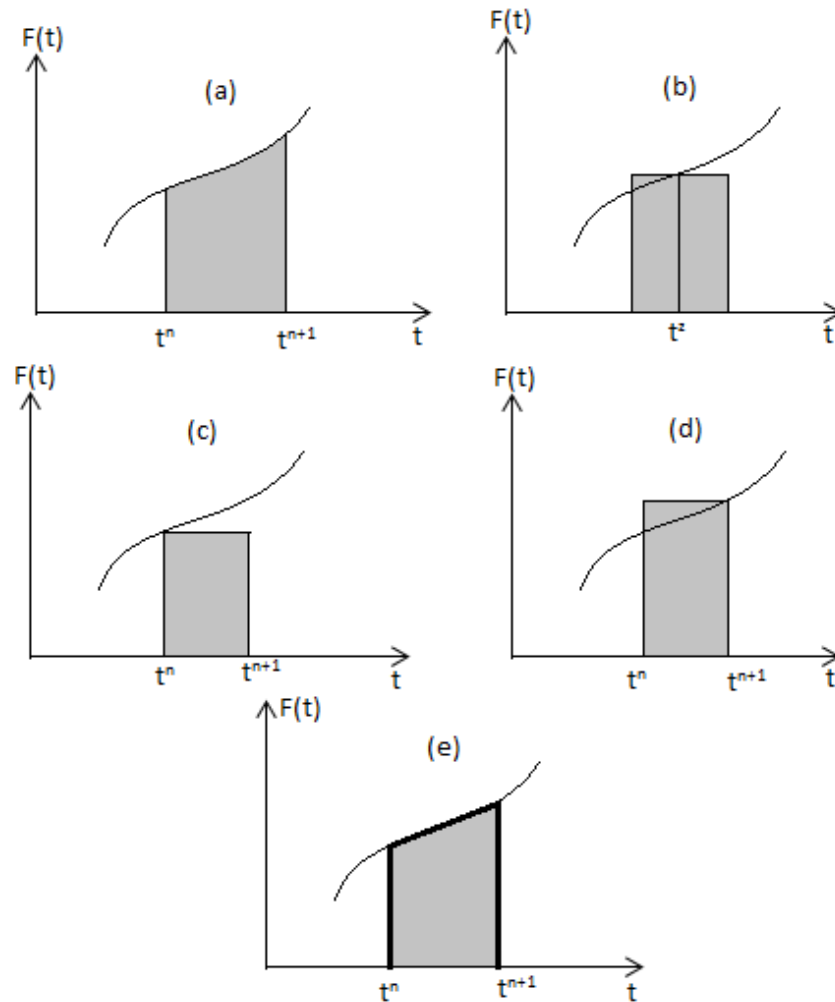


Figure 2.4: Engineering and classical approaches [8].

2.3 Problems in Convective Term Discretization

The spatial inaccuracy problems of multiphase flow equations mainly arise from unknown relative permeability terms at grid block faces. This fact is deduced from the analytical solution (frontal advance solution) of immiscible displacement of oil by water both of which are assumed incompressible. In order to calculate inlet flux into and outlet from a grid block, saturations at grid block faces have to be known. Therefore, higher order techniques may help to obtain closer prediction of saturation values at grid block faces.

A second problem in finite differencing techniques is observation of unphysical oscillations. Another important problem is the stability limitations. In 1981, Leonard investigated the stability of (specially suppressing of unnecessary perturbations) of many elementary and high order differencing schemes using the concept of feedback sensitivity. He concluded that in order to have a numerically stable solution the differencing scheme must have negative feedback sensitivity. A feedback sensitivity analysis showed that, upstream differencing techniques have negative feedback sensitivity so these methods are more stable than central differencing methods. Therefore, any scheme employed should be ensured to have negative feedback sensitivity regardless of its truncation error or accuracy.

The spatial accuracy or truncation errors are directly related the order scheme employed. In order to reduce the truncation errors especially in chemical reservoir simulation models [10], researchers mostly opted to use second order and third order upstream schemes. Using higher order upstream techniques instead of first order upstream method, gives to more reliable reservoir simulation models. In 1996, Wolcott et al. explained advantage (sharper flood front) of using higher order techniques. Researchers have shown that when the mobility terms are discretized using higher than first order schemes, sharper and potentially more accurate flood fronts are predicted [11].

Although there is no any analytical solution of 2D and 3D reservoir simulation, analytical solution of 1D incompressible two-phase immiscible displacement reservoir simulation is available. Analytical solution of 1D reservoir simulation was developed by Buckley et al. in 1941 [12]. It is very significant for us to compare our numerical results with analytical solution. Also this analytical solution has been used by a number of researchers [13-22] in their studies.

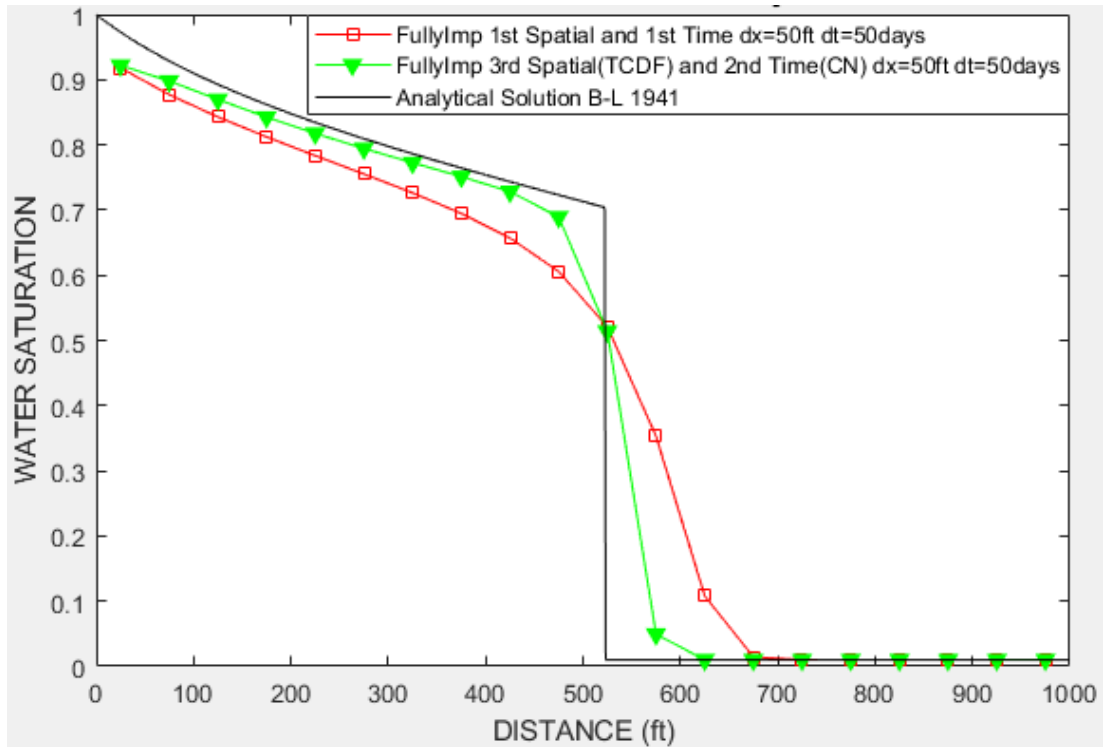


Figure 2.5: Comparison of higher and first order techniques.

Figure 2.5 shows a comparison of first and third order methods to simulate the Buckley Leveret immiscible displacement solution in a linear flooding geometry. Figure 2.5 exhibits that the higher order technique produces sharper flood front and lesser numerical dispersion and hence is much closer to analytical solution than first order method.

The main inaccuracy of caused by higher numerical dispersion is an early breakthrough of the injected water.

In 2017, Kayode et al. pointed out the importance of water breakthrough time. During history matching of observed production data of brown fields, one of the key matching parameters is the water break-through time and its accurate prediction is great significance for constructing proper surface treatment installations [23].

Figure 2.6 shows breakthrough time of first order and the higher order technique where first order method cause 200 days earlier breakthrough time which adversely affect prediction of oil reservoir performance.

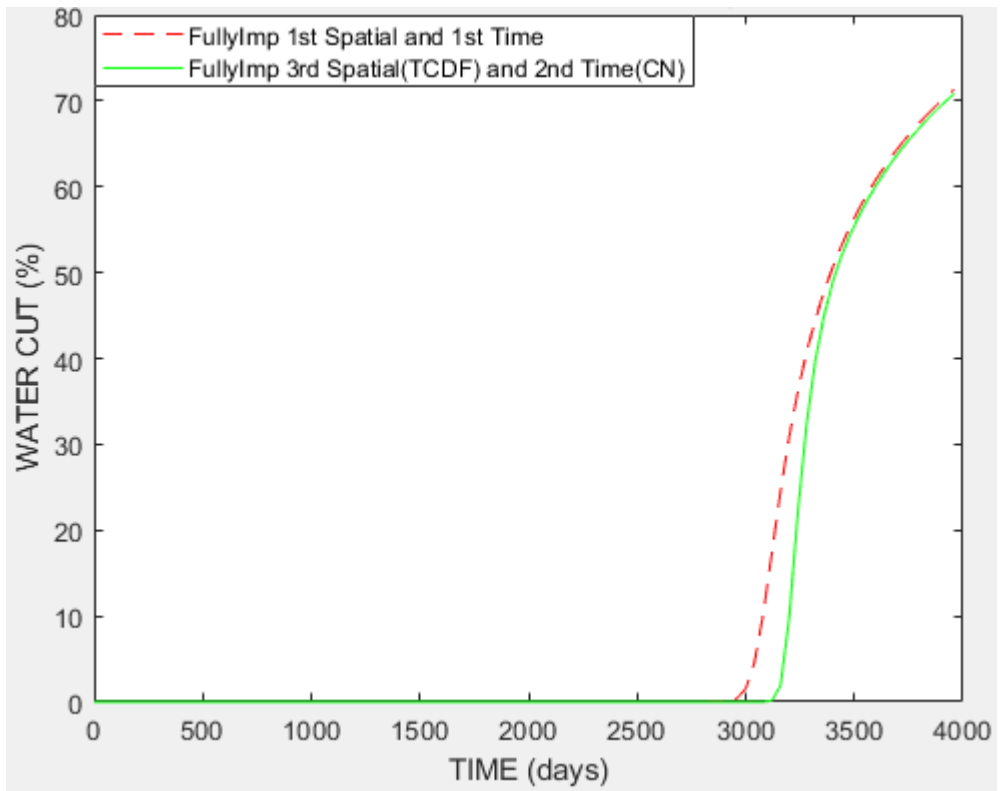


Figure 2.6: Breakthrough times of higher and first order methods.

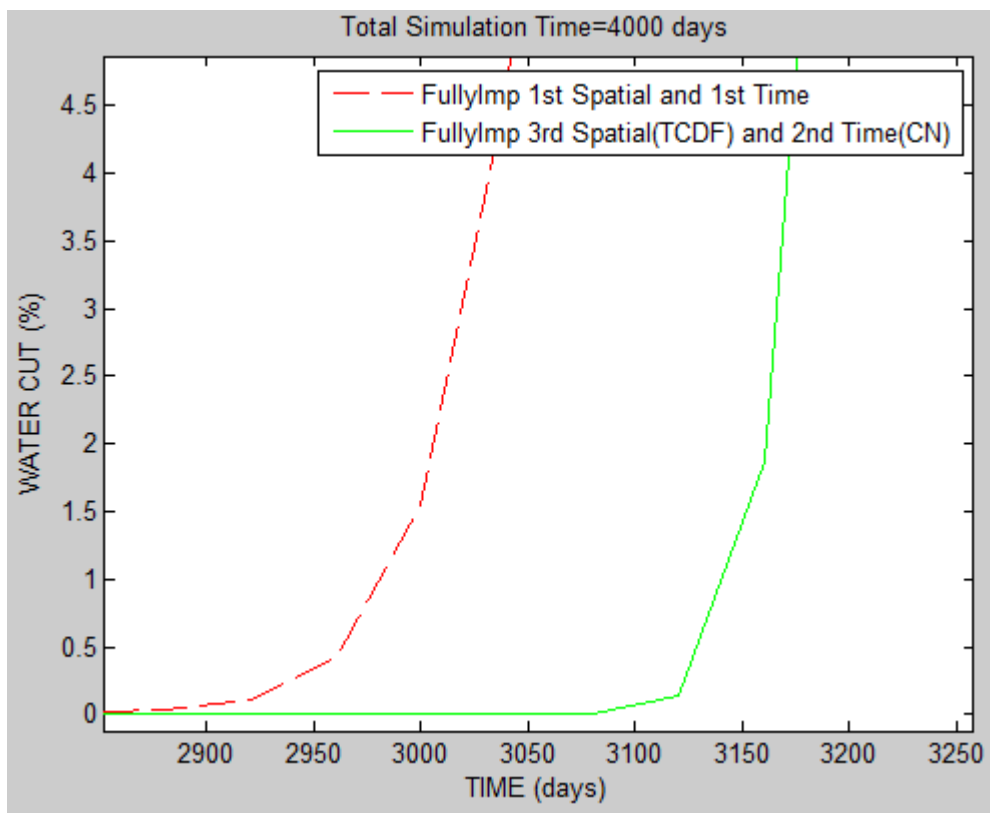


Figure 2.7: Breakthrough times of higher and first order methods in detail.

It is very important question that why earlier breakthrough time is observed using first order method. In numerical reservoir simulation, only block center saturations

and pressures are known but saturation and pressure values at interface of two grid blocks are not known. Main problems arise from that point in numerical reservoir simulation for spatial discretization. Because according to Darcy Law, interface water saturations have to be known to calculate fluid flow between two grid blocks. In figure 2.8, suppose that there are five grid blocks, first grid block is injection grid block and fifth grid block is production grid block. Normally, in fully implicit solution, there are five water equations and five oil equations in order to solve five pressure unknowns and five saturation unknowns but so as to simplify understanding of early breakthrough for first order methods, only left side water flow of third grid block will be taken into account. In order to calculate water flow from second grid block to third grid block, interface water saturation between second and third grid block requires. In first order method, due to lack of interface water saturation between second and third grid block, it is assumed that interface water saturation between second and third grid block is equal to second grid block water saturation. Because of the fact that first grid block is injection grid block and first grid block has highest water saturation, second grid block is upstream to third grid block. Therefore, saturation of second grid block is higher than saturation of third grid block as well as interface water saturation between second and third grid block. In first order method, selection of water saturation of second grid block for interface water saturation between second and third grid block causes assumption of higher water saturation than it should be. Assumption of higher water saturation for interface water saturation between second and third grid block also causes easy water flow from second grid block to third grid block because according to Darcy Law, water flow is directly proportional to relative permeability of water and relative permeability of water is also directly proportional to water saturation. There are two important results of easy water flow from second grid block to third grid block using first order method. One of them is advantage, one another is disadvantage. Advantage of first order method can be defined as there is no any accumulation of water at second grid block therefore there is no any oscillation at second grid block thanks to easy water flow. On the other hand, easy water flow from second grid block to third grid block causes numerical dispersion as well as earlier breakthrough time that can be explained as main disadvantage of first order method.

The main objectives of this study are to reduce numerical dispersion using a higher order differencing and at the same time avoid entropy violations namely to diminish nonphysical oscillation using a limiter function. There are a number of higher order spatial discretization technique for which limiter function is employed. One of the earliest application of limiter function is on the second order spatial discretization, called as TVD (Total Variation Diminishing) method [24]. This second order spatial discretization TVD Method can be easily applied IMPES as well as Fully Implicit Methods. In order to apply second order spatial discretization TVD Method on left hand side fluid flow of third grid block in figure 2.8; second, third and fourth grid block water saturations should be compared. So as to determine or predict interface water saturation between second and third grid block, firstly select lesser water saturation differences of second-third grid blocks or third-fourth grid blocks. Secondly, subtract selected differences from second grid block water saturation. Thanks to second order spatial discretization TVD Method, interface water saturation between second and third grid block was easily calculated. Calculated interface water saturation between second and third grid block is lesser than second grid block water saturation therefore lesser numerical dispersion and later water breakthrough time can be observed. Another advantage of second order spatial discretization TVD Method is to suppress the effect of oscillation using selection of lesser saturation differences. Other higher order techniques described in this study are third order spatial discretization TVD-Leonard Method [11], third order spatial discretization TCDF Method [6], second-third order time accuracy Runge-Kunta Method [24] and second order time accuracy Crank-Nicholson Method [4].

Ultimate aim of this study is to obtain combination of third order spatial accuracy TCDF Method and second order time accuracy Crank-Nicholson Method (TCDF-CN).

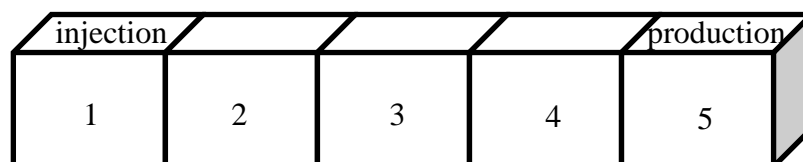


Figure 2.8: 1D five grid blocks.

3. MATHEMATICAL DEVELOPMENTS FOR MISCIBLE DISPLACEMENT SIMULATIONS

The general governing partial differential equation of miscible displacement simulation is given by equation 3.1 called as classical convection dispersion equation [4].

$$D \frac{\partial^2 C}{\partial x^2} - u \frac{\partial C}{\partial x} = \frac{\partial C}{\partial t} \quad (3.1)$$

Where C , D and u are referred to as the concentration, the dispersion coefficient, interstitial velocity respectively. The problematic first derivative, accounting for the convective transport, requires the knowledge of grid block face values for approximating the first derivative in discretized form of equation 3.1. Finite difference approximation of the convection term is given by equation 3.2.

$$-u \frac{\partial C}{\partial x} \approx -u \frac{C_{i+\frac{1}{2}} - C_{i-\frac{1}{2}}}{\Delta x} \quad (3.2)$$

3.1 Miscible Displacement Simulations Using Elementary Difference Schemes

The general forms of the elementary differencing schemes at block faces are provided by Peacemeane in his classical work as follows [4]:

$$F_{i+\frac{1}{2}} = W(F_i) + (1 - W)(F_{i+1}) \quad (3.3)$$

$$F_{i-\frac{1}{2}} = W(F_{i-1}) + (1 - W)(F_i) \quad (3.4)$$

Where for upstream differencing $W=1$, mid-point differencing $W=0.5$ and downstream differencing $W=0$ in equation 3.3 and 3.4 distance weighting methods.

Also, note that equation 3.3 and equation 3.4 show east side and west side face values respectively for different distance weighting methods [4].

The second order diffusive transport term in equation 3.1 can be accurately discretized by using a midpoint (central) differencing.

The the full and most general discretized form of equation 3.1 with elementary differencing schemes can be written as in equation 3.5:

$$\begin{aligned}
\frac{D\Delta t}{2\Delta x^2} (U_{i+1,n+1} - 2U_{i,n+1} + U_{i-1,n+1} + U_{i+1,n} - 2U_{i,n} + U_{i-1,n}) \\
- \frac{vf'\Delta t}{\Delta x} [Q\{(1-W)U_{i+1,n+1} + (2W-1)U_{i,n+1} \\
- (W)U_{i-1,n+1}\} \\
+ (1-Q)\{(1-W)U_{i+1,n} + (2W-1)U_{i,n} \\
- (W)U_{i-1,n}\}] = U_{i,n+1} - U_{i,n}
\end{aligned} \tag{3.5}$$

Where Q represents time weighting factor. Similar to spatial differencing time differencing, the three cases are as follows implicit Q=1, center-in-time Q=0.5 and explicit Q=0.

Note that the weighting factors, W and Q, are varied only for the convection term, Peaceman has used central differencing for both time and space discretization of dispersion term as they yield more accurate results than those of other weighting factors for the dispersion term [4].

Figure 3.1 [4] shows first order upstream distance weighting and second order Crank-Nicolson time weighting numerical solution of equation 3.6 using Matlab Code (see fig. 10B in Peaceman's book [4]).

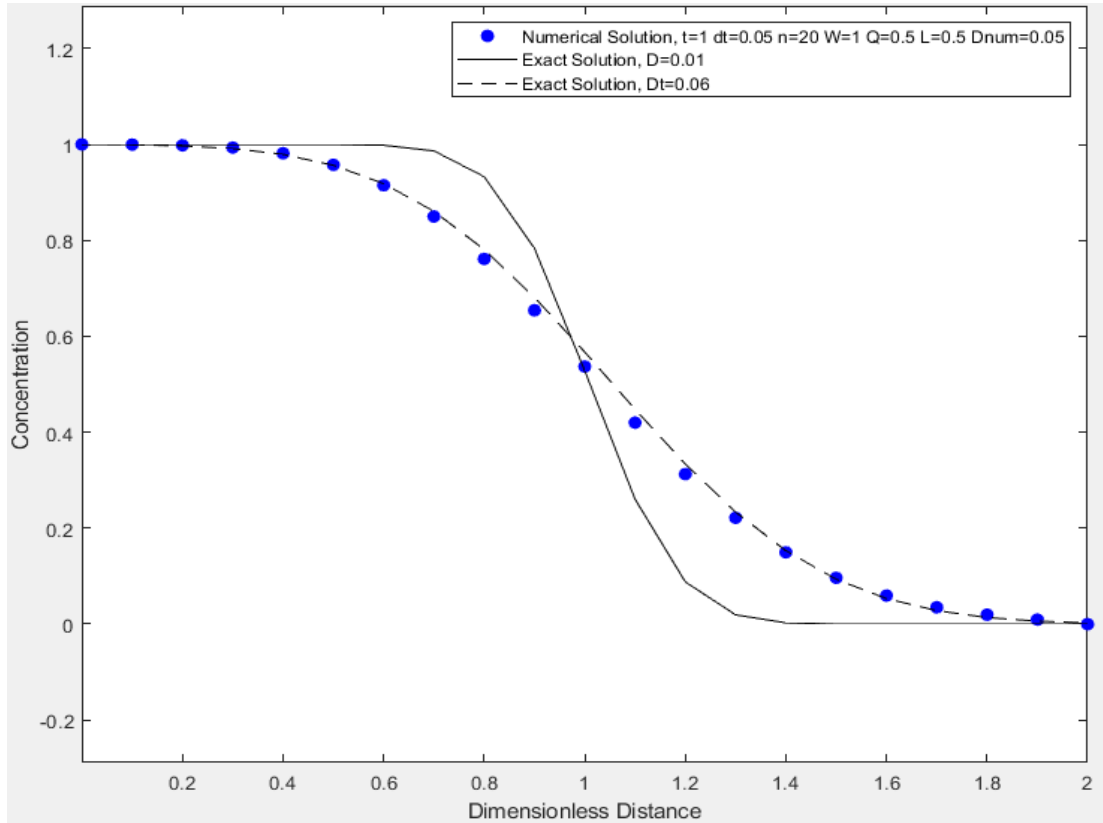


Figure 3.1: 1st order space and 2nd order time (using Matlab code).

3.2 Feedback Sensitivity and Improved Discretization Techniques

Feedback sensitivity is a techniques used by Leonard to understand investigate the stability of the numerical solutions stability with respect to oscillatory perturbations [5]. For stable numerical solutions, negative feedback sensitivity is required. Feedback sensitivity, σ , is defined as the derivative of the difference operator with respect to node for which derivative is approximated (see APPENDIX A). Leonard has pointed out that for stable numerical solutions negative feedback sensitivity is required. In addition, the greater the absolute value of the feedback sensitivity the more capable is the scheme to suppress the oscillations. For example, consider the upstream differencing of first derivative of convection term (equation 3.6):

$$-u \frac{\partial C_i}{\partial x} \cong -u \frac{C_i^n - C_{i-1}^n}{\Delta x} \quad (3.6)$$

Then, the feedback sensitivity of convection term becomes (equation 3.7):

$$\sigma = \frac{-u}{\Delta x} \quad (3.7)$$

Since the difference operator has always a negative feedback sensitivity assuring damping of oscillation, the central differencing works very well for the second order derivatives (see APPENDIX A) [5].

Also, consider the central differencing of first derivative of convection term (equation 3.8):

$$-u \frac{\partial C_i}{\partial x} \cong -u \frac{C_{i+1}^n - C_{i-1}^n}{2\Delta x} \quad (3.8)$$

Thus, the feedback sensitivity of convection term is zero as in equation 3.9:

$$\sigma = 0 \quad (3.9)$$

This differencing operator has a second order discretization error the same as that of diffusion operator. However, this operator has neutral (zero) feedback sensitivity that has a high potential of producing unphysical oscillations. In fact, Leonard states that neutral sensitivity is a characteristic of all central difference methods of any order when applied to odd order derivatives [5]. Therefore, he has resort to employing a third order upstream scheme. Equation 3.10 shows a third order upstream scheme of the first order derivative (the convection term) developed by Leonard [25].

$$-u \frac{\partial C_i}{\partial x} \cong -u \frac{2C_{i+1}^n + 3C_i^n - 6C_{i-1}^n + C_{i-2}^n}{6\Delta x} \quad (3.10)$$

The feedback sensitivity of equation 3.10 becomes:

$$\sigma = \frac{-3u}{6\Delta x} \quad (3.11)$$

This negative feedback sensitivity of the third order discretization operator assures damping of oscillations and a leads to a third order truncation error [5]. However, magnitude of feedback sensitivity of the third order discretization operator is lesser than magnitude of feedback sensitivity of the first order discretization operator. Therefore, first order upstream method is better than third order upstream technique to suppress unphysical oscillation. On the other hand, first order method has huge numerical dispersion compared with third order technique.

In 2000, Kocabas and Margoub combined the third order upstream (Leonard) distance weighting and second order Crank-Nicolson time weighting method [5] in order to take advantage of both methods higher order accuracy and unconditionally stable nature of implicit treatment. Figure 3.2 shows the concentration profiles obtained using Kocabas and Margoub approach coded in Matlab.

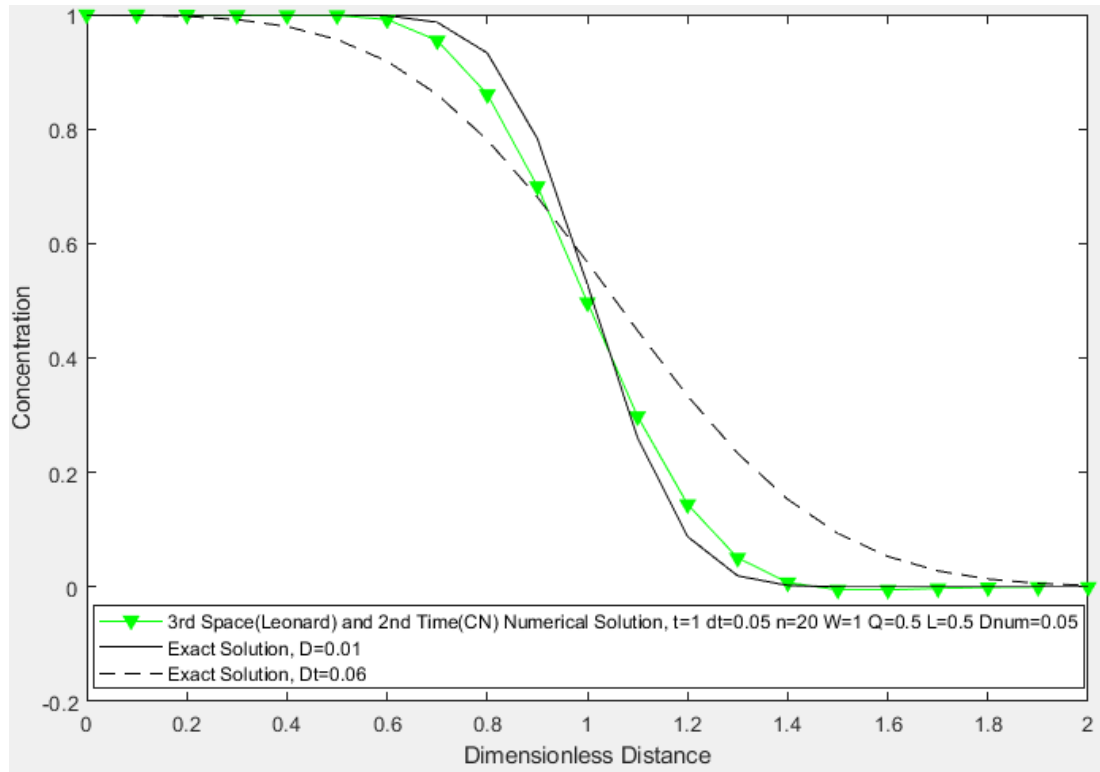


Figure 3.2: 3rd order space and 2nd order time (using Matlab code).

After that point, three different cases (Explicit, Implicit and Crank-Nicolson) using improved technique will be investigated following part in detail.

3.2.1 In Depth Investigation of the Explicit Numerical Schemes

In this section, we present an in depth investigation of elementary differencing operators, namely upstream weighting, mid-point weighting and the third order accurate Leonard technique operator, called as QUICK method, explicit schemes. Also in this section, six figures are presented for various Courant numbers and Cell Peclet numbers, which are both functions of spacial grid size and time increment.

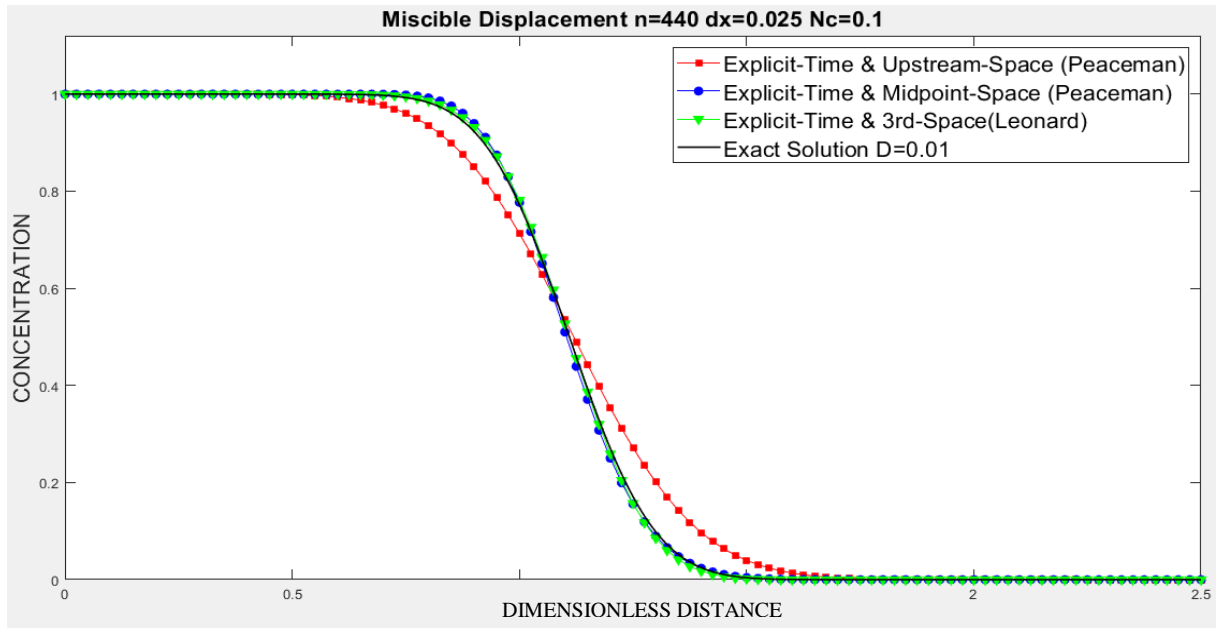


Figure 3.3: Improved method $n=440$ $dx=0.025$ $Nc=0.1$ (Explicit).

Figures 3.3, 3.4 and 3.5 show simulations with small space intervals (same cell peclt number) but gradually increasing courant numbers (Nc).

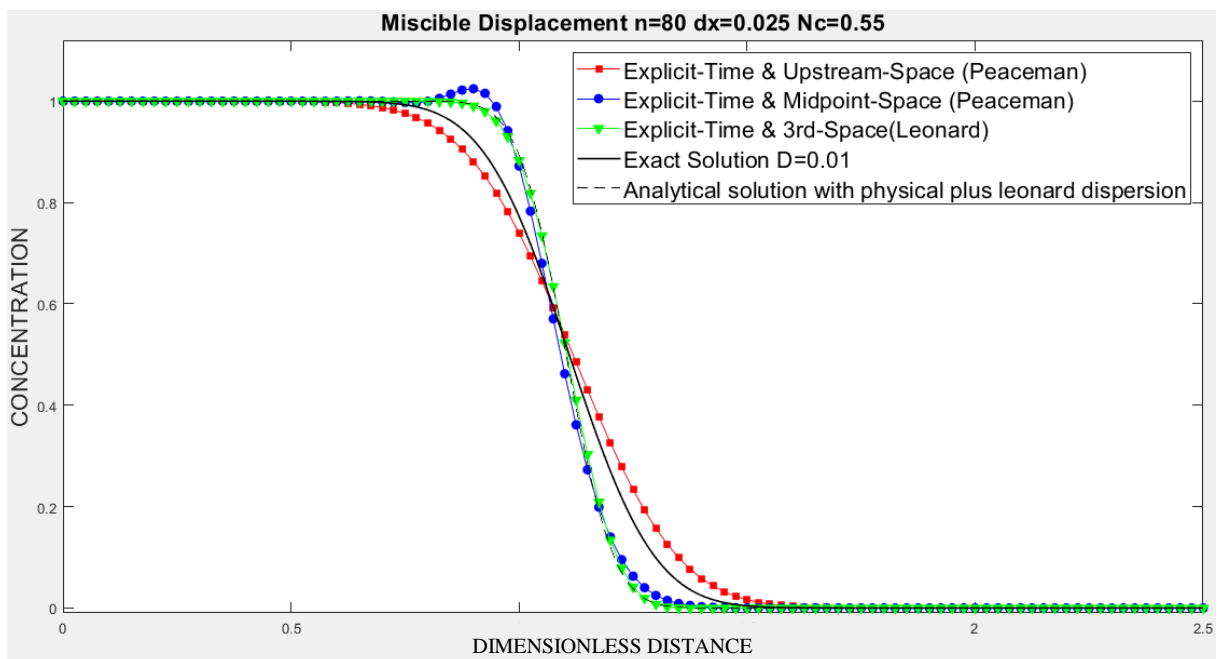


Figure 3.4: Improved method $n=80$ $dx=0.025$ $Nc=0.55$ (Explicit).

Figure 3.3 gives to same profiles for both higher (second and third) order spatial discretization techniques but the first order upstream method exhibits significant numerical dispersion. No unphysical oscillation is observed for any of the methods. Figure 3.4, exhibits a very interesting behavior namely, negative numerical dispersion effect in all methods thus and hence they are not considered as stable any more.

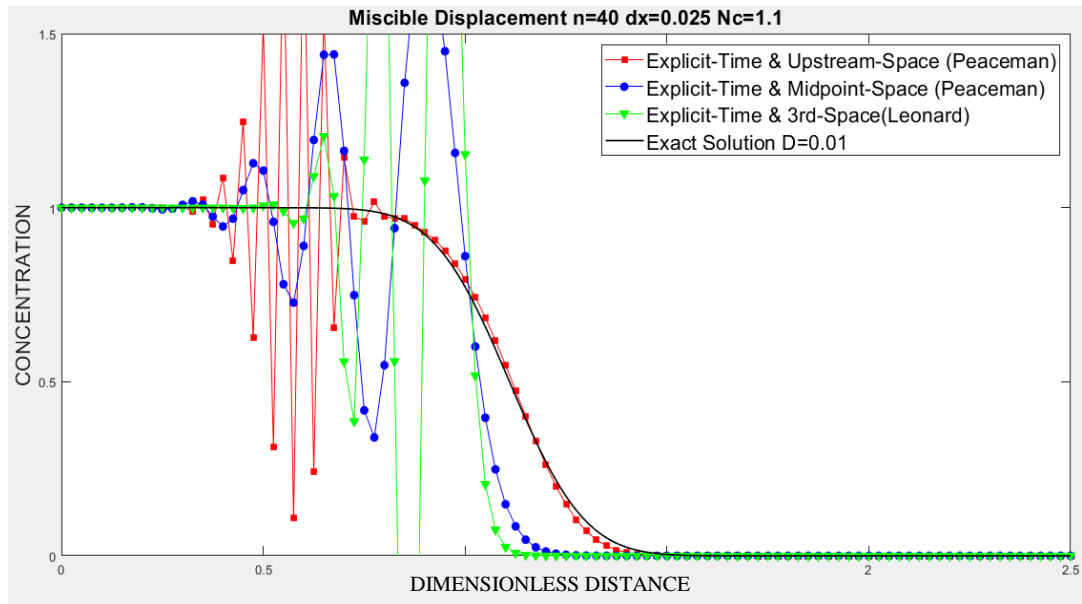


Figure 3.5: Improved method $n=40$ $dx=0.025$ $Nc=1.1$ (Explicit).

At the courant number, Nc , is further increases (figure 3.5), all solution methods becomes unstable and produce unphysical and unacceptable oscillations.

Figure 3.6 shows the profiles generated for a large space increment (i.e. large cell Peclet number Pe_{cl} , and small Courant Number, Nc). Comparing the profiles in figure 3.3 and figure 3.6 one may reach the following conclusion. Increasing the space increment, the dispersion in the upstream method becomes more prominent and leads to separation of the profile from analytical solution significantly in figure 3.7. Also in figure 3.7, while the mid-point method exhibits a pronounced unphysical oscillation, Leonard methods closely matches the analytical solution.

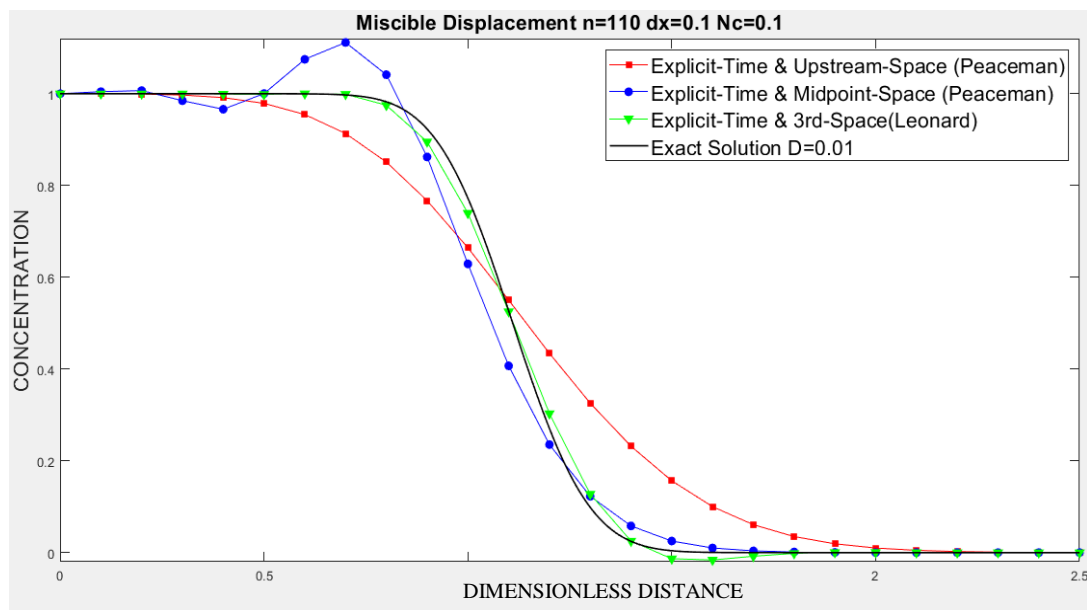


Figure 3.6: Improved method $n=110$ $dx=0.1$ $Nc=0.1$ (Explicit).

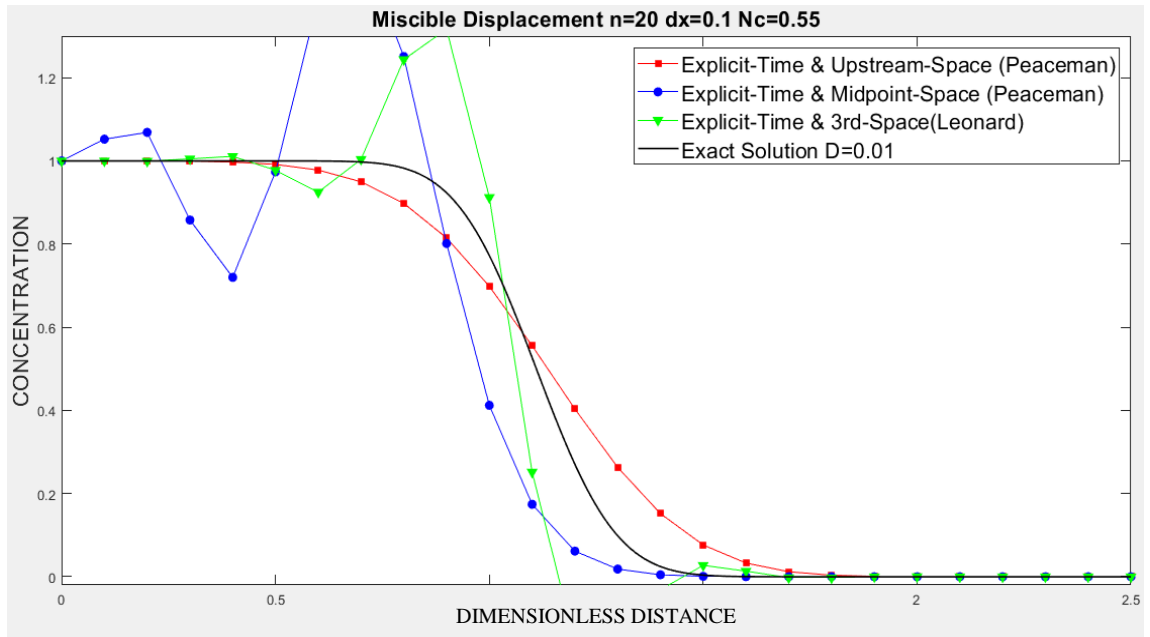


Figure 3.7: Improved method $n=20$ $dx=0.1$ $Nc=0.55$ (Explicit).

Figure 3.7 shows that for the same large cell Peclet number, increasing the Courant number to 0.55 (larger time step), the higher order methods become unstable exhibiting wild unphysical oscillations. Interestingly however, the first order upstream method yields a smooth apparently stable profile with really large numerical dispersion. One can conclude that this pseudo stable appearance is due to the fact that vastly large numerical dispersion smears out the instability oscillations from the first order upstream method.

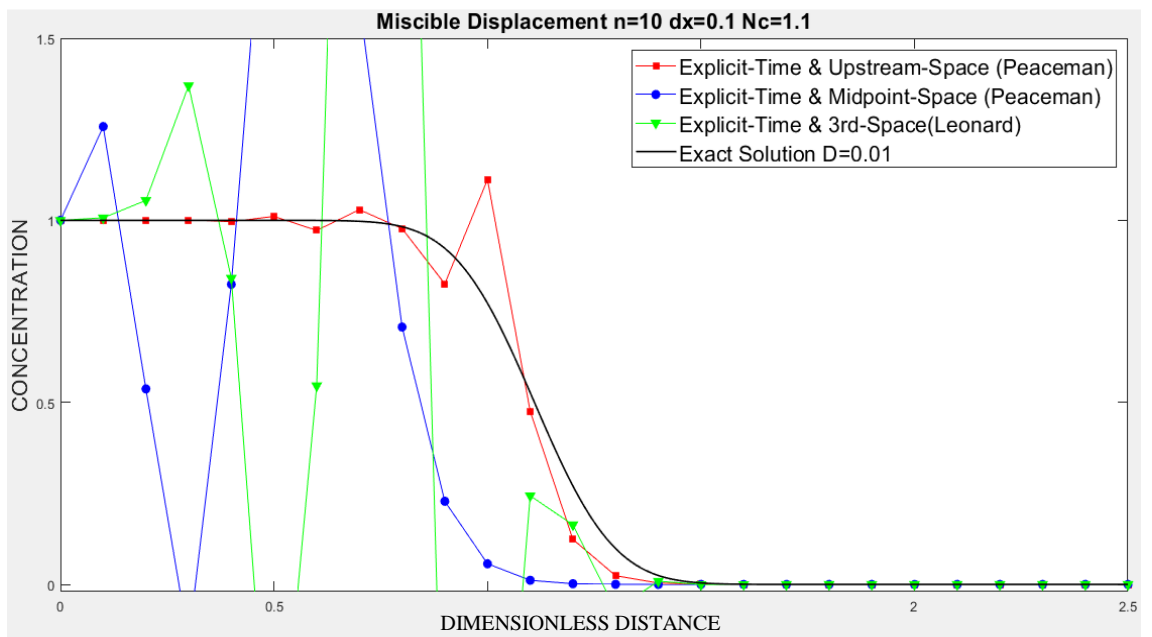


Figure 3.8: Improved method $n=10$ $dx=0.1$ $Nc=1.1$ (Explicit).

Further increase in the Courant number to 1.1 as shown in Fig. 3.9 leads totally unstable solutions for all explicit schemes of any order. This can be deduced from the stability conditions developed for each method.

In summary:

- As Δx grows truncation errors and hence numerical dispersion grows for all of explicit schemes.
- The stability condition is best for upstream scheme among the elementary schemes detailed by Peaceman.
- Explicit mid-point methods are unstable with oscillations at large Courant number.
- Quick explicit method exhibits no oscillation and negligible numerical dispersion and hence matches the front perfectly but only for very small N_c close to 0.1.
- For explicit Quick method the range of stability region for N_c must be determined before the actual simulations using analytical solutions where either oscillations or negative numerical dispersion or both are observed.

3.2.2 In Depth Investigation of the Implicit schemes

The stability of all explicit schemes are limited by the magnitude of the Courant number, N_c . Thus, large Courant numbers leads to unphysical oscillations and hence unstable solutions.

The figures 3.9-3.11 show the profiles of the implicit solution for the same cell Peclet number and Courant numbers of figures 3.3-3.5. These implicit methods are all unconditionally stable and hence increasing Courant numbers should influence the results only slightly. One can observe that figure 3.9 produces the same result that of figure 3.3 which is expected as N_c is small and explicit methods has no problem of stability in this case.

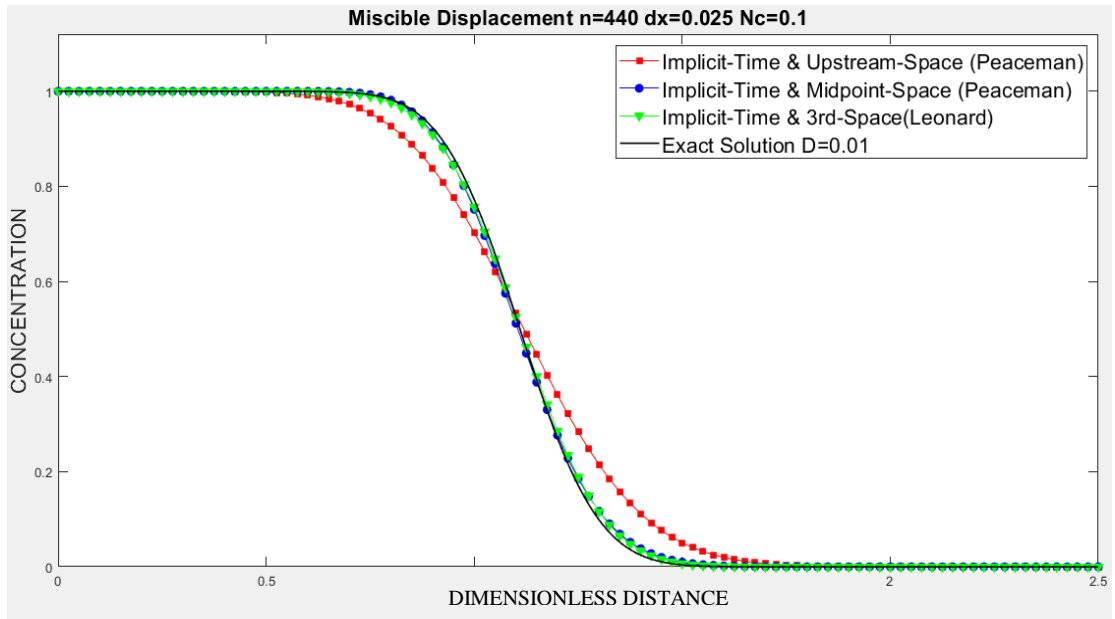


Figure 3.9: Improved method $n=440$ $dx=0.025$ $Nc=0.1$ (Implicit).

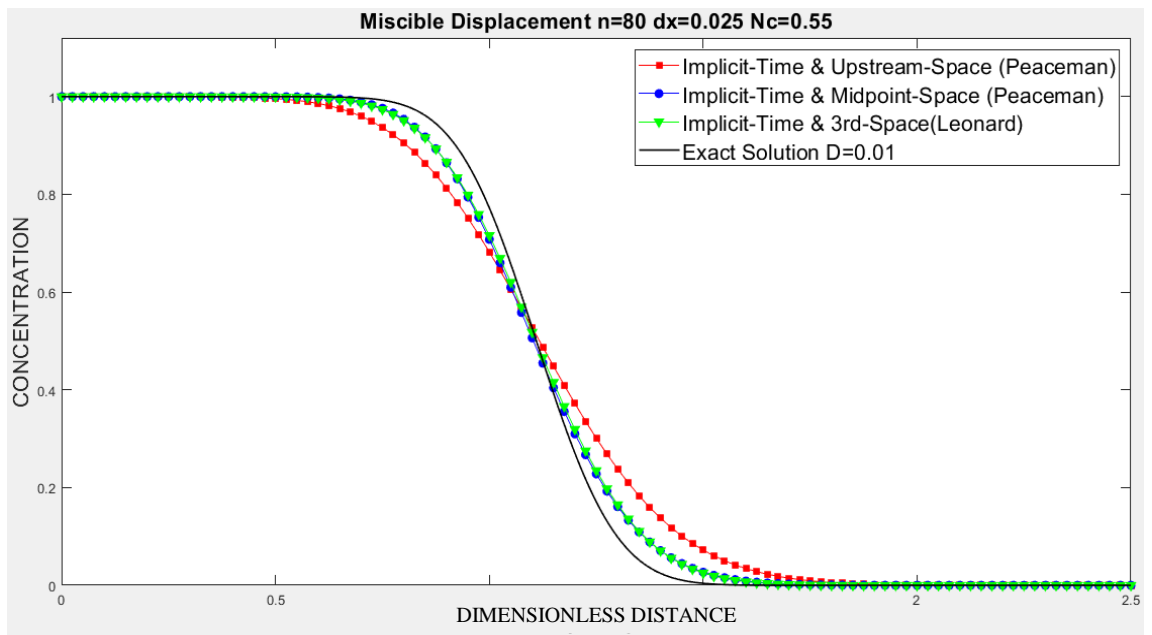


Figure 3.10: Improved method $n=80$ $dx=0.025$ $Nc=0.55$ (Implicit).

Figures 3.9, 3.10 and 3.11 show that the all the implicit methods being unconditionally stable exhibit smooth profiles separating away from the analytical solution according to the numerical dispersions they contain. The largest numerical dispersion is observed in the first order spatial upstream method as expected.

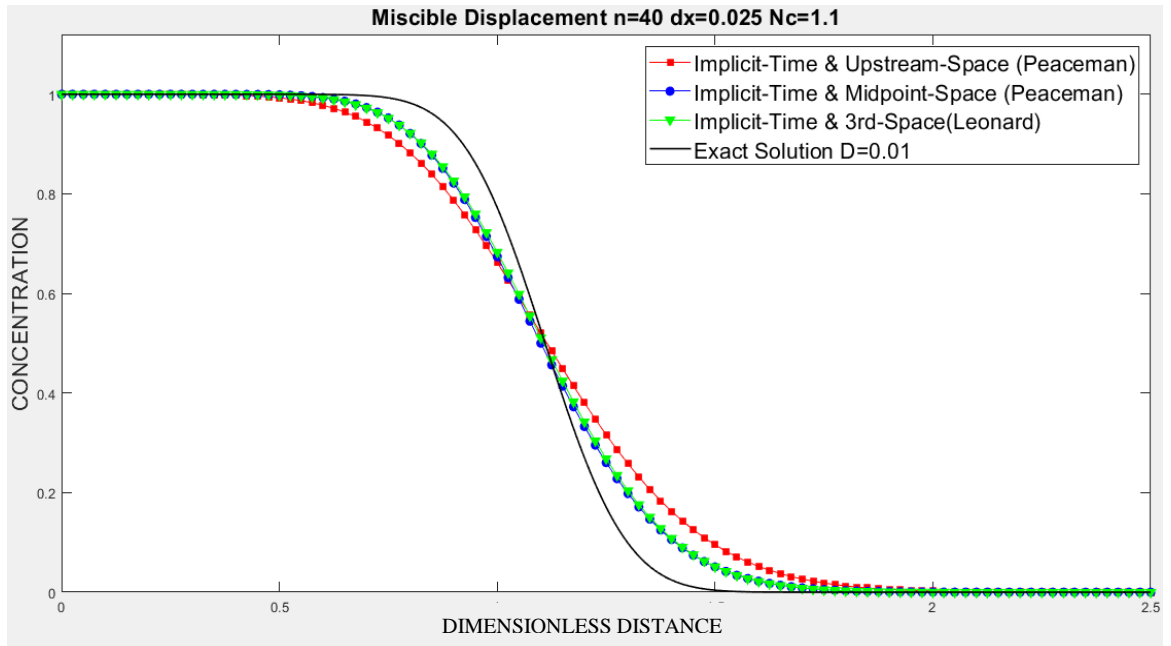


Figure 3.11: Improved method $n=40$ $dx=0.025$ $Nc=1.1$ (Implicit).

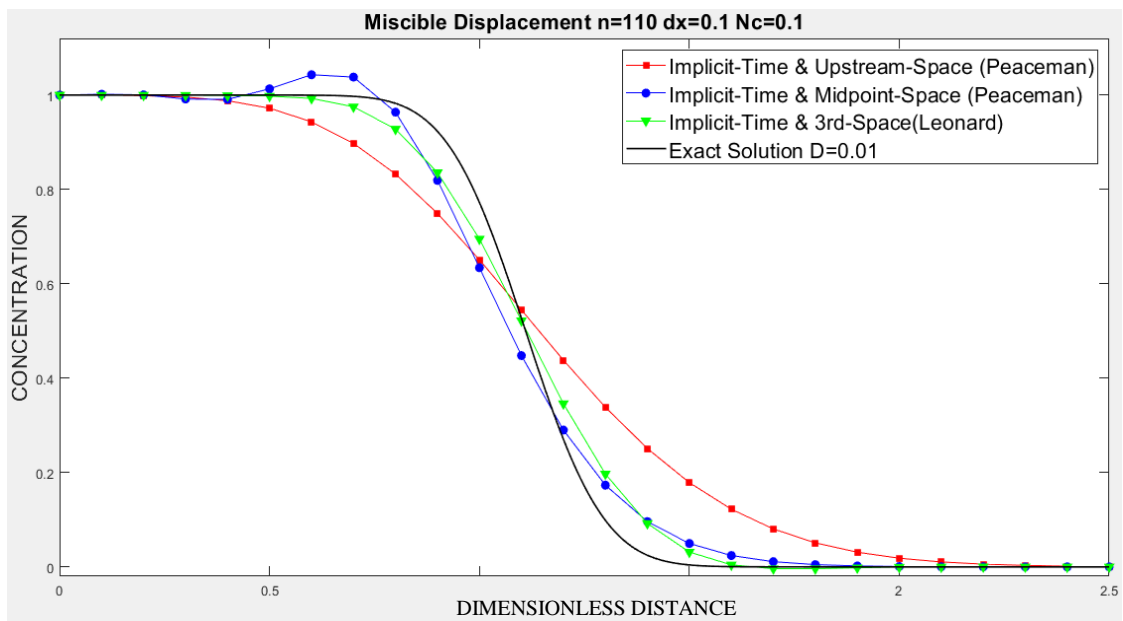


Figure 3.12: Improved method $n=110$ $dx=0.1$ $Nc=0.1$ (Implicit).

The midpoint space discretized method yields a hump-which violates entropy condition- close to the actual front, however this makes the midpoint front exhibiting a sharper dispersive profile in figure 3.12.

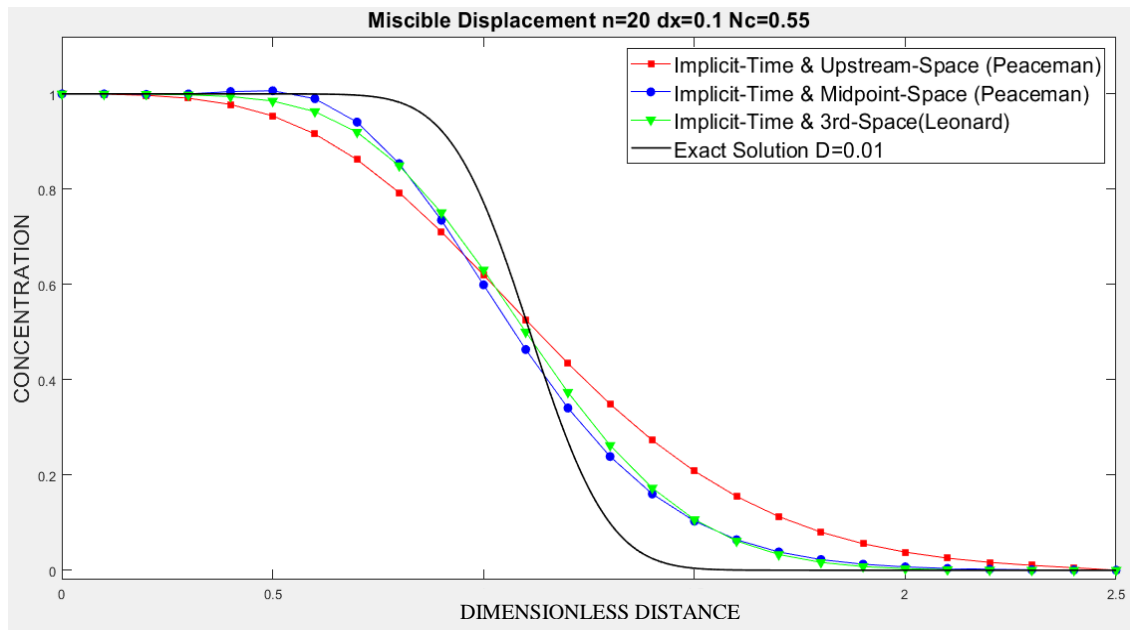


Figure 3.13: Improved method $n=20$ $dx=0.1$ $Nc=0.55$ (Implicit).

When the Courant number is increased the unphysical hump disappears due to larger numerical dispersion involved and the method shows a relatively sharper front compared to third order discretization making a false impression of as if having a smaller numerical dispersion as in figure 3.13 and 3.14.

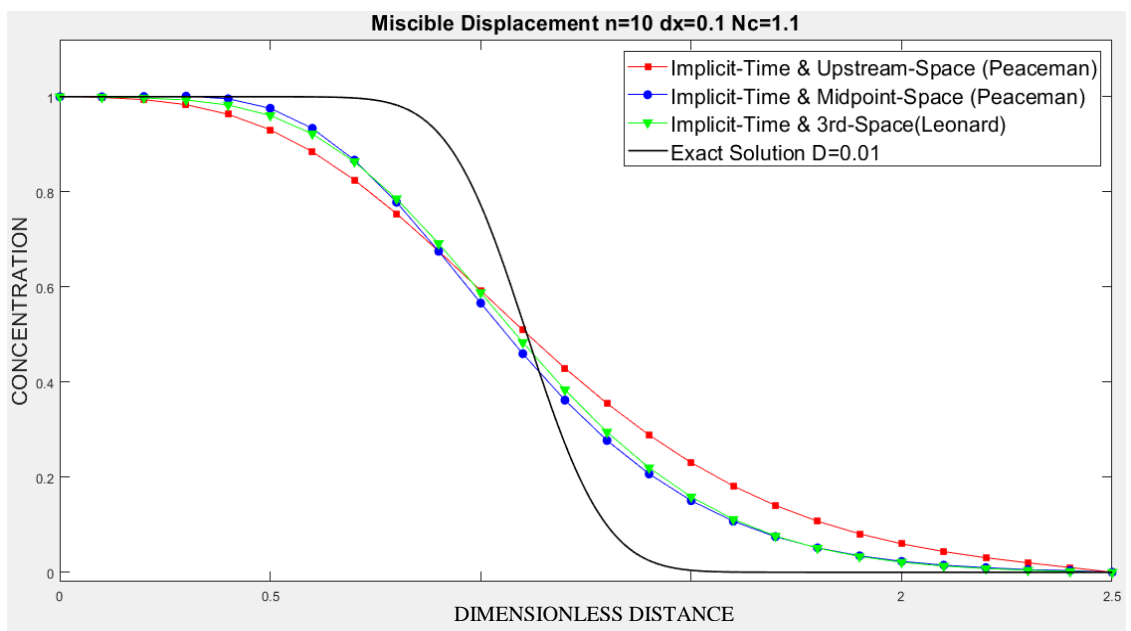


Figure 3.14: Improved method $n=10$ $dx=0.1$ $Nc=1.1$ (Implicit).

3.2.3 In Depth Investigation of Semi-implicit schemes

As the Crank-Nicolson method is of second order accurate in time discretization we have also investigated the influence of this improvement on the elementary and high

order discretization schemes. The following figures of 3.15-3.17 investigate the role of the Courant number for a fixed small cell Peclet number, Pe_{cl} .

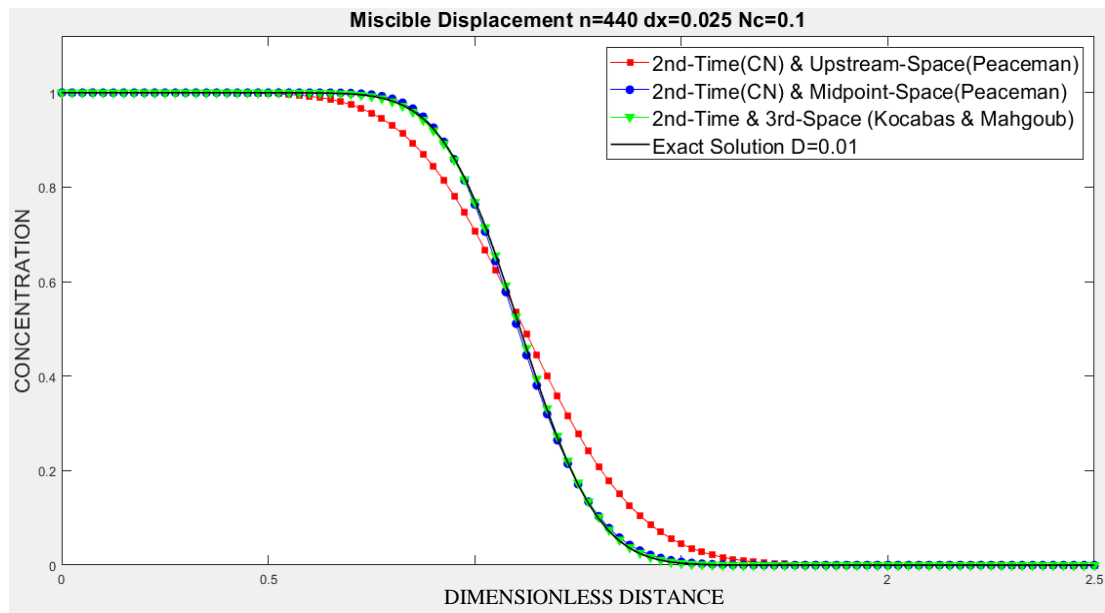


Figure 3.15: Improved method $n=440$ $dx=0.025$ $Nc=0.1$ (C-N).

For small spatial interval (figure 3.15, 3.16 and 3.17), both higher order spatial accuracy methods coincide the analytical solution even large time step or high Courant number but first order upstream method has still numerical dispersion.

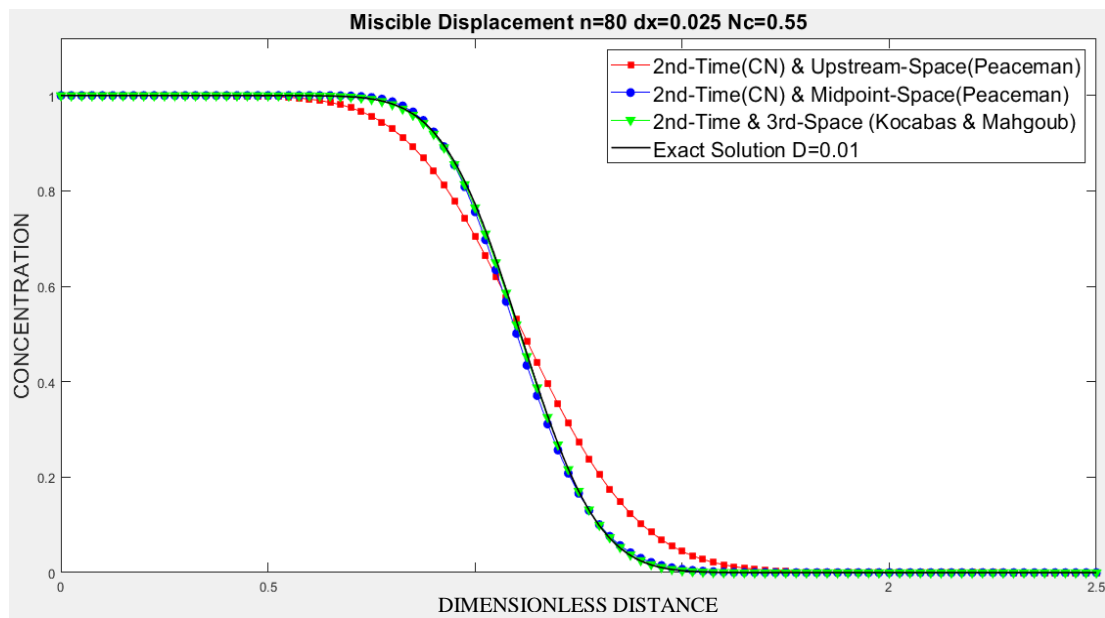


Figure 3.16: Improved method $n=80$ $dx=0.025$ $Nc=0.55$ (C-N).

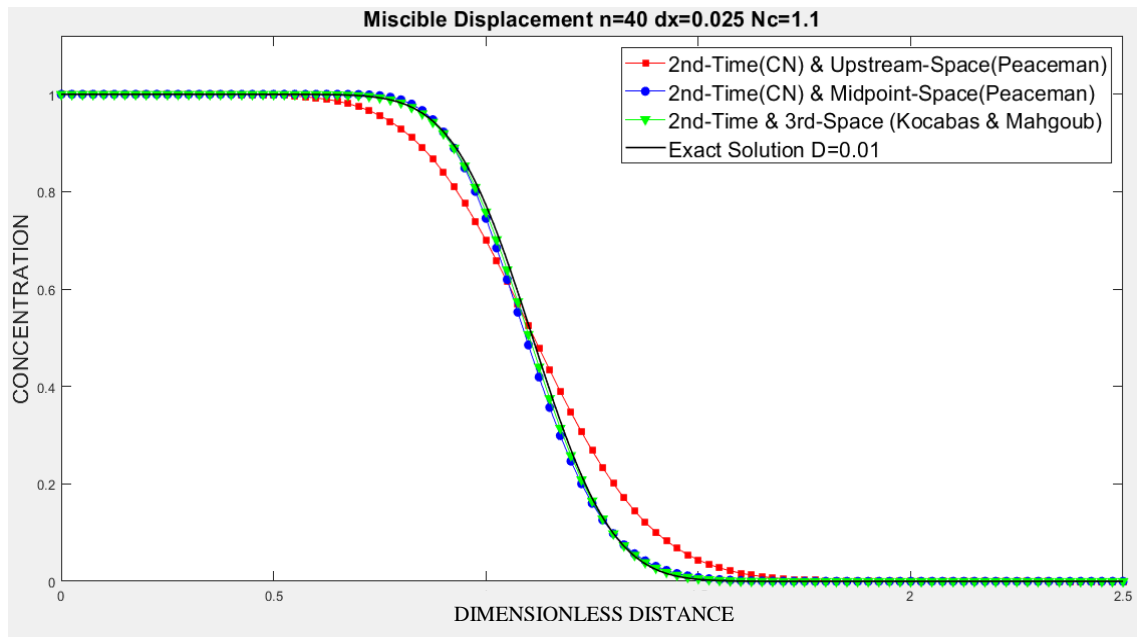


Figure 3.17: Improved method $n=40$ $dx=0.025$ $Nc=1.1$ (C-N).

First order upstream method has larger numerical dispersion for large space interval compared to small space interval. As time step increases, numerical dispersion of upstream method increases step by step.

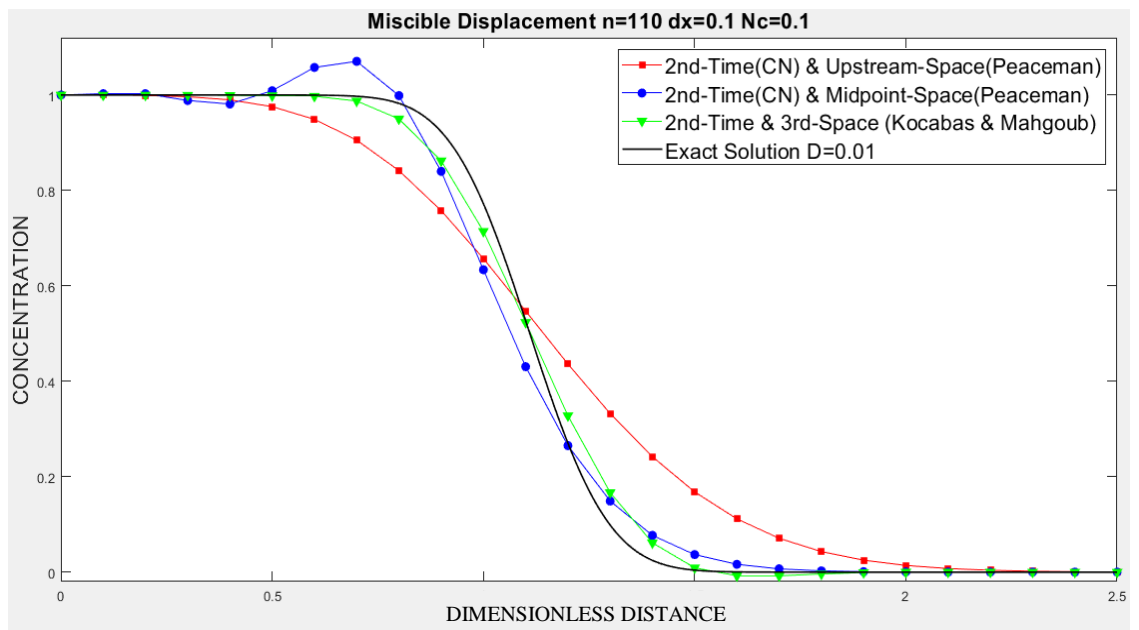


Figure 3.18: Improved method $n=110$ $dx=0.1$ $Nc=0.1$ (C-N).

The figures 3.18-3.20 shows the role of courant number on the profiles for again a fixed but large cell Peclet number.

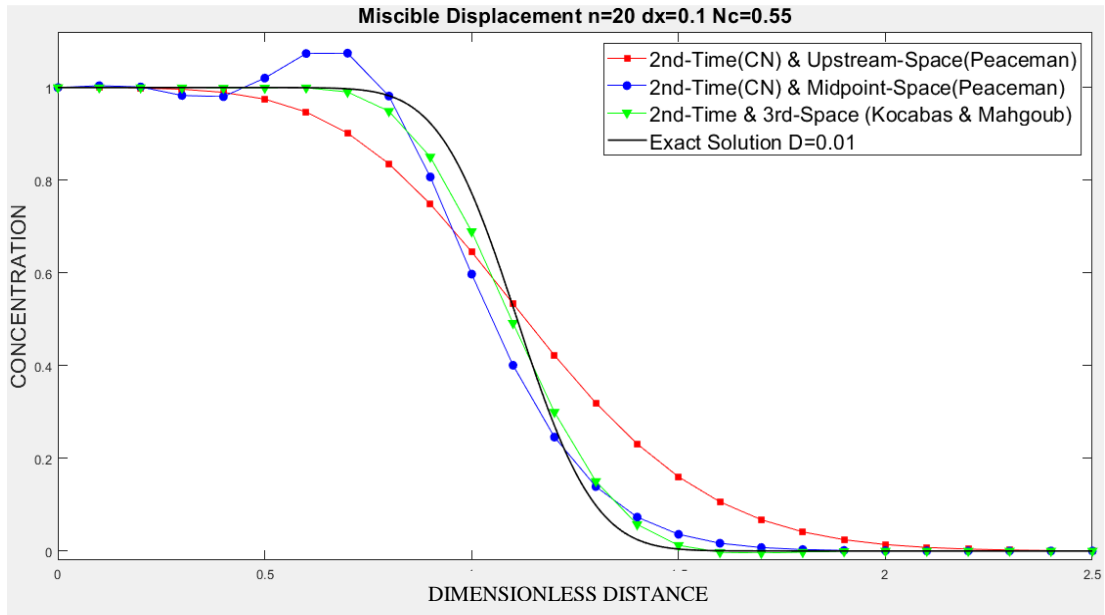


Figure 3.19: Improved method $n=20$ $dx=0.1$ $Nc=0.55$ (C-N).

For large space interval (figure 3.18, 3.19 and 3.20), advantage of third order Leonard technique become prominent. As courant number increases, oscillation of mid-point increases. On the other hand, third order Leonard with Crank-Nicolson (Kocabas and Mahgoub) technique has very small numerical dispersion with nearly non-unphysical oscillation even large time step.

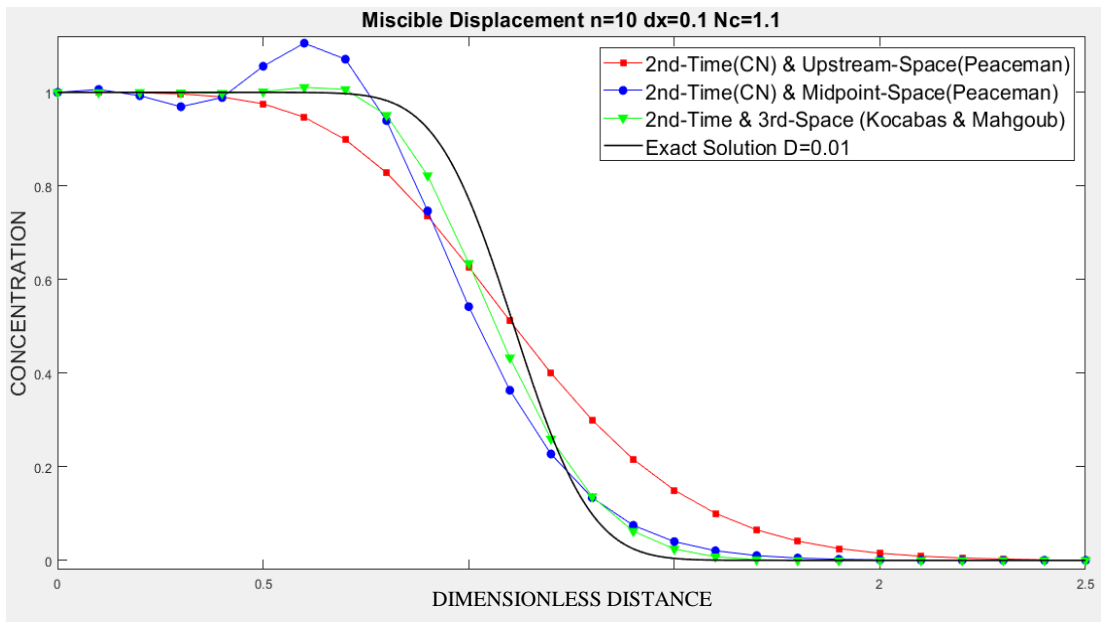


Figure 3.20: Improved method $n=10$ $dx=0.1$ $Nc=1.1$ (C-N).

Results of semi-implicit schemes:

- Upstream scheme is still unconditionally stable but second order time accuracy did not reduce numerical dispersion significantly.

- Mid-point scheme is working fine for small Δx but displacing unphysical oscillations for high Courant numbers and Δx .
- Quick-CN (Kocabas and Margoup) method reduces both the unphysical oscillation of Quick-explicit and the numerical dispersion of Quick-implicit methods. Thus, it yields both stable and highly accurate profiles compared to all previous methods for all ranges.
- For these observations, we hoped that Quick CN method would be successful for simulating convection dominated immiscible displacement.
- Mid-point and Quick have same accuracy for larger diffusion cases in stable region (which corresponds to small Δx and small Courant number).
- Difference of Mid-point and Quick methods becomes quite distinct in case of small dispersion.
- Quick explicit shows almost zero numerical dispersion for small Courant number and hence matches the front profile perfectly, outstanding all other schemes.
- However, when the Δt increases and hence Courant number is increased Quick-explicit becomes totally unstable thus prohibiting the scheme for use in actual simulations which are usually carried out with large time steps.
- Note that despite being unconditionally stable Quick-CN do exhibit unphysical oscillations and fairly large numerical dispersion for high Courant number raised to 1.5.
- This leads to investigation of flux limiters in simulation practices in CFD society.
- Since the main objective of this thesis work is to simulate convection dominated immiscible displacement all simulations were carried out using Quick-CN combined with various flux limiter. Such another suitable flux limiter has resulted in the discovery of flexible flux limiters as a notable outcome of this research.

4. CONVECTIVE DISPERSIVE NATURE OF IMMISCIBLE DISPLACEMENT SIMULATIONS

Peaceman has shown that immiscible displacement saturation equation is in indeed of convective dispersive nature. In fact, immiscible displacement of oil by water assuming incompressible fluids leads to a purely convective transport equation and its analytical solution is known as frontal advance solution developed by Buckley and Leveret.

In order to simulate the frontal advance displacements a number of simulations were carried out and the results are presented in this section.

For all one and two dimensional reservoir simulations (impes simulations and fully Implicit simulations) following input data are used.

Table 4.1: Input data for one and two dimensional simulations.

Array of blocks for 1D	i=25	j=1	k=1
Dimensions of block for 1D	dx=40 ft	dy=100 ft	dz=100 ft
Array of blocks for 2D	i=10	j=10	k=1
Dimensions of block for 2D	dx=100 ft	dy=100 ft	dz=10 ft
Porosity	20%		
Permability	kx=300 mD ky=300 mD		
Viscosity of water	1 cp		
Viscosity of oil	1 cp		
Time increment	2.5 days		
Total simulation time	tt=1500 days		
Irreducible water saturation	0.363		
Residual oil saturation	0.205		
Initial pressure	5000 psia		

In order to avoid nonunique solutions to an ill posed problem, at least one grid block pressure have to be fixed according during process of solving the governing equations numerically [7]. Therefore, the first grid block's location (1,1) and pressure was fixed at 5000 psia. Water is assumed to be injected at a rate of 65 barrel/day in the first block. Owing to incompressible nature of flowing fluids the production rate must also be fixed as 65 bbl/d at the production blocks, namely the

last block in 1D coordinate of (1,25) and in 2D coordinate of (25,25). Note also that capillary pressure is neglected included in development of the governing equations.

Figure 4.1 shows artificially generated water wet relative permeability curves in which initial water saturation and residual oil saturation data were borrowed from Ertekin et al. [7] and permeability functions are borrowed from Ahmad [26].

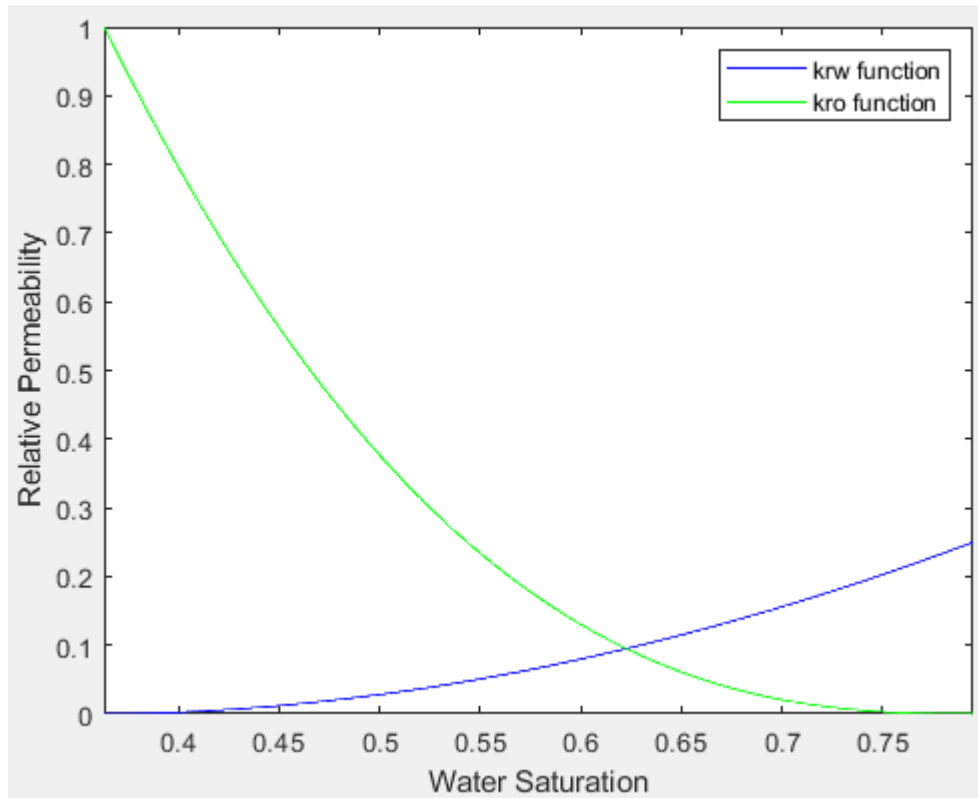


Figure 4.1: Relative permeability curves.

The relative permeability functions in figure 4.1 leads to the following fractional flow curve in figure 4.2. Welge graphical technique is used to determine the flood front water saturation of Buckley Leveret solution as in also figure 4.2.

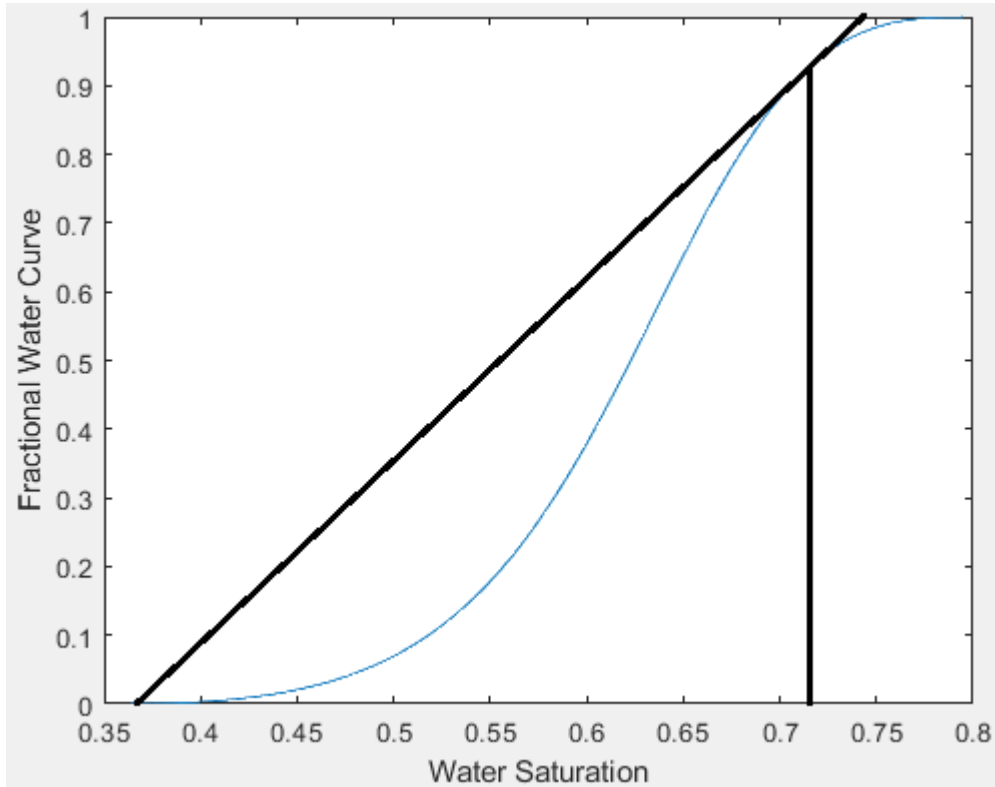


Figure 4.2: Determination of flood front water saturation (0.7131).

The following frontal advance solution (Buckley-Leverett solution) is used to determine plot saturation profiles for an immiscible incompressible displacement of oil by water.

$$x_{sw} = \left(\frac{5.615i_w t}{\phi A} \right) \left(\frac{df_w}{dS_w} \right) \quad (4.1)$$

In equation 4.1, i_w is injected water flow rate, t is total simulation time, ϕ is porosity, A is cross sectional area, f_w is fraction of water and x_{sw} is location of water saturation.

Note that in order to determine the location of any saturation behind the front you need only two parameters total flow rate and the derivative of the fractional flow equation for that saturation.

Almost all commercial and propriety simulators have employed the first order upstream space discretization and implicit time treatment owing to its simplicity, and unconditional stability. The numerical dispersion in this approach was tried to be minimized by using small spatial grids but this was almost impossible due to the

necessity of having large grid size to cover vast distances involved in petroleum reservoir simulations.

A second and more subtle source of error in immiscible displacement is due to the difficulty of predicting the grid block interface saturations. Frontal advance equation is stating that the flow in and out of a block is solely dependent on the end point saturations whereas in all simulation studies only average block saturations are calculated and known. Therefore, basing the face saturations on the average block saturations inherently involves significant errors on the estimation of fluid fluxes. For instance let's assume that at a time step the flood front has reached two third length of a certain block and still away from the outlet face. Then in reality the displacing fluid flux out of this block must be zero, however, as the simulators consider the average block saturation and this saturation may well be above irreducible water saturation then simulated flux out of this flux will be greater than zero. This is a major problem to be considered as pointed by Crotti [27, 28] for the first time.

In order to validate our Matlab codes of first order and third order schemes we have used with Buckley-Leverett analytical solution as a benchmark in the following section. Then, we have investigated various approaches of employing limiter functions in the third order schemes to obtain non-oscillation results for higher Courant numbers.

4.1 In depth Investigation of IMPES First Order Space and Time Solutions

In petroleum engineering literature, IMPES simulator a simulator that treats pressures implicitly saturations explicitly. Therefore, the simulation process consists of two stages.

4.1.1 First order pressure solution

The general form of first order (FO) pressure solutions are shown by equation 4.2 [4]:

$$\nabla \cdot (m_w + m_o) \nabla p + q = 0 \quad (4.2)$$

Where m_w , m_o , p and q corresponds to mobility of water, mobility of oil, pressure differences and source term respectively. The source term (q) represents either

injection or production rate. While the injection rate assumes a positive value, production rate is assumed to be negative.

Using a first order upstream distretization equation 4.2 may be written as equation 4.3 for the block i in a horizontal linear displacement.

$$\frac{m_{tw_i} \frac{p_i - p_{i-1}}{\Delta x} - m_{te_i} \frac{p_{i+1} - p_i}{\Delta x}}{\Delta x} + q_i = 0 \quad (4.3)$$

Where m_{tw_i} means total mobility at west face (left) of (i)th grid block. m_{te_i} means total mobility at east (right) face of (i)th grid block.

Assuming the right face phase saturations are represented by the average phase saturation of the left block (i-1)th block, the mobility can be written as equation 4.4.

$$m_{tw_i} = -0.001127 \left[\frac{k_x \times k_{rw}(S_{w_{i-1}})}{\mu_w} + \frac{k_x \times k_{ro}(S_{w_{i-1}})}{\mu_o} \right] \quad (4.4)$$

Similarly, east(right face saturations) are assumed and the corresponding mobility becomes:

$$m_{te_i} = -0.001127 \left[\frac{k_x \times k_{rw}(S_{w_i})}{\mu_w} + \frac{k_x \times k_{ro}(S_{w_i})}{\mu_o} \right] \quad (4.5)$$

Such saturation representations, where only one grid block water saturation is used, leads to first order upstream relative permeability weighting solution [7]. A major advantage of using upstream relative permeability values is to prevent excessive accumulation in the grid block under consideration, which violates entropy generation leads to unphysical oscillations.

Using the above approach, the system discretized equations for a simple five block system can be written as follows in equations 4.6-4.10.

- ✓ Pressure equation for first grid block;

$$\frac{0 - m_{te_1} \frac{p_2 - p_1}{\Delta x}}{\Delta x} + q_{1,inj} = 0 \quad (4.6)$$

- ✓ Pressure equation for second grid block;

$$\frac{m_{tw_2} \frac{p_2 - p_1}{\Delta x} - m_{te_2} \frac{p_3 - p_2}{\Delta x}}{\Delta x} + 0 = 0 \quad (4.7)$$

- ✓ Pressure equation for third grid block;

$$\frac{m_{tw_3} \frac{p_3 - p_2}{\Delta x} - m_{te_3} \frac{p_4 - p_3}{\Delta x}}{\Delta x} + 0 = 0 \quad (4.8)$$

- ✓ Pressure equation for fourth grid block;

$$\frac{m_{tw_4} \frac{p_4 - p_3}{\Delta x} - m_{te_4} \frac{p_5 - p_4}{\Delta x}}{\Delta x} + 0 = 0 \quad (4.9)$$

- ✓ Pressure equation for fifth grid block;

$$\frac{m_{tw_5} \frac{p_5 - p_4}{\Delta x} - 0}{\Delta x} + q_{5,prd} = 0 \quad (4.10)$$

As the saturation values are assumed to be known from the previous time steps, the unknown pressure values can be easily solved using simple matrix solvers.

4.1.2 First order saturation solution

The second stage of the IMPES method is the computation of saturations for the new time step. As pressure values have been already determined in the first stage, therefore, velocity as well as saturation values of each grid block can be determined using the following saturation equation.

$$\nabla \cdot (u_t \times f_w) + q = \phi \frac{\partial S_w}{\partial t} \quad (4.11)$$

Where u_t and f_w are total Darcy velocity and fractional water flow respectively [4].

$$u_t = (m_w + m_o) \nabla p \quad (4.12)$$

As the pressure values for each grid block are known, the total velocity values can be calculated by substituting equation 4.12 and 4.13 into equation 4.11.

$$f_w = \frac{m_w}{m_w + m_o} \quad (4.13)$$

$$\nabla \cdot \left((m_w + m_o) \nabla p \times \frac{m_w}{m_w + m_o} \right) + q = \phi \frac{\partial S_w}{\partial t} \quad (4.14)$$

Equation 4.13 can be simplified as:

$$\nabla \cdot (m_w \nabla p) + q = \phi \frac{\partial S_w}{\partial t} \quad (4.15)$$

Discretizing equation 4.15 one obtains:

$$S_w^{n+1} = S_w^n + \left[\frac{u_w - u_e}{\Delta x} + q \right] \times \frac{5.614583 \times \Delta t}{\phi} \quad (4.16)$$

New time step water saturation of each grid block can be calculated using equation 4.16.

$$u_w = -0.001127 \frac{k_x \times k_{rw}(S_{w_{i-1}})}{\mu_w} \times \frac{P_i - P_{i-1}}{\Delta x} \quad (4.17)$$

It is important note that; in equation 4.16 and 4.17, relative permeability of water is function of water saturation only.

$$u_e = -0.001127 \frac{k_x \times k_{rw}(S_{w_i})}{\mu_w} \times \frac{P_{i+1} - P_i}{\Delta x} \quad (4.18)$$

The two dimensional simulations using IMPES of first order space and time are presented in APPENDIX B for future referencing.

Figure 4.3 compares of 1D Buckley-Leverett analytical solution and our 1D first order Matlab code results.

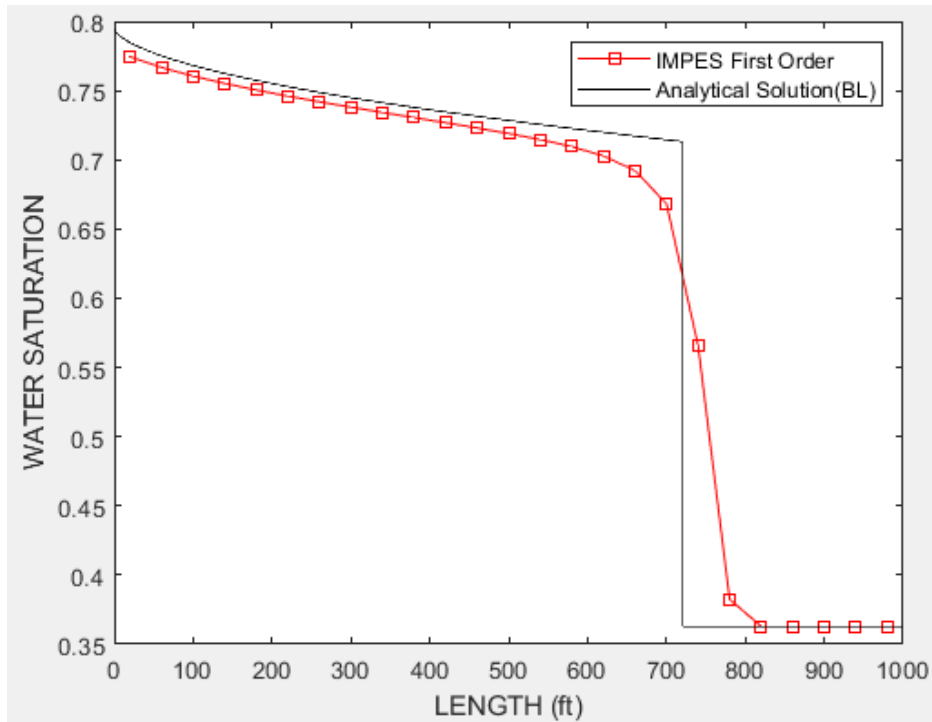


Figure 4.3 : Impes first order Matlab result.

A major advantage of first order upstream differencing is its ability to dampen the unphysical oscillations due to its large magnitude negative feedback sensitivity. However, it is greatly limited by the stability conditions which require small time steps and large Δx values. Since the large Δx values lead to large numerical dispersion, this apparently stable (smeared nonphysical oscillations) techniques suffers from large number of time steps and large numerical dispersion. An interesting observation we have made is rendered in the following figure 4.4 for which we have selected a large Δx . As Δx grows the negative feedback sensitivity decreases and hence the solution becomes more prone to oscillations. Apparent in Fig. 4.4 is the significant numerical dispersion in the IMPES numerical solution.

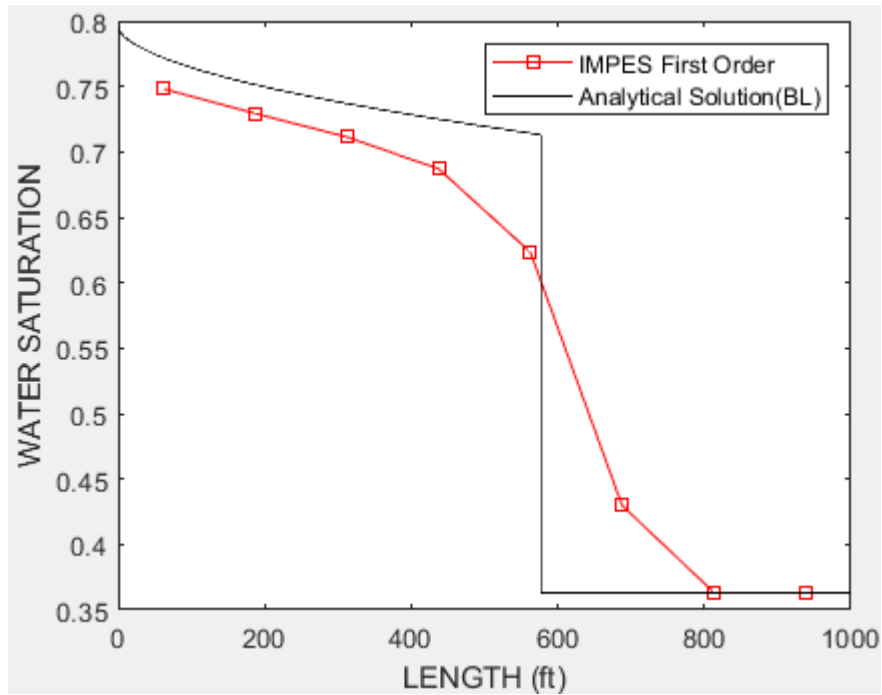


Figure 4.4: First order method for large Δx .

Such an oscillation can be observed at an intermediate simulation time as in figure 4.5. However, as the simulation continues for greater times then the numerical dispersion overcomes the oscillation but shows a larger dispersion of the front as in figure 4.6.

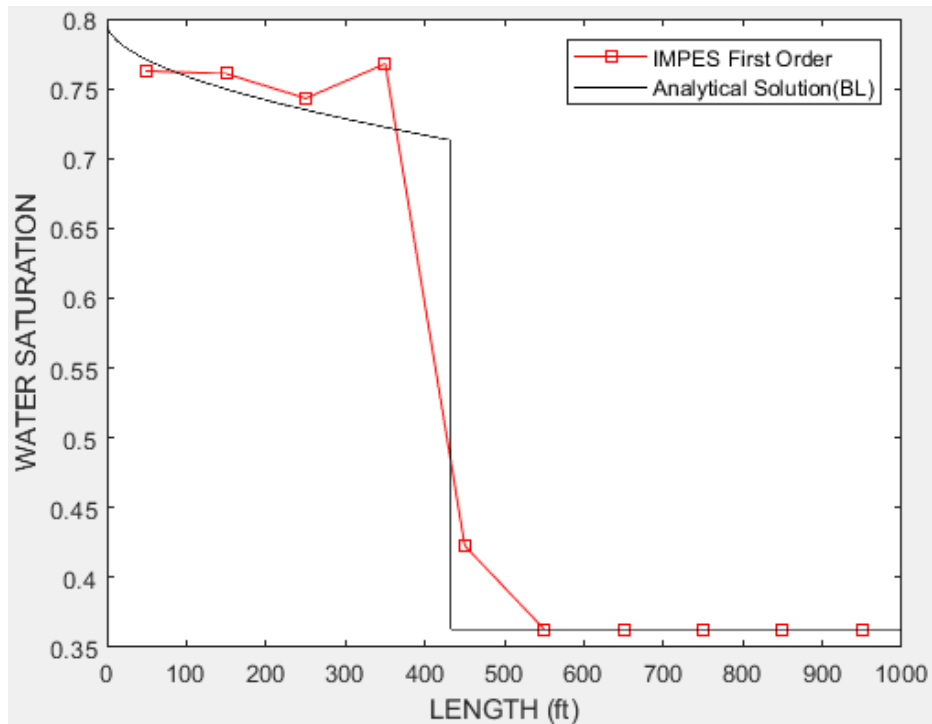


Figure 4.5: First order method for intermediate simulation time.

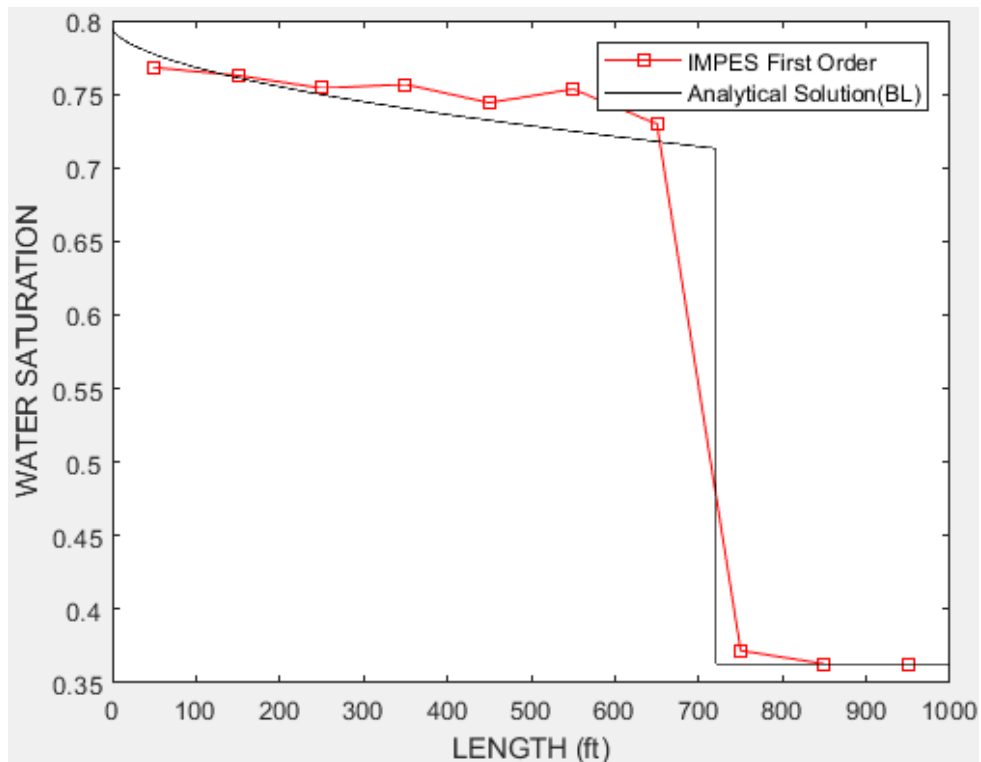


Figure 4.6: First order method for intermediate simulation time.

Figure 4.7 shows the first order IMPES solution obtained using the 2D IMPES Matlab code. Chen [24] mentions the disadvantage of this IMPES method suffering from grid orientation effect in two-dimensional simulations.

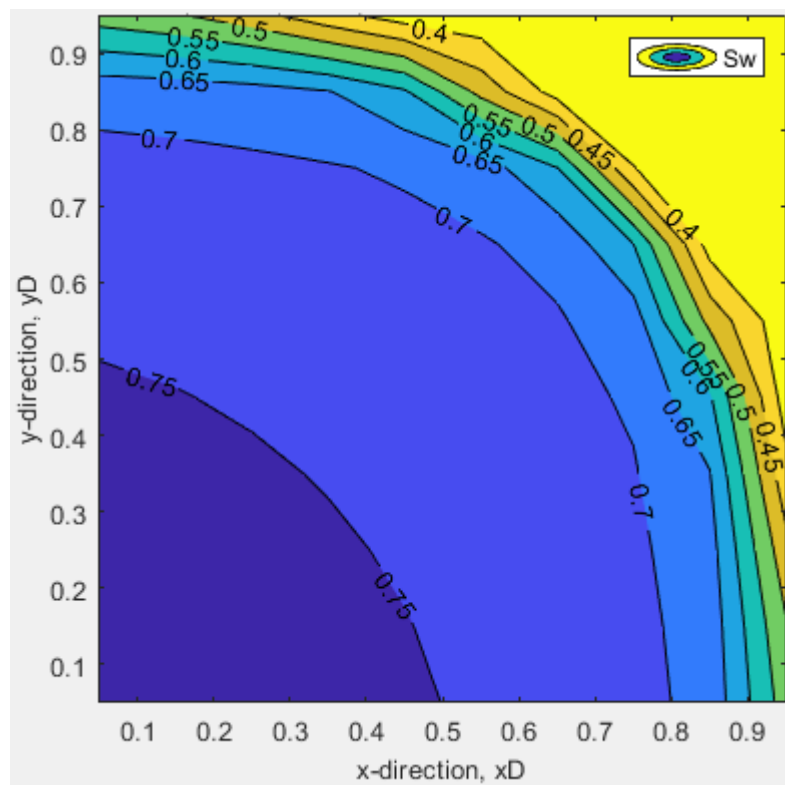


Figure 4.7 : 2D Impes first order Matlab result.

4.2 Impes Second Order (TVD) Space and Time Solutions

Higher order differencing method were investigated to mitigate the large numerical dispersion in the first order differencing solutions. Therefore, a second order upstream method has been developed to reduce the numerical dispersion but this even order methods suffer more in unphysical oscillations as pointed out by Leonard. Nevertheless, researchers applied this method combined with a technique called as TVD (total variation diminishing) technique. Impes second order method consists of two stages solution which are pressure and saturation steps. In both steps, relative permeability values will be calculated as second order spatial accuracy. In saturation solution step, saturation values will be calculated as second order time accuracy.

4.2.1 TVD pressure solution

Recall equation 4.3 which describes solutions of pressure (equation 4.19).

$$\frac{m_{twi} \frac{p_i - p_{i-1}}{\Delta x} - m_{tei} \frac{p_{i+1} - p_i}{\Delta x}}{\Delta x} + q_i = 0 \quad (4.19)$$

Application of the second order Total Variation Diminishing (TVD) method [24] to equation 4.19 can be explained as follows:

The main objective of this method is to reduce the numerical dispersion which is mainly cause by the fast propagation of the grid block average saturations to the grid faces. In ther words in the upstream method we assume the west face saturation of the grid block i is equated to the average saturation of the block (i-1). Similarly the east face of saturation of the grid block I is equated to average saturation of i. Thus the saturations are allowed to propagate faster leading to large numerical dispersion. In order to alleviate the numerical dispersion, TVD is applied as follows:

Let's define the differential of saturation as the difference between saturations of (i-1) and (i-2) grid blocks as:

$$dv_w = S_{wi-1} - S_{wi-2} \quad (4.20)$$

Similarly, for grid blocks of (i) and (i-1) may be defined as:

$$dw_w = S_{w_i} - S_{w_{i-1}} \quad (4.21)$$

Based on the two saturation differentials a flux limiter is defined as follows:

$$\Delta i_w = \text{sign}(dv_w) \times \max(0, \min[|dv_w|, dw_w \times \text{sign}(dv_w)]) \quad (4.22)$$

Equation 4.22 describes limiter function of the flux for the west face saturation term. The west face saturation is now defined as the (i-1) block saturation less the half of the Δi_w , note that Δi_w subtraction leads to a smaller west face saturation than that is obtained by propagating the (i-1) average saturation. It is this limiter that reduces the numerical dispersion and therefore it is also called as anti-diffusive term [29] employment/addition.

Using this algorithm allows us to represent, the west face mobility term with a second order spatial accuracy as follows:

$$m_{tw_i} = -0.001127 \left[\frac{k_x \times k_{rw}(S_{w_{i-1}} + 0.5 \times \Delta i_w)}{\mu_w} + \frac{k_x \times k_{ro}(S_{w_{i-1}} + 0.5 \times \Delta i_w)}{\mu_o} \right] \quad (4.23)$$

Similarly, equations 4.24 through 4.27 represent the development of the second order TVD scheme for the east face of the block (i).

$$dv_e = S_{w_i} - S_{w_{i-1}} \quad (4.24)$$

$$dw_e = S_{w_{i+1}} - S_{w_i} \quad (4.25)$$

$$\Delta i_e = \text{sign}(dv_e) \times \max(0, \min[|dv_e|, dw_e \times \text{sign}(dv_e)]) \quad (4.26)$$

$$m_{te_i} = -0.001127 \left[\frac{k_x \times k_{rw}(S_{w_i} + 0.5 \times \Delta i_e)}{\mu_w} + \frac{k_x \times k_{ro}(S_{w_i} + 0.5 \times \Delta i_e)}{\mu_o} \right] \quad (4.27)$$

Pressure solutions of second order TVD IMPES schemes are quite analogous to pressure solutions of first order IMPES.

4.2.2 TVD saturation solution

TVD saturation equation is solved by using two steps Runge Kutta algorithm. First step of Runge Kutta algorithm is S1 and second one is S2.

$$S1_w^n = S_w^n + FO \quad (4.28)$$

Equation 4.29 means first order time term (FO). However, it is important note that, FO time term in equation 4.28 has second order spatial accuracy.

$$FO = \left[\frac{u_w - u_e}{\Delta x} + q \right] \times \frac{5.614583 \times \Delta t}{\phi} \quad (4.29)$$

In equation 4.29, u_w and u_e values are calculated by equation 4.30 and 4.31 respectively.

$$u_w = -0.001127 \frac{k_x \times k_{rw}(S_{w_{i-1}} + 0.5 \times \Delta i_w)}{\mu_w} \times \frac{P_i - P_{i-1}}{\Delta x} \quad (4.30)$$

Again u_w and u_e values have second order spatial accuracy.

$$u_e = -0.001127 \frac{k_x \times k_{rw}(S_{w_i} + 0.5 \times \Delta i_e)}{\mu_w} \times \frac{P_{i+1} - P_i}{\Delta x} \quad (4.31)$$

Second order TVD saturation solutions are shown by equation 4.32.

$$S_w^{t+1} = S_w^t + 0.5 \times FO + 0.5 \times SO \quad (4.32)$$

In equation 4.32, calculations of second order (SO) time term very similar to FO time term. Equation 4.33, 4.34 and 4.35 describes SO time term. Again, it is important not that SO time term has also second order spatial accuracy.

$$SO = \left[\frac{u_{w1} - u_{e1}}{\Delta x} + q \right] \times \frac{5.614583 \times \Delta t}{\phi} \quad (4.33)$$

$$u_{w1} = -0.001127 \frac{k_x \times k_{rw}(S1_{w_{i-1}} + 0.5 \times \Delta i_w)}{\mu_w} \times \frac{P_i - P_{i-1}}{\Delta x} \quad (4.34)$$

$$u_{e1} = -0.001127 \frac{k_x \times kr_w(S1_{wi} + 0.5 \times \Delta i_e)}{\mu_w} \times \frac{P_{i+1} - P_i}{\Delta x} \quad (4.35)$$

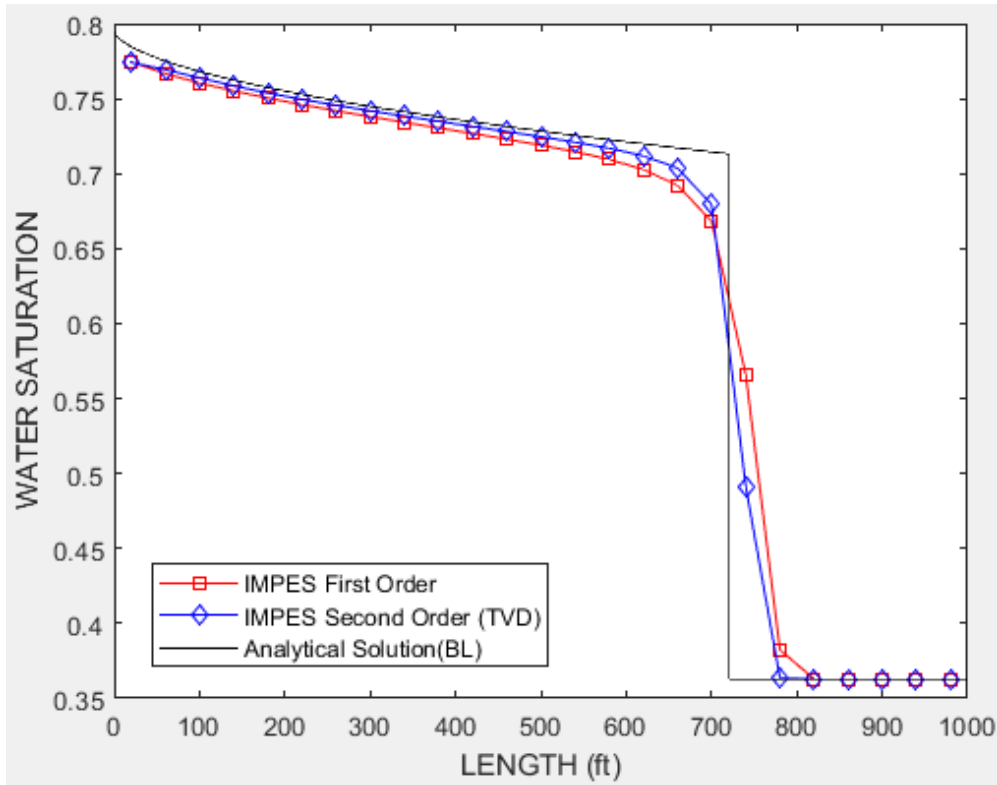


Figure 4.8 : Impes second order (TVD) result.

Figures 4.8 and 4.9 are IMPES TVD method with small and large Δx respectively. Figure 4.9 shows that adding a TVD algorithm reduces the numerical dispersion.

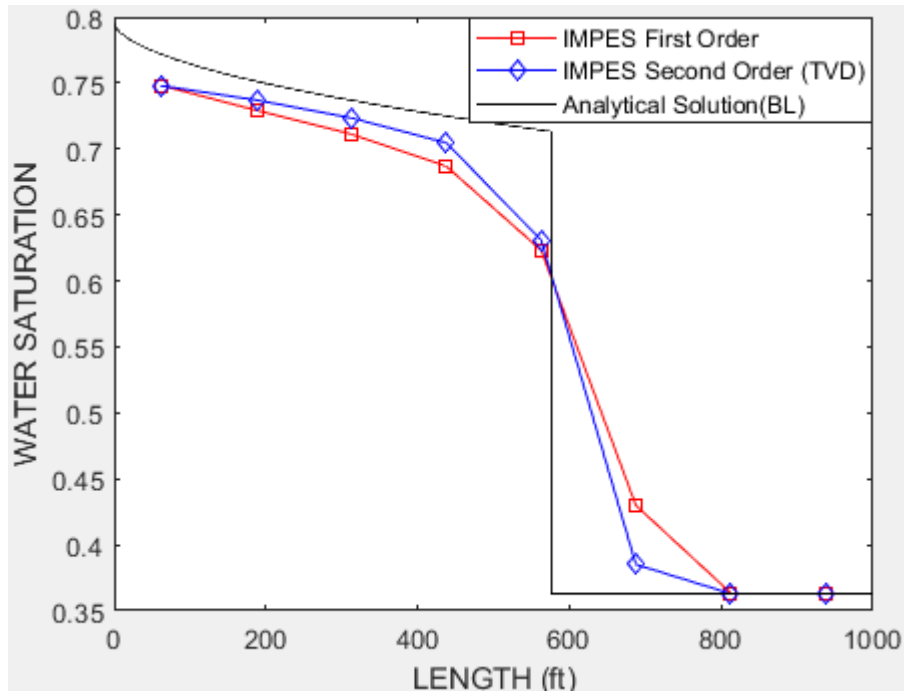


Figure 4.9: IMPES TVD with large Δx .

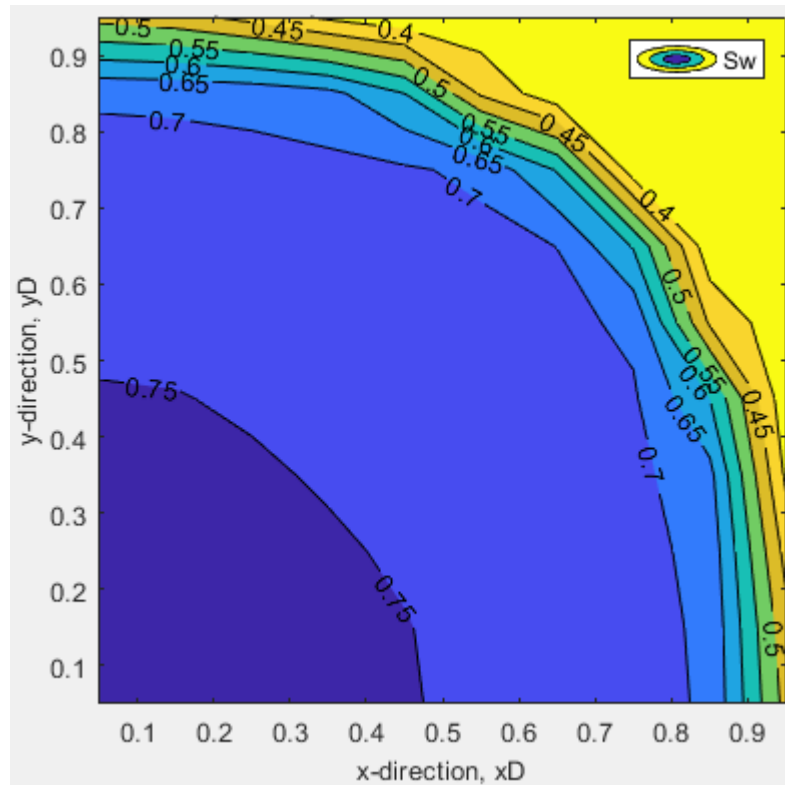


Figure 4.10 : 2D Impes second order (TVD) Matlab result.

Figure 4.10 shows results of 2D simulation for second order (TVD) displaying two dimensional dispersion in colours.

4.3 Impes Third Order (TVD- Leonard) Space and Time Solutions

The third order Leonard method is known to yield much smaller numerical dispersion than first order method and has greater ability to dampen introduced oscillations than second order (in fact all even high order) methods. As the absolute value of feedback sensitivity of Leonard method slightly smaller than that of first order upstream method it is more prone to oscillations than first order method. Therefore the researchers wanted to take advantage of Leonard method combined with TVD algorithm.

Note that Leonard third order differencing is a specific TVD algorithm itself. Sweby has noticed this feature and then formalized the stability region for flux limiters as follows. Wolcott [11] et al has also noticed this feature and they pointed out that the flux limiters can be applied to any of the variables including saturations, velocities, mobilities and fractional flow.

For any variable, the general flux limiter can be expressed as:

$$f_{i+1/2} = f_i + 0.5 \times \phi_{i+1/2} \times (f_{i+1} - f_i) \quad (4.36a)$$

Where ϕ is the flux limiter of flux ratio, r , is given by equation 4.36b:

$$r_{i+1/2} = \frac{f_i - f_{i-1}}{f_{i+1} - f_i} \quad (4.36b)$$

Sweby [30] has noticed that the stability region for the flux limiter as a function of flux ratio can be derived as in figure 4.11.

It is imported note that in 1984, Harten [31] has introduced the Total Variation Diminishing (TVD) scheme which aims eliminating the unphysical oscillations that violate the entropy condition. In the same year, Sweby has published a classical work which specified the stability region for the TVD schemes.

In equation 4.36a; if flux limiter (anti-difusive term) is constant as $(r+2)/3$, red straight line will be obtained in figure 4.11. The anti-difusive term of Leonard's method may be expressed as equation 4.37:

$$f_{i+1/2} = f_i + 0.5 \times \frac{r+2}{3} \times (f_{i+1} - f_i) \quad (4.37)$$

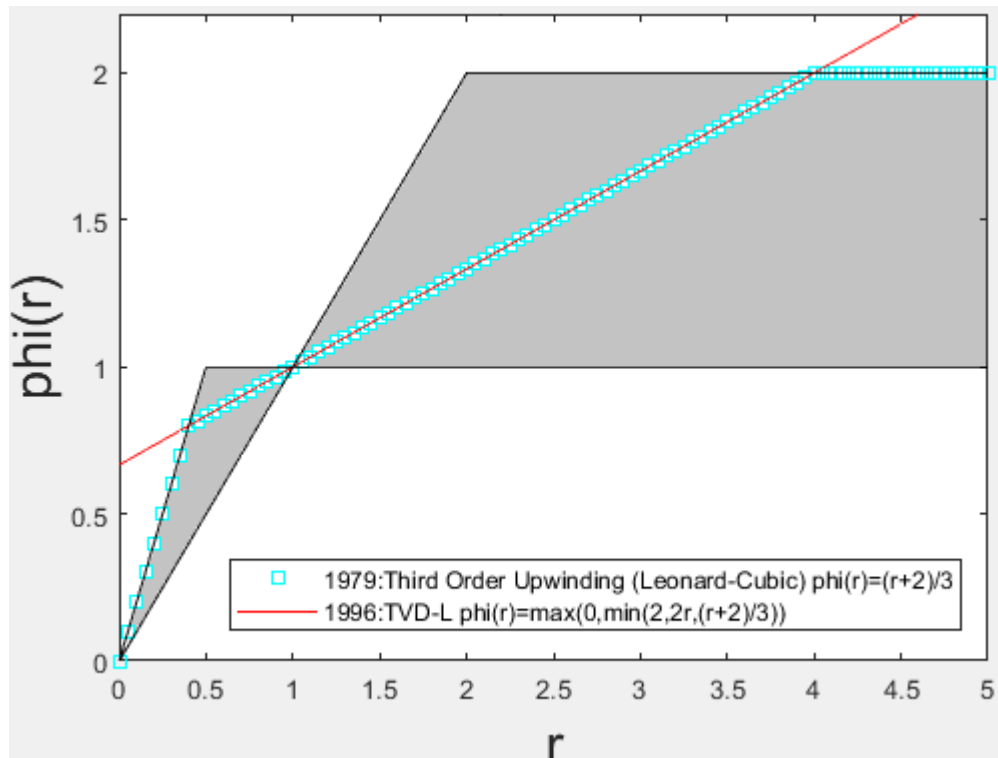


Figure 4.11: TVD region.

Note that in figure 4.11 Leonard's flux limiter (Leonard scheme expressed as a flux limiter) is shown as a red straight line for which a large range of flux ratios would fall into the shaded stability region. Any limiter which is in this region is at least second order accurate; if it falls on the Leonard line, it is exactly third order accurate.

In order to take advantage of this stability region, the Leonard flux limiter can be modified as needed when it falls outside the stability region. Therefore, the TVD method can also be successfully applied to the Leonard scheme as in the following section.

4.3.1 TVD- Leonard pressure solution

Recall equation 4.2 that describes solutions of pressure (equation 4.38).

$$\frac{m_{twi} \frac{p_i - p_{i-1}}{\Delta x} - m_{tei} \frac{p_{i+1} - p_i}{\Delta x}}{\Delta x} + q_i = 0 \quad (4.38)$$

Implementing third order TVD-Leonard scheme in IMPES method [17] [11], represents west and east side total mobility terms with a third order spatial accuracy. In order to calculate the west side total mobility term of a grid block; in addition to the saturation values of the same grid block, the two preceding block saturations are also considered.

➤ In this method firstly, the west side total mobility term, m_{twi} is written as:

$$m(1) = -0.001127 \left[\frac{k_x \times kr_w(S_{wi-2})}{\mu_w} + \frac{k_x \times kr_o(S_{wi-2})}{\mu_o} \right] \quad (4.39)$$

$$m(2) = -0.001127 \left[\frac{k_x \times kr_w(S_{wi-1})}{\mu_w} + \frac{k_x \times kr_o(S_{wi-1})}{\mu_o} \right] \quad (4.40)$$

$$m(3) = -0.001127 \left[\frac{k_x \times kr_w(S_{wi})}{\mu_w} + \frac{k_x \times kr_o(S_{wi})}{\mu_o} \right] \quad (4.41)$$

Equations 4.39, 4.40 and 4.41 are used to define the flux limiter's flux ratio, equation 4.42.

$$r = (m(2) - m(1))/(m(3) - m(2)) \quad (4.42)$$

Equation 4.42 is used to determine the flux limiter function from figure 4.11.

For achieving stability the limiter function must fall in the shaded stability region in figure 4.11. If the vertical line drawn from the flux limiter intersects the Leonard limiter function line then the value corresponding to Leonard limiter is used. In other words Leonard scheme is use with no modification of its original limiter [11]. However, if the vertical line crosses Leonard's line outside the stability region then a new limiter function value is selected within the shaded area. Such a selection of the flux limitier is achieved using equation 4.43.

$$L_f = \max[0, \min(2, 2r, (2 + r)/3)] \quad (4.43)$$

Finally, the west side mobility is determined using the flux limiter from 4.43 as:

$$m_{tw_i} = m(2) + 0.5 \times L_f \times (m(3) - m(2)) \quad (4.44)$$

➤ Similarly for east side total mobility, m_{te_i} the equations, 4.45 through 4.50 must be used to determine the east side mobility.

$$m(1) = -0.001127 \left[\frac{k_x \times kr_w(S_{w_{i-1}})}{\mu_w} + \frac{k_x \times kr_o(S_{w_{i-1}})}{\mu_o} \right] \quad (4.45)$$

$$m(2) = -0.001127 \left[\frac{k_x \times kr_w(S_{w_i})}{\mu_w} + \frac{k_x \times kr_o(S_{w_i})}{\mu_o} \right] \quad (4.46)$$

$$m(3) = -0.001127 \left[\frac{k_x \times kr_w(S_{w_{i+1}})}{\mu_w} + \frac{k_x \times kr_o(S_{w_{i+1}})}{\mu_o} \right] \quad (4.47)$$

$$r = (m(2) - m(1))/(m(3) - m(2)) \quad (4.48)$$

$$L_f = \max[0, \min(2, 2r, (2 + r)/3)] \quad (4.49)$$

$$m_{te_i} = m(2) + 0.5 \times Lf \times (m(3) - m(2)) \quad (4.50)$$

The solutions to pressure equations of TVD- Leonard are analogous to pressure solutions of first order IMPES method.

4.3.2 TVD-Leonard saturation solution

The Leonard TVD saturation equations are solved explicitly by using a three step (third order time accurate) Runga Kutta technique. For the first Runga Kutta iteration is he saturation equation is given by Eq. 4.48:

$$S1_w^t = S_w^t + \left[\frac{u_w - u_e}{\Delta x} + q \right] \times \frac{5.614583 \times \Delta t}{\phi} \quad (4.51)$$

➤ The west and east side velocity, u_w , u_e values are calculated using TVD Leonard technique as follows:

$$uw(1) = -0.001127 \left[\frac{k_x \times kr_w(S_{w_{i-2}})}{\mu_w} \right] \quad (4.52)$$

$$uw(2) = -0.001127 \left[\frac{k_x \times kr_w(S_{w_{i-1}})}{\mu_w} \right] \quad (4.53)$$

$$uw(3) = -0.001127 \left[\frac{k_x \times kr_w(S_{w_i})}{\mu_w} \right] \quad (4.54)$$

$$rw = (uw(2) - uw(1))/(uw(3) - uw(2)) \quad (4.55)$$

$$Lfw = \max[0, \min(2, 2r, (2 + r)/3)] \quad (4.56)$$

$$u_w = [uw(2) + 0.5 \times Lf \times (uw(3) - uw(2))] \times \frac{P_i - P_{i-1}}{\Delta x} \quad (4.57)$$

For east face values:

$$ue(1) = -0.001127 \left[\frac{k_x \times kr_w(S_{wi-1})}{\mu_w} \right] \quad (4.58)$$

$$ue(2) = -0.001127 \left[\frac{k_x \times kr_w(S_{wi})}{\mu_w} \right] \quad (4.59)$$

$$ue(3) = -0.001127 \left[\frac{k_x \times kr_w(S_{wi+1})}{\mu_w} \right] \quad (4.60)$$

$$re = (v(2) - v(1))/(v(3) - v(2)) \quad (4.61)$$

$$Lfe = \max[0, \min(2, 2r, (2 + r)/3)] \quad (4.62)$$

$$u_e = [ue(2) + 0.5 \times Lf \times (ue(3) - ue(2))] \times \frac{P_{i+1} - P_i}{\Delta x} \quad (4.63)$$

Substituting 4.57 and 4.63 into 4.51 gives the first iteration via Runge Kutta. Similarly using the values obtained from the first iteration we can calculate the saturation for the second iteration as equation 4.64 and the results of the second iteration is substituted into the third iteration equations to finally obtain equation 4.65 as a order time accurate, Runge-Kutta solution [24] which employed the Leonard TVD algorithm.

$$S2_w^t = \frac{3}{4} S_w^t + \frac{1}{4} S1_w^t + \frac{1}{4} \times \left[\frac{v1_w - v1_e}{\Delta x} + q \right] \times \frac{5.614583 \times \Delta t}{\phi} \quad (4.64)$$

$$S_w^{t+1} = \frac{1}{3} S_w^t + \frac{2}{3} S2_w^t + \frac{2}{3} \times \left[\frac{v2_w - v2_e}{\Delta x} + q \right] \times \frac{5.614583 \times \Delta t}{\phi} \quad (4.65)$$

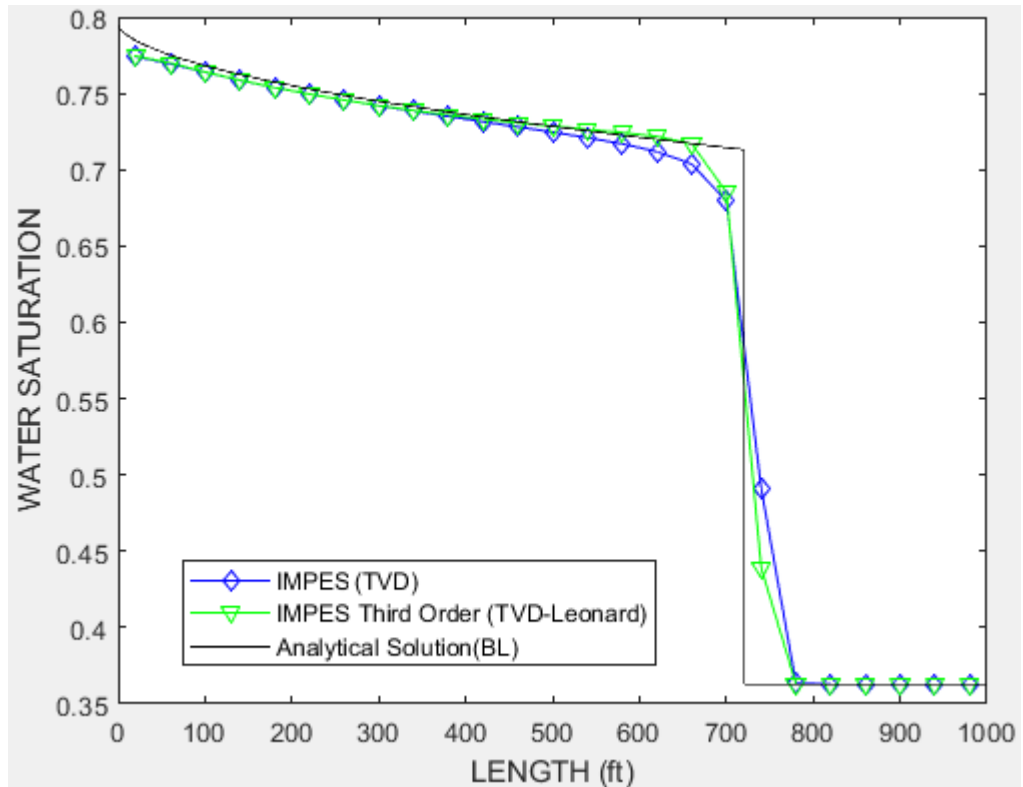


Figure 4.12 : IMPES TVD-Leonard for small Δx .

Fig. 4.12 compares IMPES TVD and third order IMPES TVD-Leonard methods for small Courant numbers and small cell Peclet number.

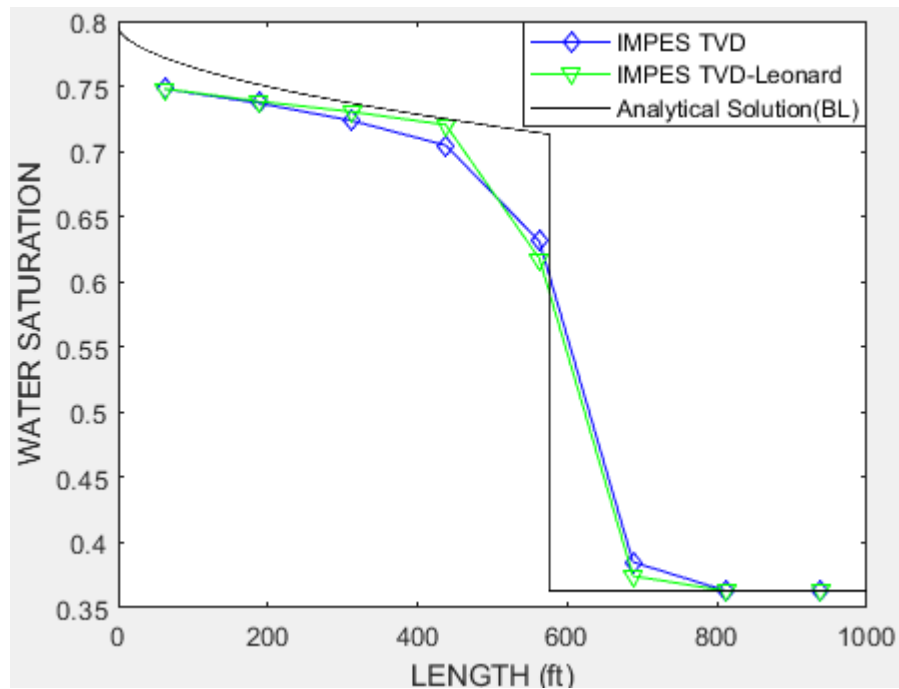


Figure 4.13: IMPES TVD-Leonard for large Δx .

Fig. 4.13 compares IMPES TVD and third order IMPES TVD-Leonard methods for large Δx . 2D equations were presented in APPENDIX C for future referencing.

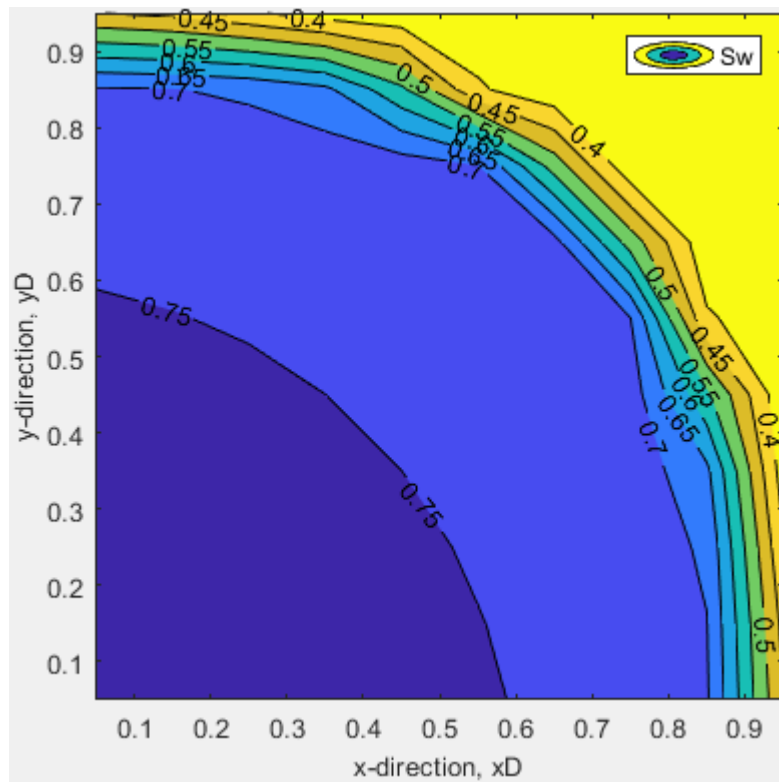


Figure 4.14 : 2D Impes third order (TVD-L) Matlab result.

Figure 4.14 shows the simulations of 2D third order (TVD-L) method displaying two dimensional dispersion in colours.

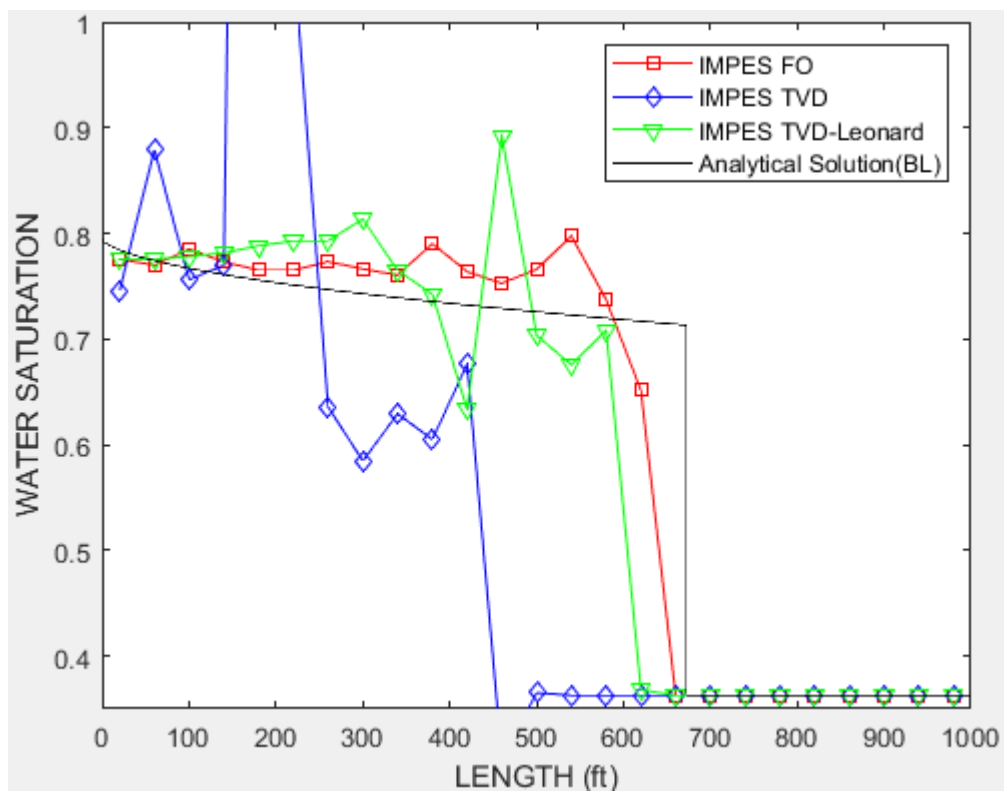


Figure 4.15: Unstability of IMPES.

Figure 4.15 shows instability of IMPES methods for Δx is 40 ft and Δt is 70 days. Therefore, we need to use unconditionally stable solution techniques as fully implicit or semi-implicit methods.

4.4 Fully Implicit First Order Space and First Order Time Solution

Fully implicit methods are proposed because of their unconditional stability characteristics. However, their high iteration requirements and large computational CPU time appears to be a disadvantage. Nevertheless, the fully implicit methods have been widely employed in petroleum reservoir simulation studies. This section provides a brief introduction and some results of the fully implicit method which employ first order discretization technique for both time and space. Using these two simple discretization scheme the discrete set of equations for second grid block can be written as equations 4.66-4.67 and 4.68-4.69 [9].

$$\begin{aligned}
 g_{w2} = & \frac{A \times k_x \times k_{rw_{1,2}} \times (P_1^{n+1} - P_2^{n+1}) \times \rho}{\mu_w \times \Delta x} \\
 & + \frac{A \times k_x \times k_{rw_{2,3}} \times (P_3^{n+1} - P_2^{n+1}) \times \rho}{\mu_w \times \Delta x} + q_{w2, mass}^{n+1} \\
 & - \frac{V_2 \times \emptyset \times \rho \times (S_{w2}^{n+1} - S_{w2}^n)}{\Delta t} = 0
 \end{aligned} \tag{4.66}$$

$$\begin{aligned}
 g_{w2} = & \frac{k_x \times k_{rw} [S_{w1}^{n+1}] \times (P_1^{n+1} - P_2^{n+1})}{\mu_w \times \Delta x^2} \\
 & + \frac{k_x \times k_{rw} [S_{w2}^{n+1}] \times (P_3^{n+1} - P_2^{n+1})}{\mu_w \times \Delta x^2} + \frac{q_{w2, volume}^{n+1}}{V_2} \\
 & - \frac{\emptyset \times (S_{w2}^{n+1} - S_{w2}^n)}{\Delta t} = 0
 \end{aligned} \tag{4.67}$$

$$\begin{aligned}
g_{o2} = & \frac{A \times k_x \times k_{ro_{1,2}} \times (P_1^{n+1} - P_2^{n+1}) \times \rho}{\mu_o \times \Delta x} \\
& + \frac{A \times k_x \times k_{ro_{2,3}} \times (P_3^{n+1} - P_2^{n+1}) \times \rho}{\mu_w \times \Delta x} + q_{o2,mass}^{n+1} \\
& - \frac{V_2 \times \emptyset \times \rho \times (-S_{w2}^{n+1} + S_{w2}^n)}{\Delta t} = 0
\end{aligned} \tag{4.68}$$

$$\begin{aligned}
g_{o2} = & \frac{k_x \times k_{ro} [S_{w1}^{n+1}] \times (P_1^{n+1} - P_2^{n+1})}{\mu_o \times \Delta x^2} \\
& + \frac{k_x \times k_{ro} [S_{w2}^{n+1}] \times (P_3^{n+1} - P_2^{n+1})}{\mu_o \times \Delta x^2} + \frac{q_{o2,volume}^{n+1}}{V_2} \\
& - \frac{\emptyset \times (-S_{w2}^{n+1} + S_{w2}^n)}{\Delta t} = 0
\end{aligned} \tag{4.69}$$

Total number of water and oil equations developed for all grids in the reservoir is equal to number of unknown pressures and saturations for all grids. The discretized set of algebraic equations are solved by a suitable matrix solver iteratively such as Newton-Rapson method [9]. Equation 4.70 shows the matrix representation of discretized set of equations.

$$\begin{bmatrix} P_1^{v+1} \\ P_2^{v+1} \\ \vdots \\ S_{w1}^{v+1} \\ S_{w2}^{v+1} \\ \vdots \end{bmatrix} = \begin{bmatrix} P_1^v \\ P_2^v \\ \vdots \\ S_{w1}^v \\ S_{w2}^v \\ \vdots \end{bmatrix} - \begin{bmatrix} \frac{df_{w1}^v}{dP_1^v} & \frac{df_{w1}^v}{dP_2^v} & \dots & \frac{df_{w1}^v}{dS_{w1}^v} & \frac{df_{w1}^v}{dS_{w2}^v} & \dots \\ \frac{df_{w2}^v}{dP_1^v} & \dots & \dots & \frac{df_{w2}^v}{dS_{w1}^v} & \dots & \dots \\ \vdots & \dots & \dots & \dots & \dots & \dots \\ \frac{df_{o1}^v}{dP_1^v} & \frac{df_{o1}^v}{dP_2^v} & \dots & \frac{df_{o1}^v}{dS_{w1}^v} & \frac{df_{o1}^v}{dS_{w2}^v} & \dots \\ \frac{df_{o2}^v}{dP_1^v} & \dots & \dots & \frac{df_{o2}^v}{dS_{w1}^v} & \dots & \dots \\ \vdots & \dots & \dots & \dots & \dots & \dots \end{bmatrix}^{-1} \times \begin{bmatrix} f_{w1}^v \\ f_{w2}^v \\ \vdots \\ f_{o1}^v \\ f_{o2}^v \\ \vdots \end{bmatrix} \tag{4.70}$$

Figure 4.16 shows first order fully implicit solution with small Δx and small Δt . Using large Δx for first order implicit solution is given by figure 4.17.

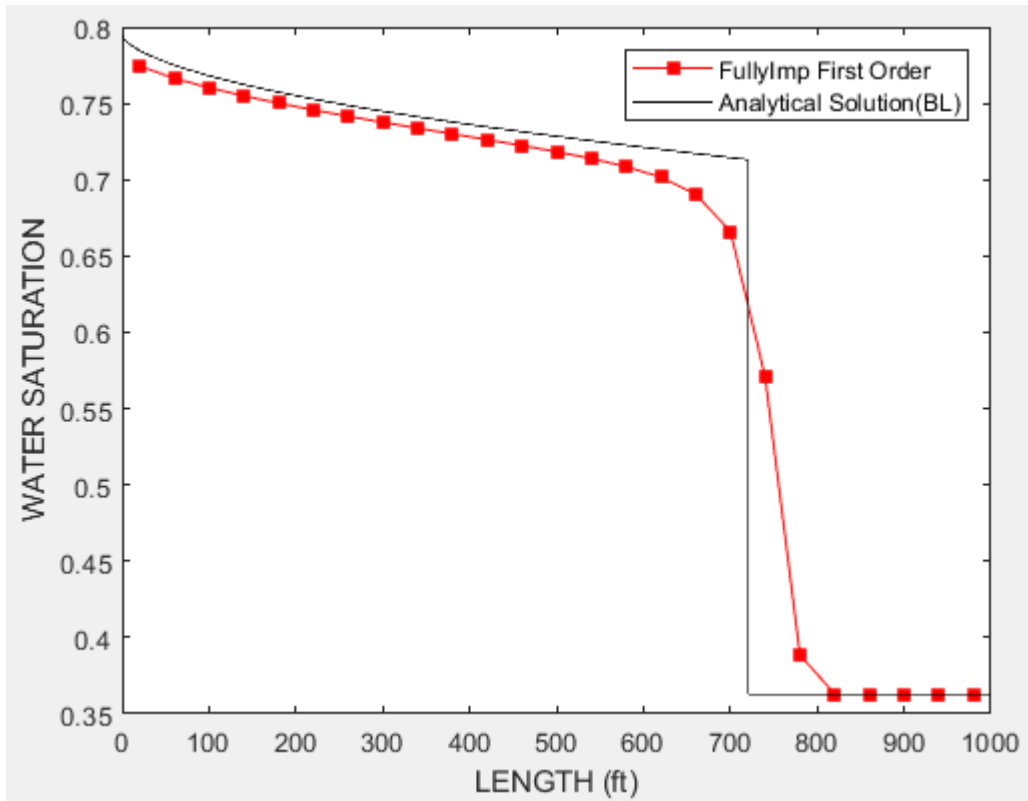


Figure 4.16 : Fully implicit first order Matlab result.

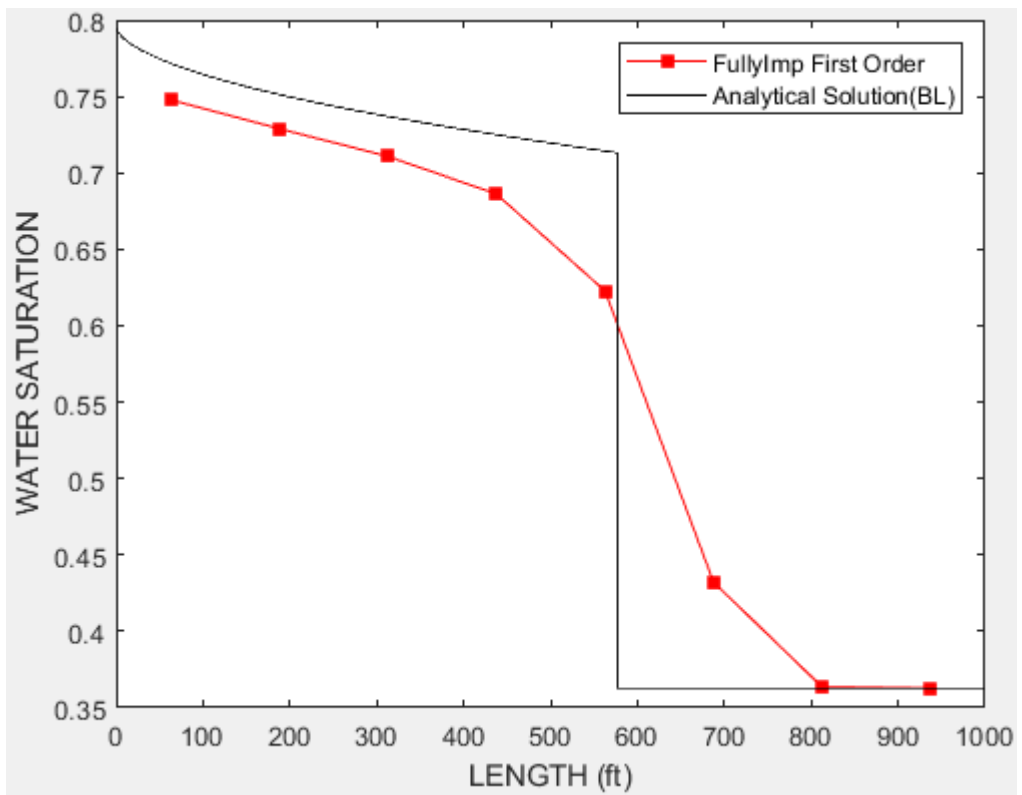


Figure 4.17: Fully implicit first order for large Δx .

Figure 4.18 shows first order implicit solution with large time step ($\Delta t=70$ days). Despite large time step, first order fully implicit solution is still stable. In that condition, all IMPES solution techniques are unstable (see figure 4.15).

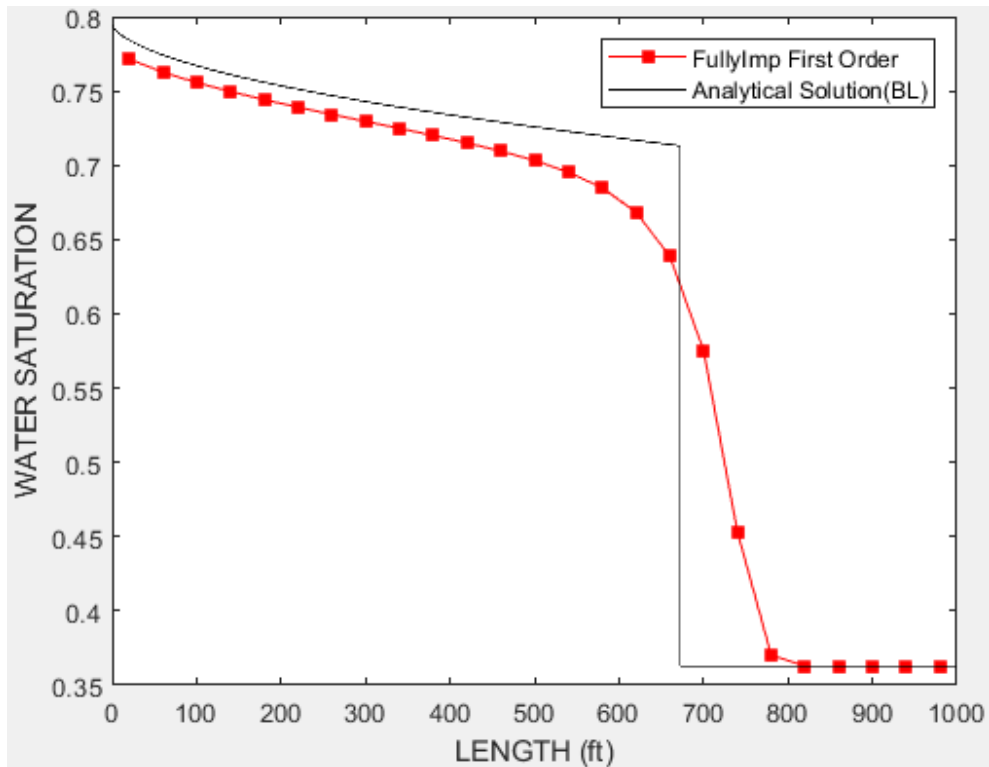


Figure 4.18: Fully implicit first order for large Δt .

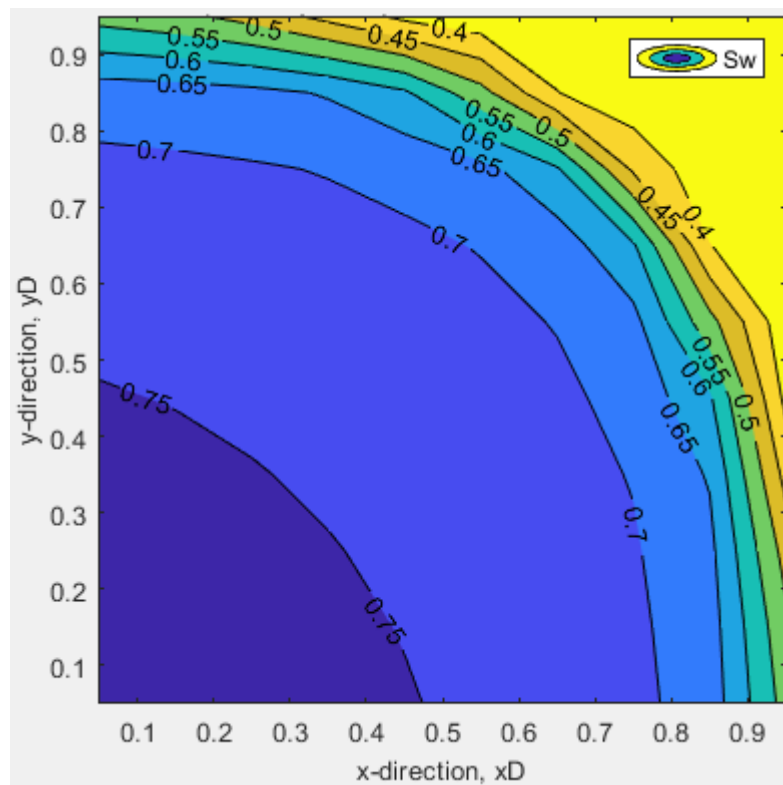


Figure 4.19 : 2D Fully implicit first order Matlab result.

The discretized equations of 2D fully implicit method is given in APPENDIX D for future referencing. Figure 4.13 shows 2D fully implicit first order Matlab code results.

4.5 TVD Implemented Fully Implicit First Order Method

The highly promising TVD method can also be implemented for fully implicit solution methods. Employing the TVD the related flow and transport equations are modified as follows:

$$\begin{aligned}
 g_{w2} = & \frac{A \times k_x \times k_{rw_1,2} \times (P_1^{n+1} - P_2^{n+1}) \times \rho}{\mu_w \times \Delta x} \\
 & + \frac{A \times k_x \times k_{rw_2,3} \times (P_3^{n+1} - P_2^{n+1}) \times \rho}{\mu_w \times \Delta x} + q_{w2,mass}^{n+1} \\
 & - \frac{V_2 \times \emptyset \times \rho \times (S_{w2}^{n+1} - S_{w2}^n)}{\Delta t} = 0
 \end{aligned} \tag{4.71}$$

Equations 4.72 to 4.78 are used to calculate limiter function.

$$v_w = S_{w_{i-1}} - S_{w_{i-2}} \tag{4.72}$$

$$w_w = S_{w_i} - S_{w_{i-1}} \tag{4.73}$$

$$\Delta i_w = \text{sign}(v_w) \times \max(0, \min[|v_w|, w_w \times \text{sign}(v_w)]) \tag{4.74}$$

$$v_e = S_{w_i} - S_{w_{i-1}} \tag{4.75}$$

$$w_e = S_{w_{i+1}} - S_{w_i} \tag{4.76}$$

$$\Delta i_e = \text{sign}(v_e) \times \max(0, \min[|v_e|, w_e \times \text{sign}(v_e)]) \tag{4.77}$$

$$\begin{aligned}
g_{w2} = & \frac{k_x \times k_{rw} [S_{w1}^{n+1} + 0.5 \times \Delta i_w] \times (P_1^{n+1} - P_2^{n+1})}{\mu_w \times \Delta x^2} \\
& + \frac{k_x \times k_{rw} [S_{w2}^{n+1} + 0.5 \times \Delta i_e] \times (P_3^{n+1} - P_2^{n+1})}{\mu_w \times \Delta x^2} \\
& + \frac{q_{w2,volume}^{n+1}}{V_2} - \frac{\emptyset \times (S_{w2}^{n+1} - S_{w2}^n)}{\Delta t} = 0
\end{aligned} \tag{4.78}$$

Using Δi_w and Δi_e limiter values, equation 4.78 has second order spatial accuracy.

$$\begin{aligned}
g_{o2} = & \frac{A \times k_x \times k_{ro,1,2} \times (P_1^{n+1} - P_2^{n+1}) \times \rho}{\mu_o \times \Delta x} \\
& + \frac{A \times k_x \times k_{ro,2,3} \times (P_3^{n+1} - P_2^{n+1}) \times \rho}{\mu_w \times \Delta x} + q_{o2, mass}^{n+1} \\
& - \frac{V_2 \times \emptyset \times \rho \times (-S_{w2}^{n+1} + S_{w2}^n)}{\Delta t} = 0
\end{aligned} \tag{4.79}$$

$$\begin{aligned}
g_{o2} = & \frac{k_x \times k_{ro} [S_{w1}^{t+1} + 0.5 \times \Delta i_w] \times (P_1^{t+1} - P_2^{t+1})}{\mu_o \times \Delta x^2} \\
& + \frac{k_x \times k_{ro} [S_{w2}^{t+1} + 0.5 \times \Delta i_e] \times (P_3^{t+1} - P_2^{t+1})}{\mu_o \times \Delta x^2} \\
& + \frac{q_{o2,volume}^{t+1}}{V_2} - \frac{\emptyset \times (-S_{w2}^{t+1} + S_{w2}^t)}{\Delta t} = 0
\end{aligned} \tag{4.80}$$

Similarly, flux limiter is applied to oil phase equation (see equations 4.79 and 4.80).

Note that the only difference between IMPES and Fully Implicit TVD methods is that the saturations and pressures are all treated at the new time step in fully implicit, while saturation are treated at old time steps in IMPES method. The same iterative solution techniques must be used for the TVD implemented fully implicit methods.

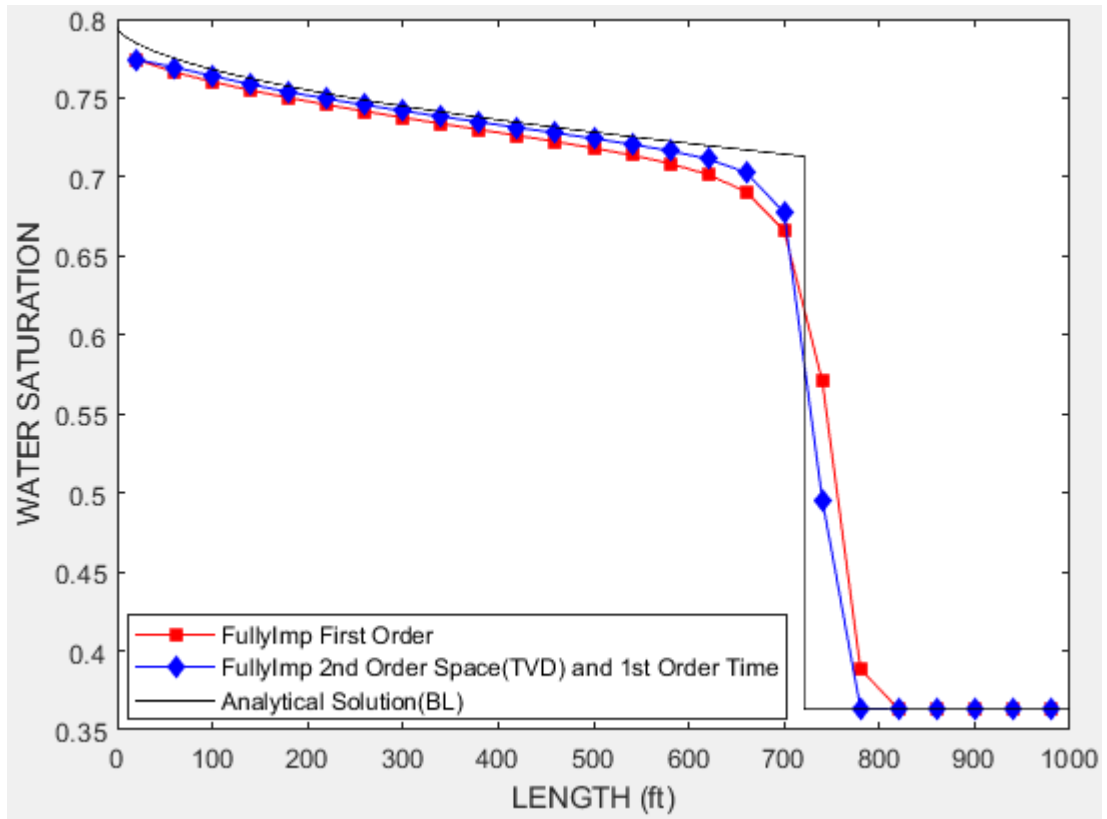


Figure 4.20 : Fully implicit second order space first order time Matlab result.

Figure 4.20 shows comparison of 1D fully implicit first order and second order TVD methods for small Δx and Δt .

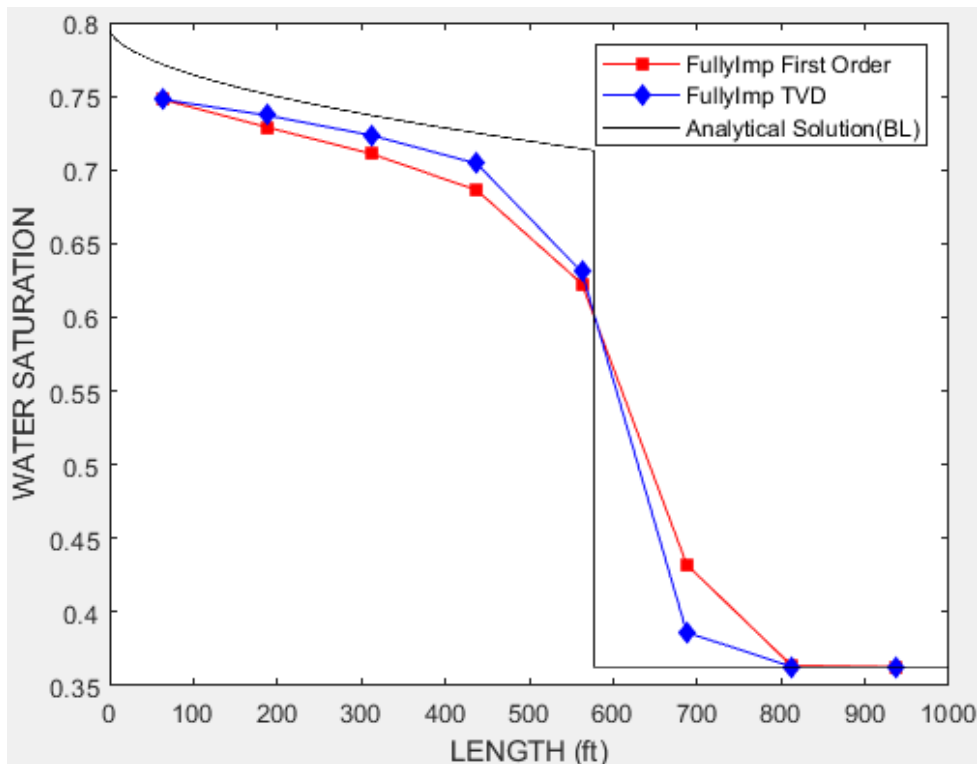


Figure 4.21: Fully implicit TVD for large Δx .

Figure 4.21 and figure 4.20 shows implicit TVD results with large Δx (125 ft) and large Δt (70 days) respectively.

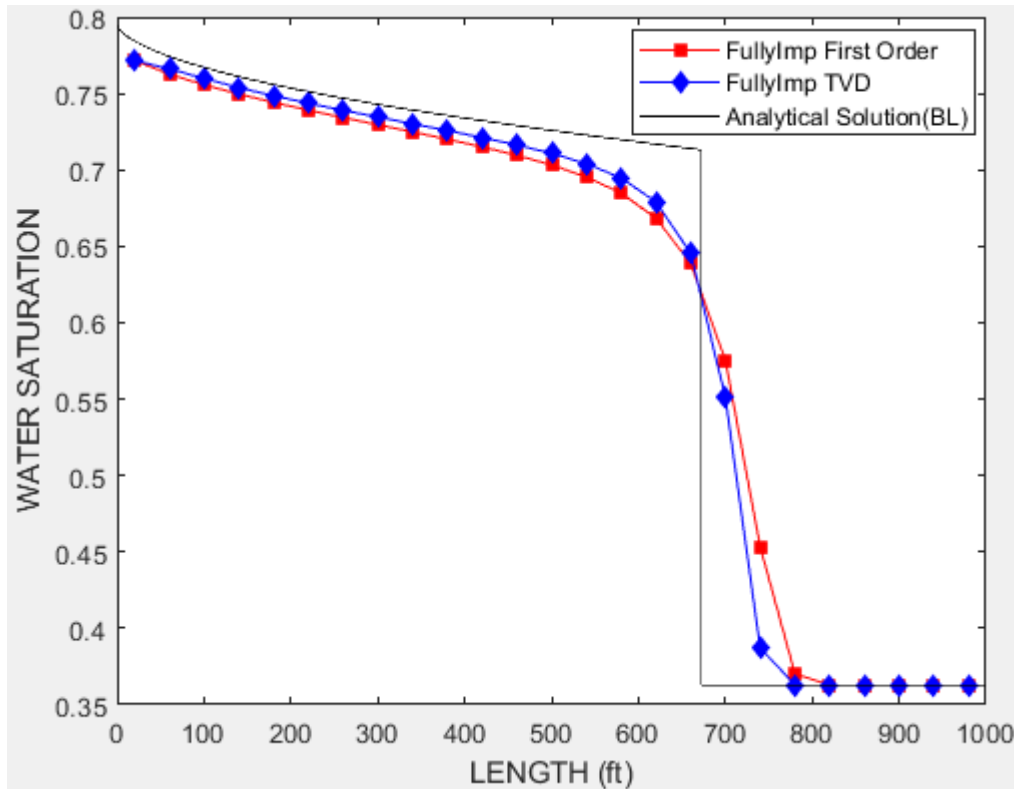


Figure 4.22: Fully implicit TVD for large Δt .

Figure 4.23 shows 2D fully implicit second order space (TVD) and first order time Matlab result.

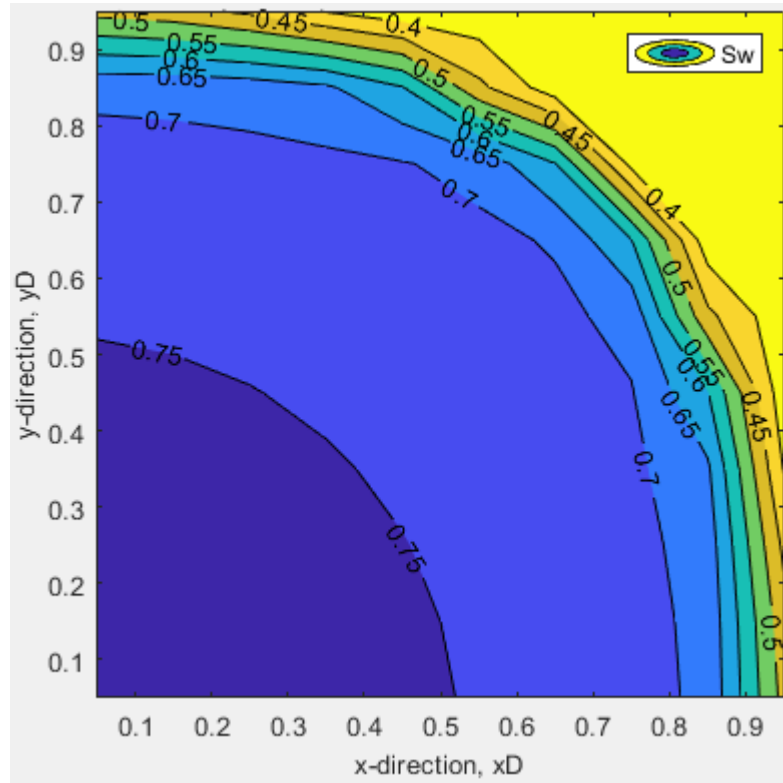


Figure 4.23: 2D Fully implicit second order space first order time Matlab result.

4.6 Fully Implicit Third Order Space (TVD-L) and First Order Time Solution

The governing equations for this technique is the same as IMPES TVD Leonard Method with the sole difference of implicit treatment of grid block saturation. Thus, the governing equations for second grid block can be written as follows:

$$\begin{aligned}
 g_{w2} = & \frac{A \times k_x \times k_{rw_{1,2}} \times (P_1^{n+1} - P_2^{n+1}) \times \rho}{\mu_w \times \Delta x} \\
 & + \frac{A \times k_x \times k_{rw_{2,3}} \times (P_3^{n+1} - P_2^{n+1}) \times \rho}{\mu_w \times \Delta x} + q_{w2,mass}^{n+1} \\
 & - \frac{V_2 \times \phi \times \rho \times (S_{w2}^{n+1} - S_{w2}^n)}{\Delta t} = 0
 \end{aligned} \tag{4.81}$$

The following equations (equations 4.82-4.87) are used to calculate water relative permeability values at a grid block's west face.

$$k(1) = kr_w(S_{wi-2}) \tag{4.82}$$

$$k(2) = kr_w(S_{w_{i-1}}) \quad (4.83)$$

$$k(3) = kr_w(S_{w_i}) \quad (4.84)$$

$$r = (k(2) - k(1))/(k(3) - k(2)) \quad (4.85)$$

$$Lf = \max[0, \min(2, 2r, (2 + r)/3)] \quad (4.86)$$

$$k_{rw_{1,2}} = k(2) + 0.5 \times Lf \times (k(3) - k(2)) \quad (4.87)$$

The following equations (equation 4.88-4.93) are used to calculate water relative permeability values at a grid block's east face.

$$k(1) = kr_w(S_{w_{i-1}}) \quad (4.88)$$

$$k(2) = kr_w(S_{w_i}) \quad (4.89)$$

$$k(3) = kr_w(S_{w_{i+1}}) \quad (4.90)$$

$$r = (k(2) - k(1))/(k(3) - k(2)) \quad (4.91)$$

$$Lf = \max[0, \min(2, 2r, (2 + r)/3)] \quad (4.92)$$

$$k_{rw_{2,3}} = k(2) + 0.5 \times Lf \times (k(3) - k(2)) \quad (4.93)$$

The oil relative permeability equations are of the same form of water equations. The oil and water functional equations may be written as equation 4.94-4.95.

$$\begin{aligned} g_{w2} = & \frac{k_x \times k_{rw_{1,2}} \times (P_1^{n+1} - P_2^{n+1})}{\mu_w \times \Delta x^2} \\ & + \frac{k_x \times k_{rw_{2,3}} \times (P_3^{n+1} - P_2^{n+1})}{\mu_w \times \Delta x^2} + \frac{q_{w2,volume}^{n+1}}{V_2} \\ & - \frac{\phi \times (S_{w2}^{n+1} - S_{w2}^n)}{\Delta t} = 0 \end{aligned} \quad (4.94)$$

$$\begin{aligned}
g_{o2} = & \frac{A \times k_x \times k_{ro_{1,2}} \times (P_1^{n+1} - P_2^{n+1}) \times \rho}{\mu_o \times \Delta x} \\
& + \frac{A \times k_x \times k_{ro_{2,3}} \times (P_3^{n+1} - P_2^{n+1}) \times \rho}{\mu_w \times \Delta x} + q_{o2, mass}^{n+1} \\
& - \frac{V_2 \times \phi \times \rho \times (-S_{w2}^{n+1} + S_{w2}^n)}{\Delta t} = 0
\end{aligned} \tag{4.95}$$

Dividing both sides of Equation 4.81 and 4.95 by the grid block volume one obtains equations 4.94 and 4.96 only as a function of Δx .

$$\begin{aligned}
g_{o2} = & \frac{k_x \times k_{ro_{1,2}} \times (P_1^{t+1} - P_2^{t+1})}{\mu_o \times \Delta x^2} + \frac{k_x \times k_{ro_{2,3}} \times (P_3^{t+1} - P_2^{t+1})}{\mu_o \times \Delta x^2} \\
& + \frac{q_{o2, volume}^{t+1}}{V_2} - \frac{\phi \times (-S_{w2}^{t+1} + S_{w2}^t)}{\Delta t} = 0
\end{aligned} \tag{4.96}$$

The TVD Leonard Fully Implicit equation can be solved iteratively similar to any fully implicit method.

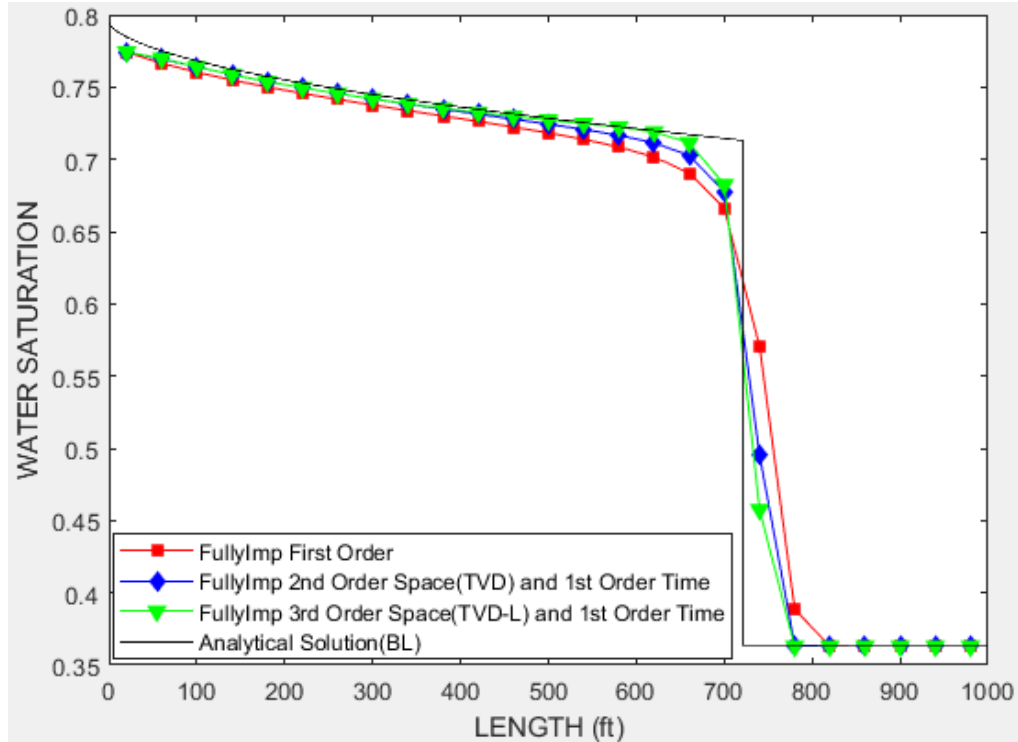


Figure 4.24 : Fully implicit third order space first order time Matlab result.

Figure 4.24 is designed by small Δx and Δt . Figure 4.25 and 4.26 show fully implicit TVD and TVD-Leonard methods with large Δx and large Δt respectively. Figure 4.26 implies that despite large Δt , higher order methods are still stable.

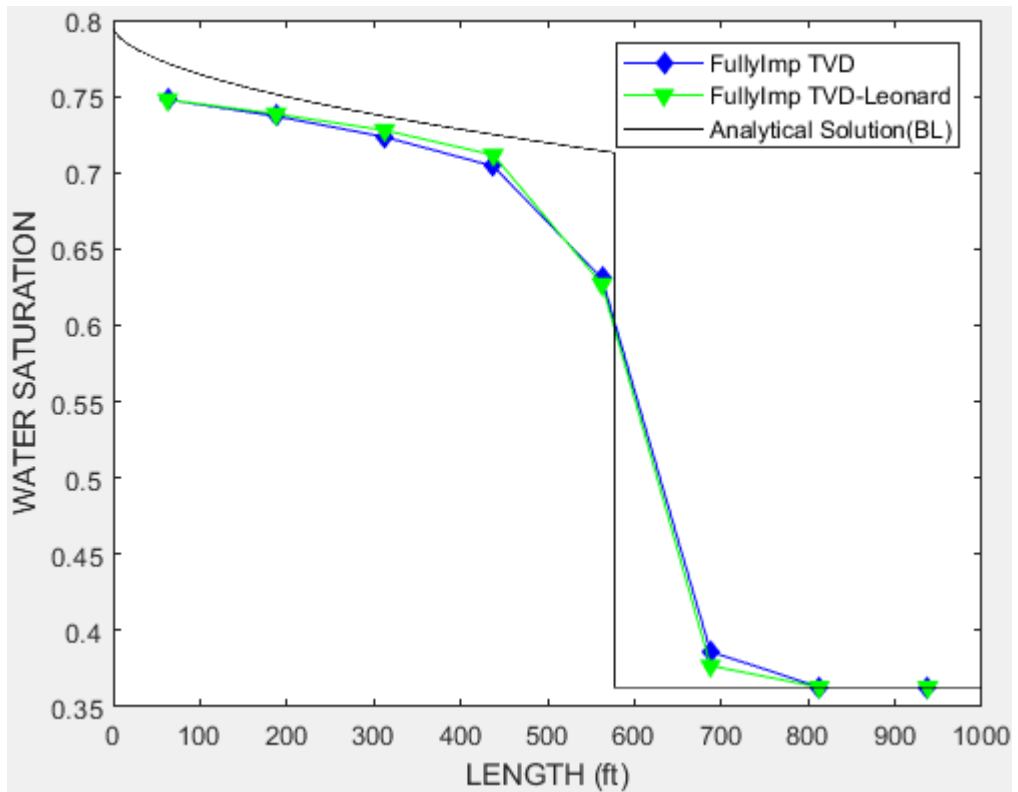


Figure 4.25: Fully implicit TVD for large Δx .

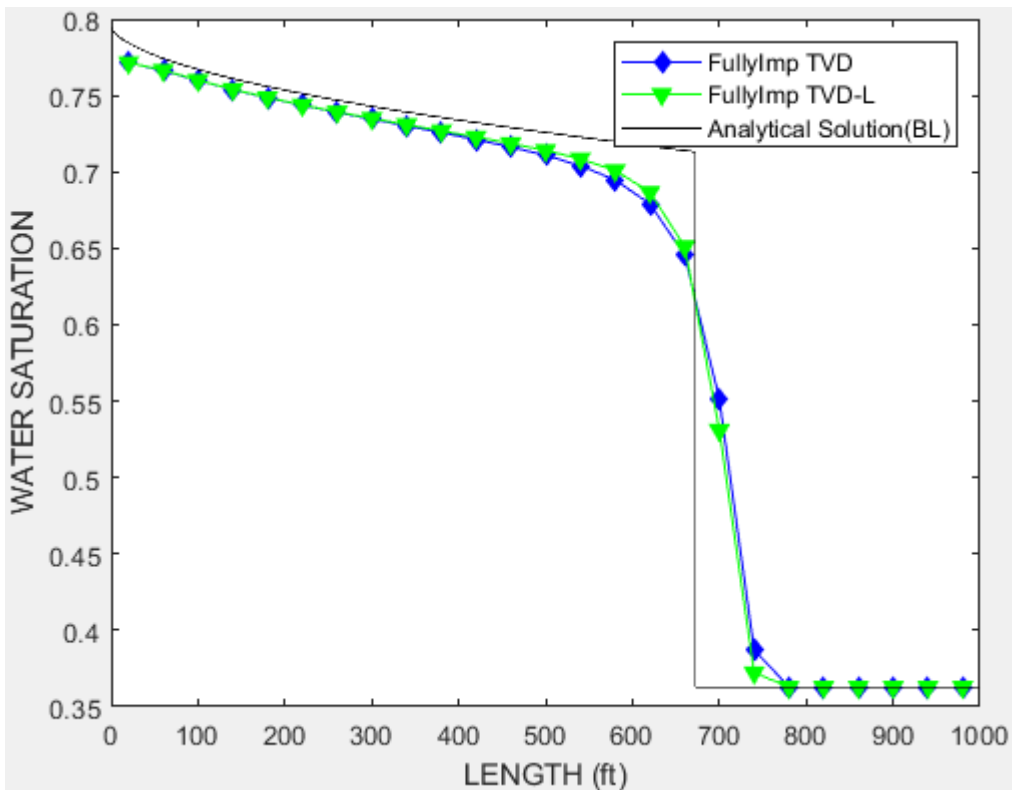


Figure 4.26: Fully implicit TVD-L for large Δt .

The equations of 2D fully implicit third order space (TVD-L) is presented in APPENDIX E. Figure 4.27 shows 2D fully implicit (TVD-L) Matlab simulations result.

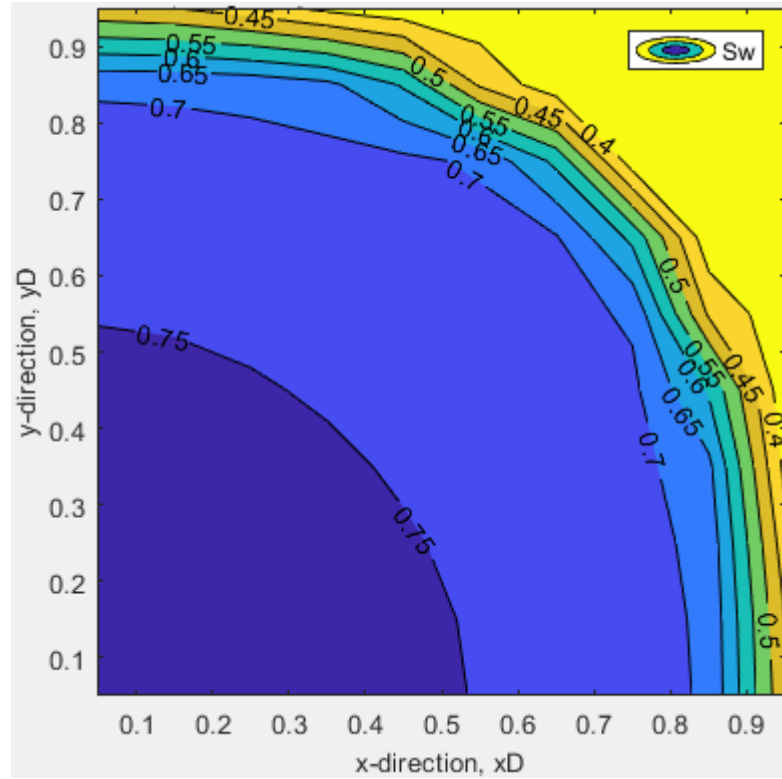


Figure 4.27 : 2D Fully implicit (TVD-L) result.

4.7 Fully Implicit Third Order Space (TCDF) and First Order Time Solution

Third-order Continuously Differentiable Function (TCDF) technique [32] improved the TVD method by changing abrupt switching of the original TVD [33-34] flux limiter to when the limiter function falls outside the stability region to a gradually switching smooth flux-limiter function[6]. The smooth flux limiter function is given by equation 4.97.

$$Lf = \begin{cases} r^3 - 2r^2 + 2r & \text{if } 0 \leq r < 0.5 \\ 0.75r + 0.25 & \text{if } 0.5 \leq r < 2 \\ \frac{2r^2 - 2r - 9/4}{r^2 - r - 1} & \text{if } 0 \leq r < 0.5 \end{cases} \quad (4.97)$$

Even though there no noticable improvement in the capturing of sharp front profiles for a large range of flux limiter values and removing oscillations for those values as shown in figure 4.28, this method requires only slightly lower iterations (171 iterations for TVD-L and 163 iterations for TCDF) for the computational work.

However, it is this method that has lead to the development of flexible flux limiter function, which is the major contribution of this thesis.

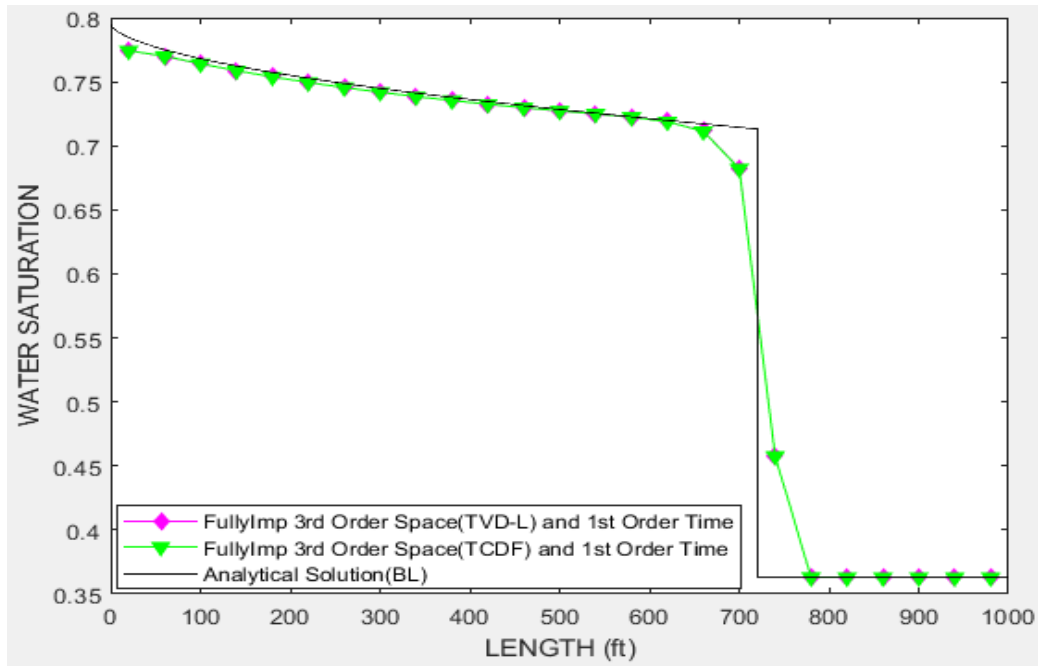


Figure 4.28 : TCDF and TVD-L methods.

Figure 4.29 shows 2D fully implicit third order space (TCDF) first order time Matlab result.

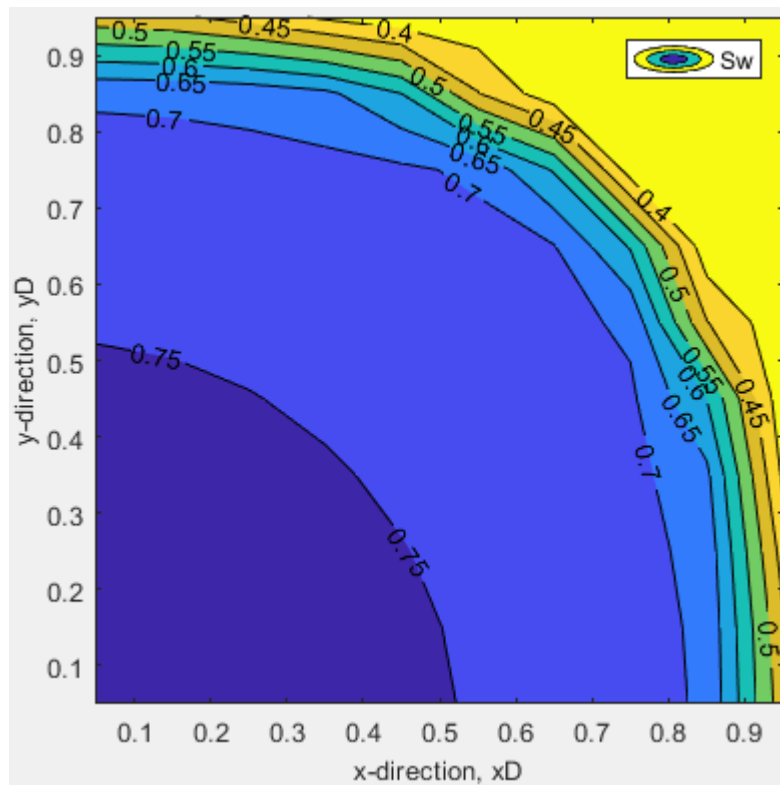


Figure 4.29 : 2D Fully implicit third order space (TCDF) first order time Matlab result.

4.8 First Order Space and Semi Implicit Second Order Time (Crank-Nicolson) Solution

Crank-Nicolson[4] (CN) method has been introduced to take advantage of both unconditional stability and second order time accuracy for the finite difference schemes. Thus, it will be implemented for both elementary and high order techniques possibly combined with TVD schemes.

This section presents the equations, from 4.98 to 4.103, for upstream first order space discretized flow equations combined with Crank Nicholson method.

$$G_{w2}^n = \frac{k_x \times k_{rw}[S_{w1}^n] \times (P_1^n - P_2^n)}{\mu_w \times \Delta x^2} + \frac{k_x \times k_{rw}[S_{w2}^n] \times (P_3^n - P_2^n)}{\mu_w \times \Delta x^2} + \frac{q_{w2,volume}^n}{V_2} \quad (4.98)$$

$$G_{o2}^n = \frac{k_x \times k_{ro}[S_{w1}^n] \times (P_1^n - P_2^n)}{\mu_o \times \Delta x^2} + \frac{k_x \times k_{ro}[S_{w2}^n] \times (P_3^n - P_2^n)}{\mu_o \times \Delta x^2} + \frac{q_{o2,volume}^n}{V_2} \quad (4.99)$$

In equations 4.98 and 4.99; saturations, pressures and flow rates are based on previous time step.

$$G_{w2}^{n+1} = \frac{k_x \times k_{rw}[S_{w1}^{n+1}] \times (P_1^{n+1} - P_2^{n+1})}{\mu_w \times \Delta x^2} + \frac{k_x \times k_{rw}[S_{w2}^{n+1}] \times (P_3^{n+1} - P_2^{n+1})}{\mu_w \times \Delta x^2} + \frac{q_{w2,volume}^{n+1}}{V_2} \quad (4.100)$$

$$G_{o2}^{n+1} = \frac{k_x \times k_{ro}[S_{w1}^{n+1}] \times (P_1^{n+1} - P_2^{n+1})}{\mu_o \times \Delta x^2} + \frac{k_x \times k_{ro}[S_{w2}^{n+1}] \times (P_3^{n+1} - P_2^{n+1})}{\mu_o \times \Delta x^2} + \frac{q_{o2,volume}^{n+1}}{V_2} \quad (4.101)$$

The saturations, pressures and flow rates are based on next time step in equation 4.100 and 4.101.

$$g_{w2} = \frac{F_{w2}^n + F_{w2}^{n+1}}{2} - \frac{\phi \times (S_{w2}^{n+1} - S_{w2}^n)}{\Delta t} = 0 \quad (4.102)$$

$$g_{o2} = \frac{F_{o2}^n + F_{o2}^{n+1}}{2} - \frac{\phi \times (-S_{w2}^{n+1} + S_{w2}^n)}{\Delta t} = 0 \quad (4.103)$$

Equation 4.102 and 4.103 are solved by using an iterative matrix solver employment similar to any fully implicit method.

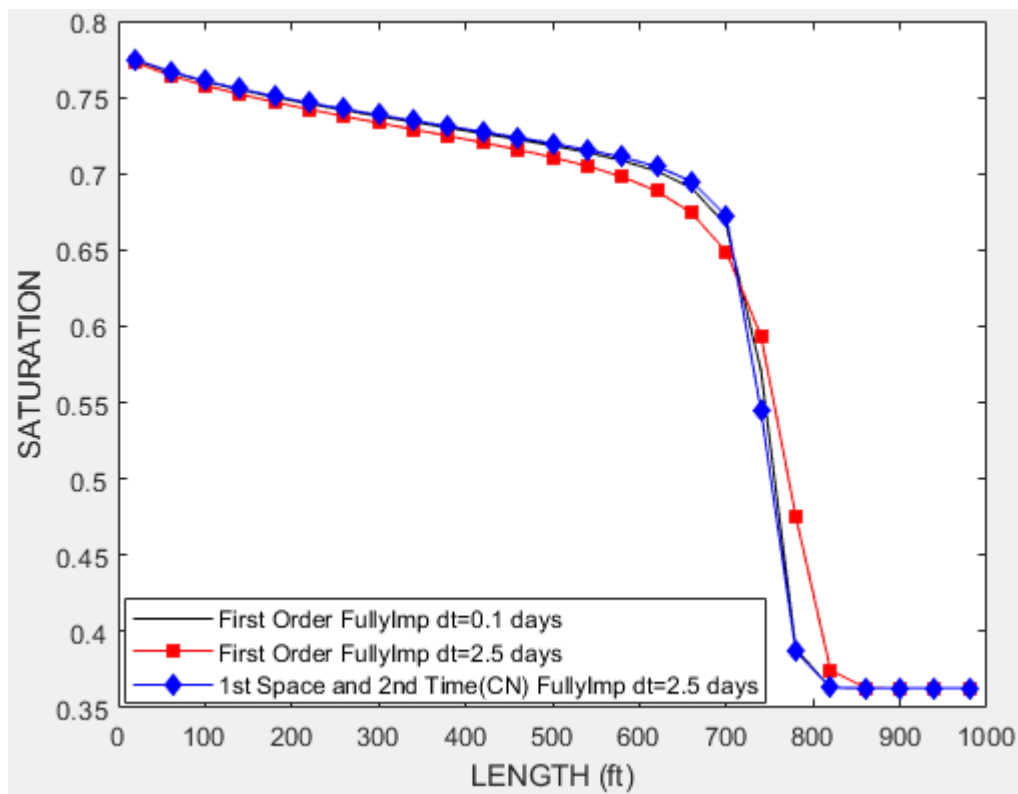


Figure 4.30 : 1D Fully implicit first order space and second order time Matlab result.

One dimensional immiscible displacement simulations of fully implicit first order and semi-implicit second order Crank Nicholson solutions are compared in figure 4.30 (small time step) and figure 4.31 (large time step). Figure 4.32 shows 2D result.

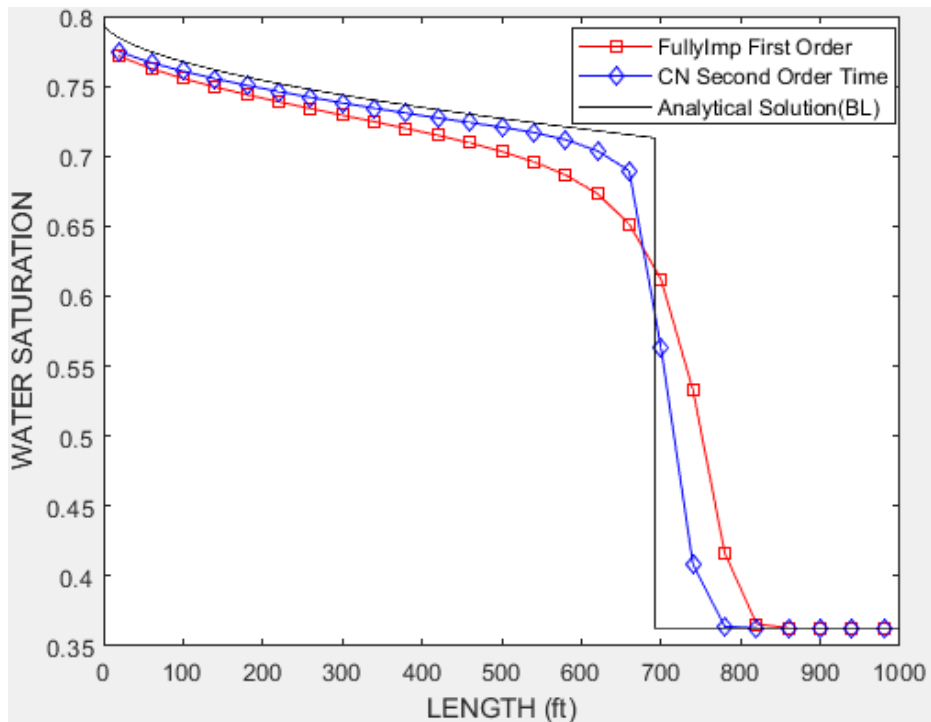


Figure 4.31: Crank-Nicholson with large time step.

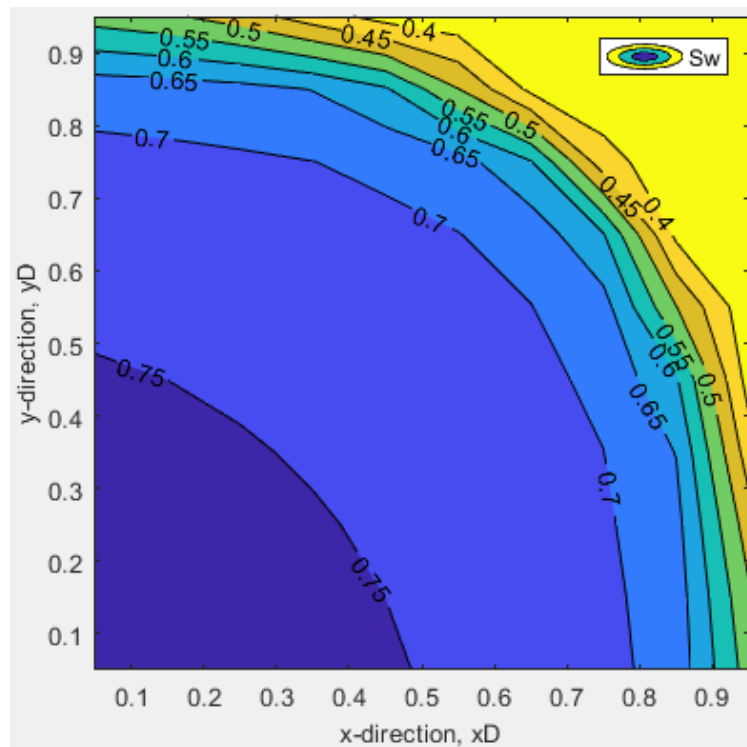


Figure 4.32 : 2D Fully implicit first order space and second order time Matlab result.

The previous mathematical developments and investigation of solution techniques has lead us to take advantage of the three findings, namely Leonard differencing for third order space accuracy, Crank Nicholson for second order time accuracy and unconditional stability and TCDF for removing oscillations with a hihger order accuracy. Thus, we have used these methods all combines as follows.

5. TCDF-LEONARD WITH CRANK NICOLSON SCHEME

In order to observe the possible advantages we have combined the TCDF Leonard with Crank Nicholson Scheme. The mathematical 1D equations for this technique is given by equations 5.1 through 5.6. Functional forms of previous time step are given by 5.1 and 5.2.

$$G_{w2}^n = \frac{k_x \times k^n_{rw_{1,2}} \times (P_1^n - P_2^n)}{\mu_w \times \Delta x^2} + \frac{k_x \times k^n_{rw_{2,3}} \times (P_3^n - P_2^n)}{\mu_w \times \Delta x^2} + \frac{q_{w2,volume}^n}{V_2} \quad (5.1)$$

$$G_{o2}^n = \frac{k_x \times k^n_{ro_{1,2}} \times (P_1^n - P_2^n)}{\mu_o \times \Delta x^2} + \frac{k_x \times k^n_{ro_{2,3}} \times (P_3^n - P_2^n)}{\mu_o \times \Delta x^2} + \frac{q_{o2,volume}^n}{V_2} \quad (5.2)$$

Functional forms in present time step are given by 5.3 and 5.4.

$$G_{w2}^{n+1} = \frac{k_x \times k^{n+1}_{rw_{1,2}} \times (P_1^{n+1} - P_2^{n+1})}{\mu_w \times \Delta x^2} + \frac{k_x \times k^{n+1}_{rw_{2,3}} \times (P_3^{n+1} - P_2^{n+1})}{\mu_w \times \Delta x^2} + \frac{q_{w2,volume}^{n+1}}{V_2} \quad (5.3)$$

$$G_{o2}^{n+1} = \frac{k_x \times k^{n+1}_{ro_{1,2}} \times (P_1^{n+1} - P_2^{n+1})}{\mu_o \times \Delta x^2} + \frac{k_x \times k^{n+1}_{ro_{2,3}} \times (P_3^{n+1} - P_2^{n+1})}{\mu_o \times \Delta x^2} + \frac{q_{o2,volume}^{n+1}}{V_2} \quad (5.4)$$

The functional form of Crank Nicholson scheme is given by 5.5 and 5.6.

$$g_{w2} = \frac{F_{w2}^n + F_{w2}^{n+1}}{2} - \frac{\phi \times (S_{w2}^{n+1} - S_{w2}^n)}{\Delta t} = 0 \quad (5.5)$$

$$g_{o2} = \frac{F_{o2}^n + F_{o2}^{n+1}}{2} - \frac{\phi \times (-S_{w2}^{n+1} + S_{w2}^n)}{\Delta t} = 0 \quad (5.6)$$

Equations 5.5 and 5.6 are solved similarly to any implicit method.

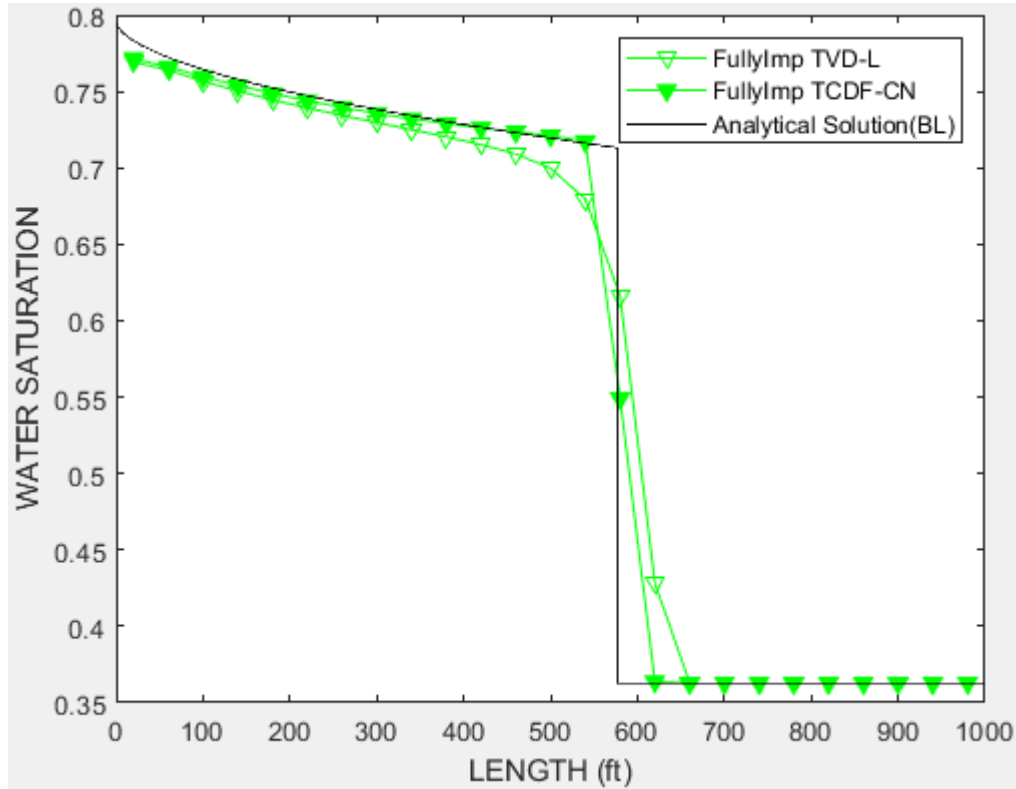


Figure 5.1: 1D Fully implicit third order space and second order time Matlab result.

Figure 5.1 shows comparison of TVD-L and TCDF-CN methods for $\Delta t=60$ days and $\Delta x=40$ ft. For higher than 60 days time step interval, TCDF-CN techniques gives oscillations in front of the front line. Therefore, we need to use flexible flux limiter to suppresses small oscillation of the TCDF-CN solution techniques. Figure 5.2 shows 2D result of TCDF-CN methods.

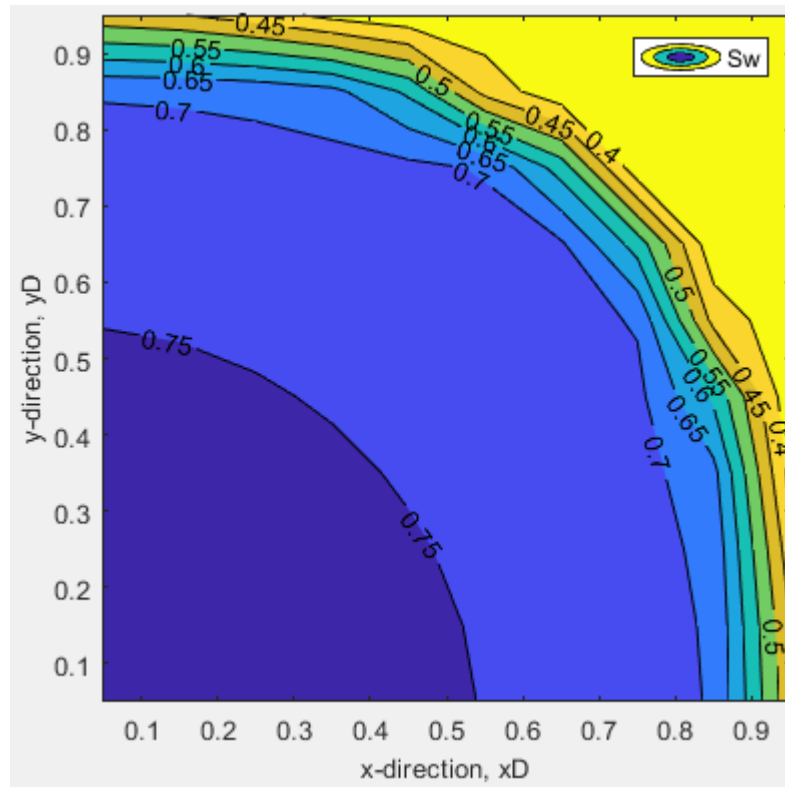


Figure 5.2: 2D Fully implicit third order space and second order time Matlab result.

6. FLEXIBLE FLUX LIMITER APPLICATIONS

In 2017, Jiang et. al. investigated in detail the implementation of flux limiter switching. They have used two TCDF switching functions that switch the limiter function smoothly but either of the two limiter values of 2 and 1.5. They have also observed that when Δt is large switching the flux limiter to 1.5 yield better results both in smoothing the oscillation and reducing the number of computational iterations.

Since the Δt values are direct indicator of Courant number we have adopted a switching method based on the Courant number magnitude. We have observed that the Courant number is very good indicator of unphysical oscillations. As the following figure 6.1 shows once the Courant Number is high enough then fixing the flux limiter to 2 or 1.5 may still yield oscillatory behavior, despite the fact that the limiter function is specified within the Sweby stability region. To determine the stable and unoscillatory flux limiter value within the Sweby stability region we have divided two, the maximum limiter value in the stability region, by the Courant number as the limiting value of the flexible flux limiter. Since this limiting value is varying depending on the Courant number we called this technique as the flexible flux limiter method. Note however that for Courant numbers smaller than one then the calculated flexible flux limiter value becomes greater than 2 which is outside the stability region. Then the flux limiter is fixed back to 2, which works very well because the time step and hence the Courant number is small.

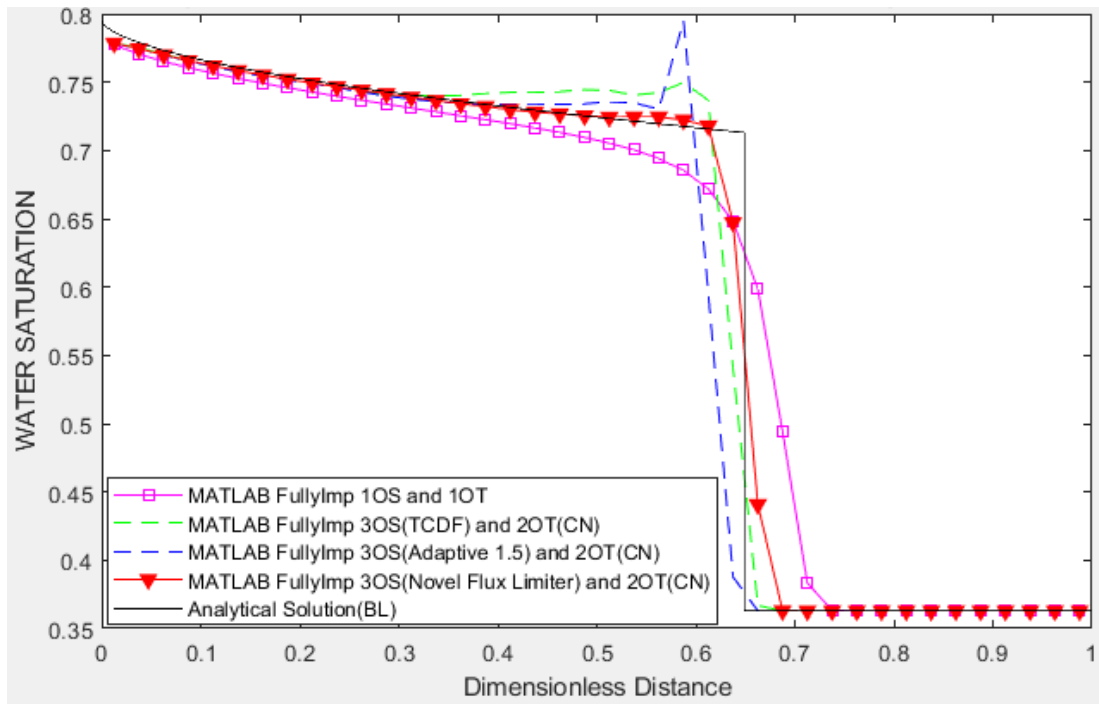


Figure 6.1: Matlab result of flexible flux limiter $N_c=1.8515$.

Figure 6.1 and 6.2 show results of flexible flux limiter method and other techniques for large time step (45 days) and small time step (10 days) respectively.

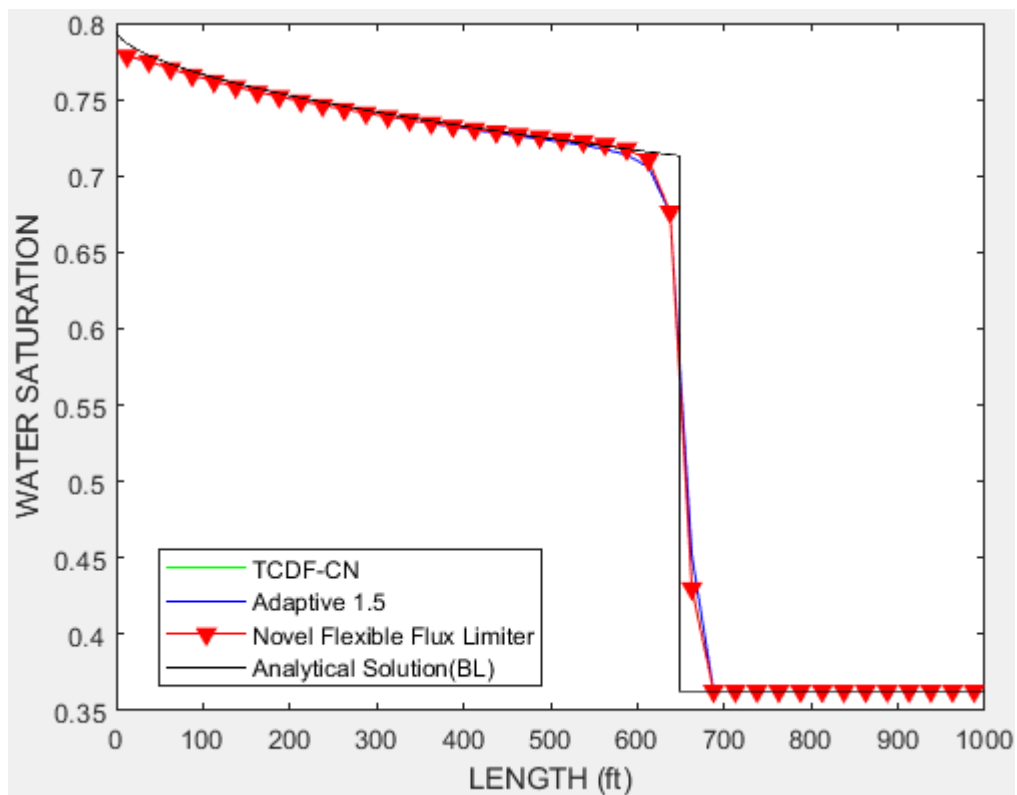


Figure 6.2: Matlab result of flexible flux limiter $N_c=0.4115$.

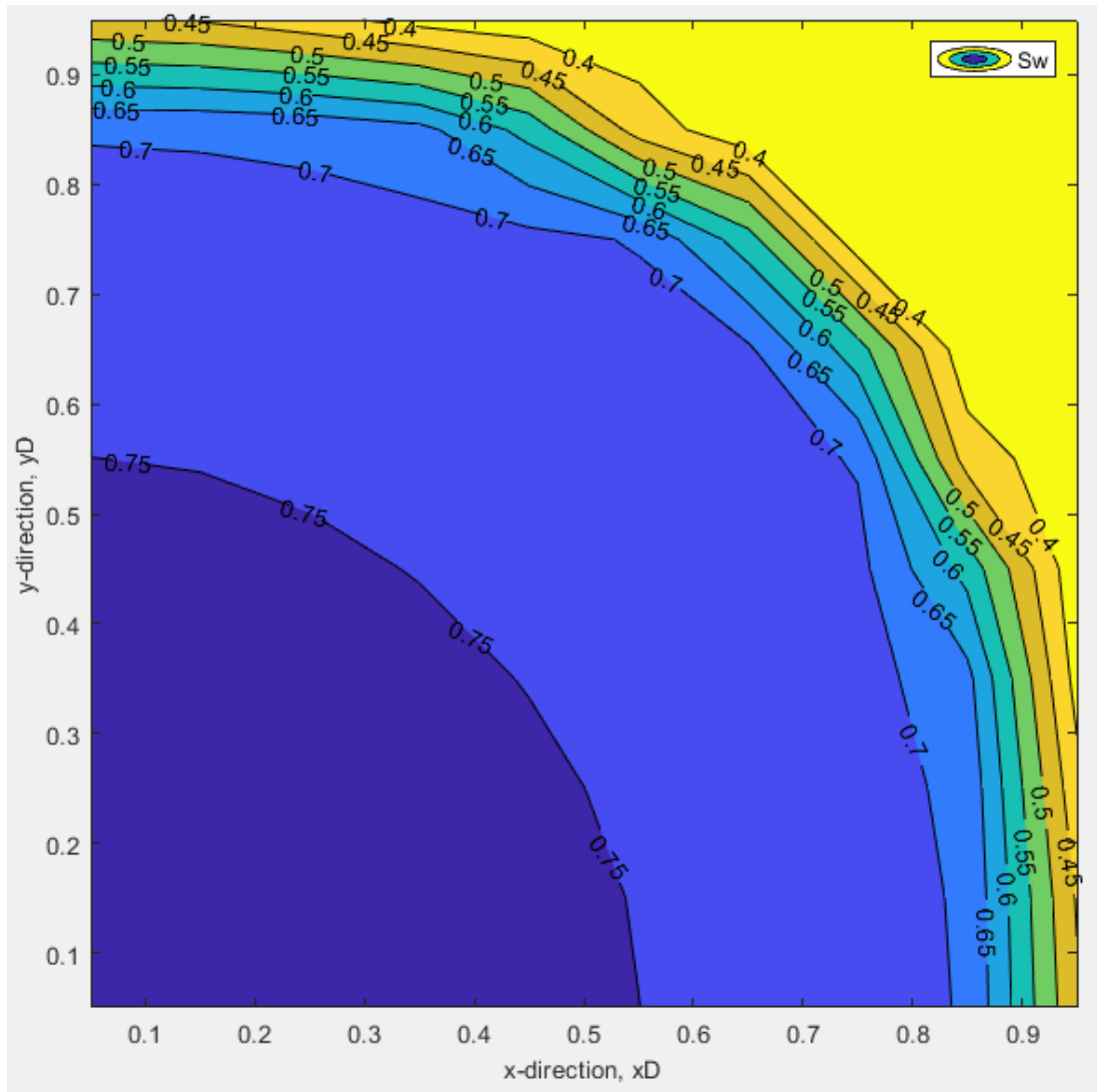


Figure 6.3: 2D Matlab result of flexible flux limiter (before breakthrough time).

Figure 6.3 (before breakthrough time) and figure 6.4 (before breakthrough time) show Matlab result of FullyImp 3OS(Novel Flux Limiter) and 2OT(CN) method.

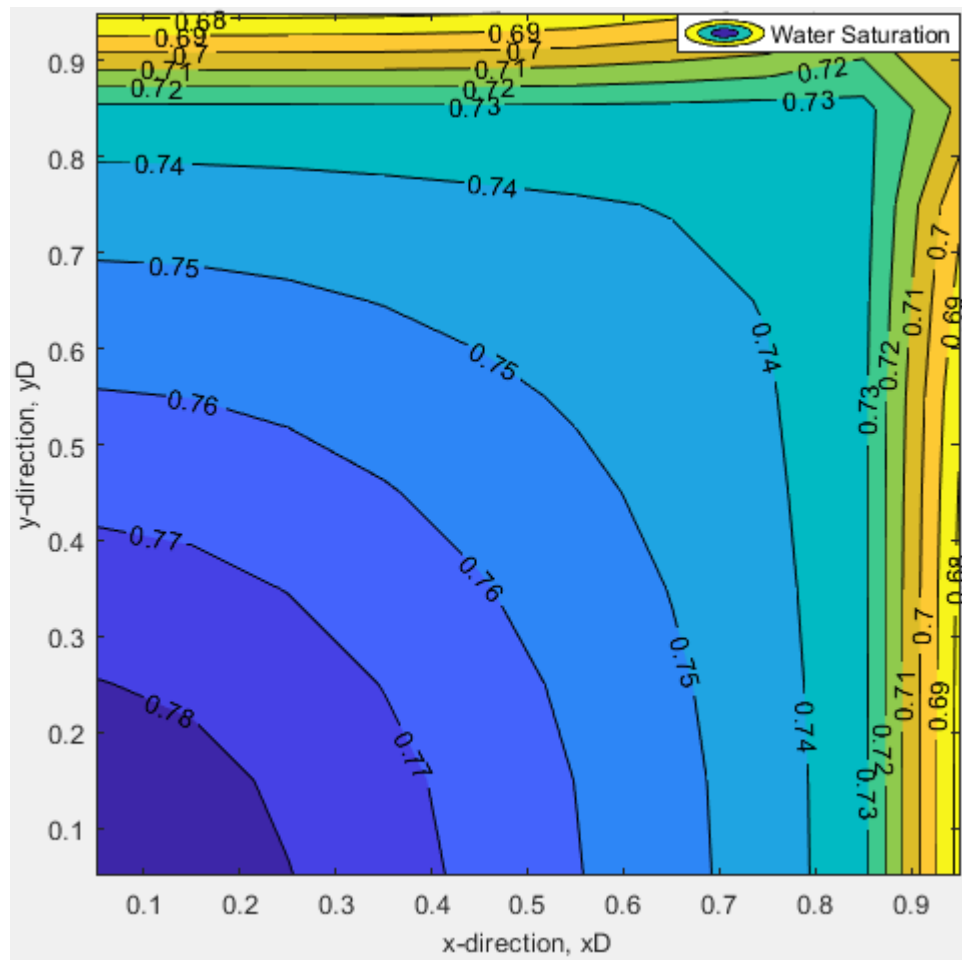


Figure 6.4: 2D Matlab result of flexible flux limiter (after breakthrough time).

7. APPLICATIONS OF THE METHODS TO DIFFERENT RESERVOIRS

7.1 Oil Wet Reservoirs

In this section, oil wet reservoir data will be used to compare solution methods. It is assumed that total simulation time is 1000 days, Δy is 100 ft, Δz is 100 ft, j -direction block is 1 and initial pressure of reservoir is 1000 psia.

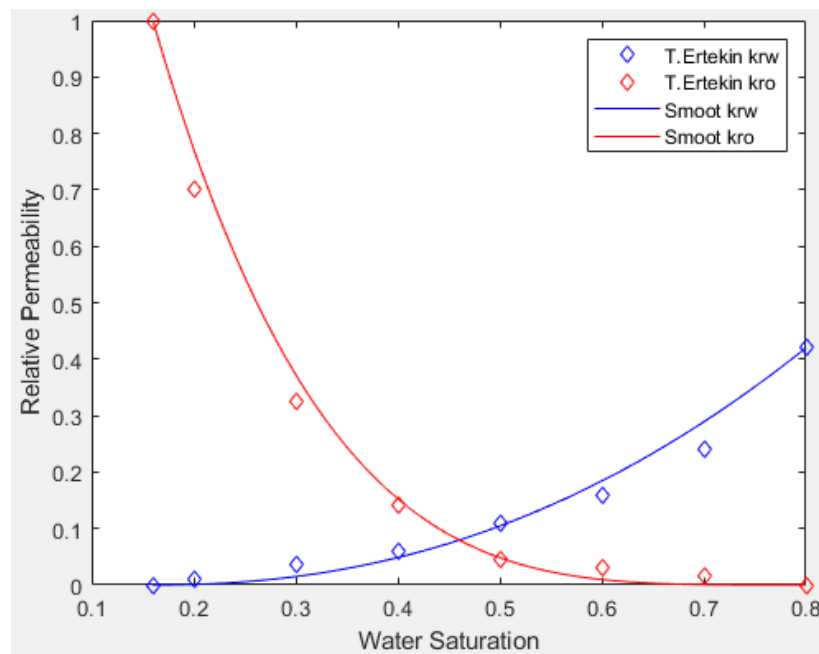


Figure 7.1: Relative permeability curves for case 2.

These reservoir simulation data and relative permeability curves data in figure 7.1 are taken from Ertekin et. al. [7]. Using regression, smoot relative permeability curves are obtained.

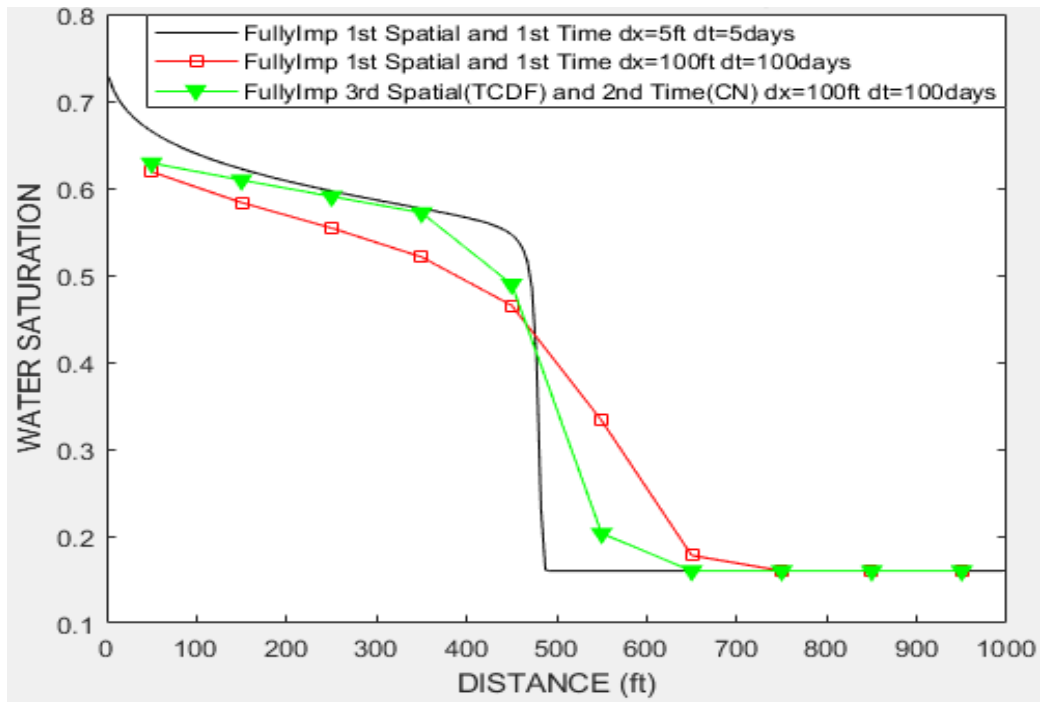


Figure 7.2: $dx=100ft$ and $dt=100days$ for oil wet reservoir.

In order to compare different reservoir simulation methods, we will use fine grid block dimension and minor time step intervals in this section. Figure 7.2-7.5 show comparison of fully implicit third order spatial (TCDF) second order time (CN) method and fully implicit first order spatial first order time method for different spatial and different time step intervals.

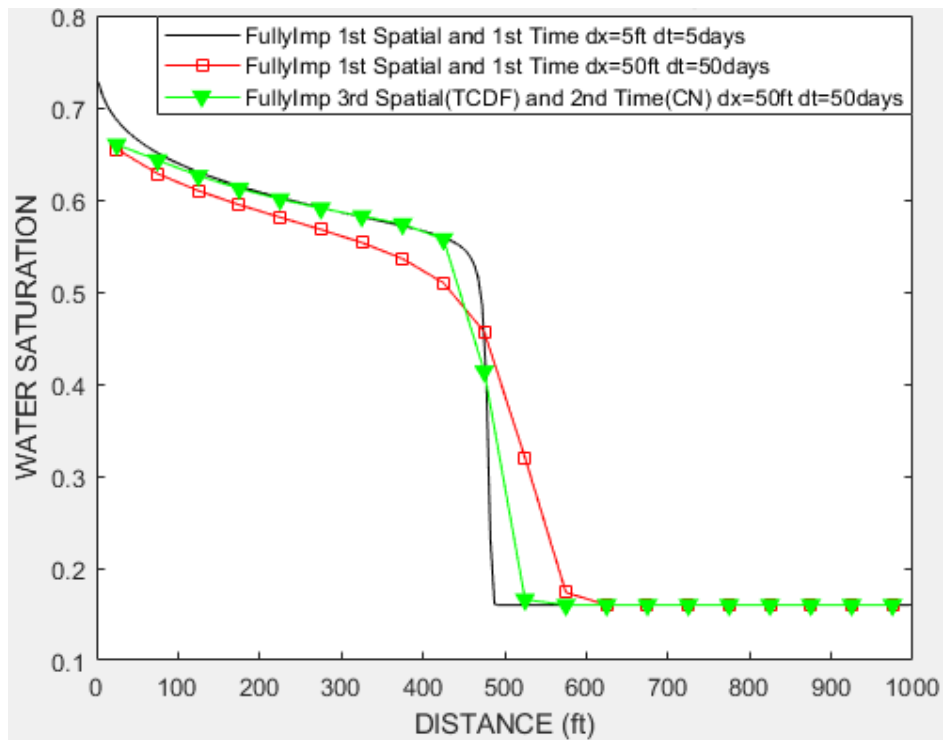


Figure 7.3: $dx=50ft$ and $dt=50days$ oil wet reservoir.

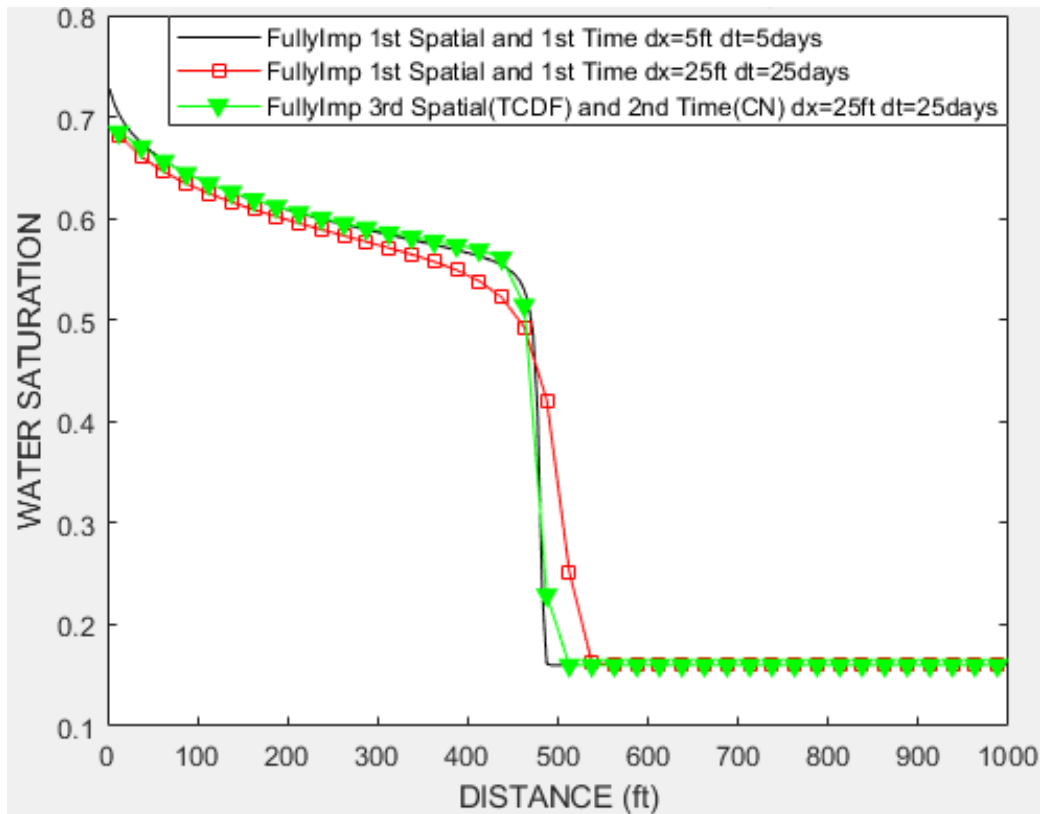


Figure 7.4: $dx=25\text{ft}$ and $dt=25\text{days}$ for oil wet reservoir.

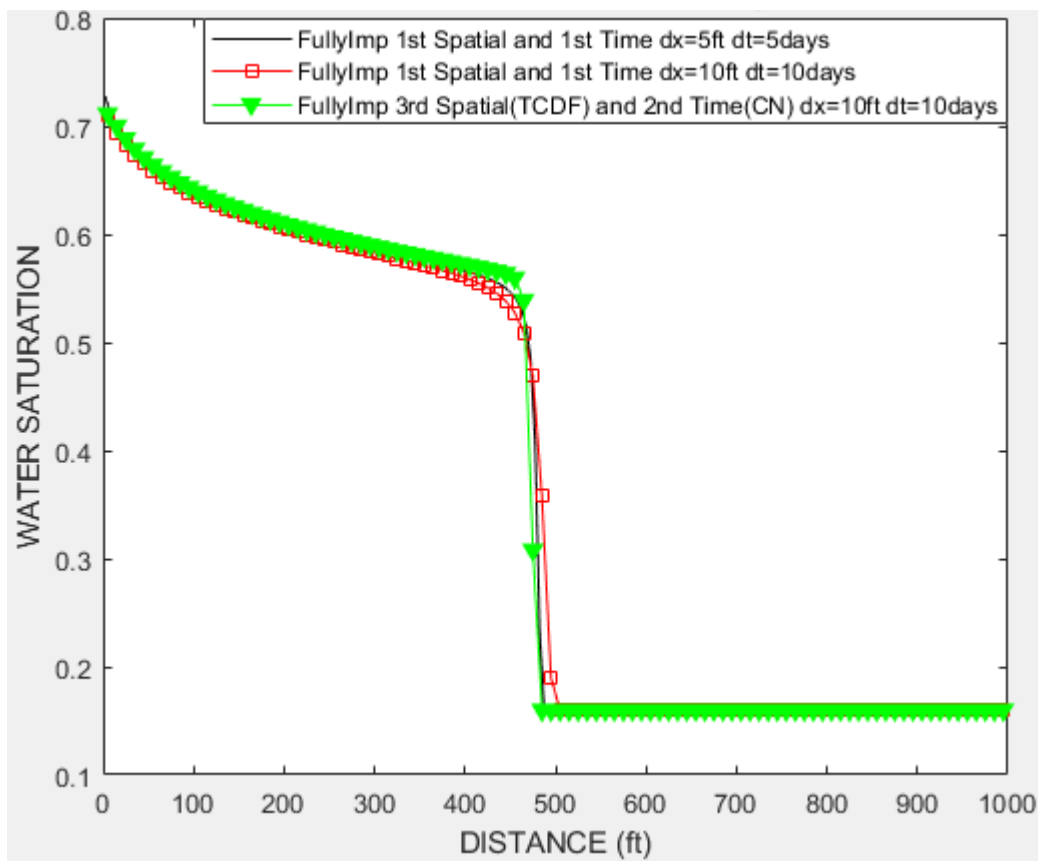


Figure 7.5: $dx=10\text{ft}$ and $dt=10\text{days}$ for oil wet reservoir.

7.2 Intermediate Wettability Reservoirs

Using fine grid block dimension and minor time step intervals is not appropriate to compare different reservoir simulation models. Because there are truncation errors even using fine grid block dimension and minor time step intervals. Therefore, we will use Buckley–Leverett [12] analytical solution in order to compare results of fully implicit third order spatial (TCDF) second order time (CN) method and fully implicit first order spatial first order time method for different spatial and different time step intervals.

In this section it is assumed that total simulation time 2000 days, Δy 100 ft, Δz 100 ft, j -direction block 1, $S_{wi}=0.01$, $S_{or}=0$, $P_i=1000$ psia. Also it is assumed that relative permeability of water is function of square of water saturation and relative permeability of oil is function of square of oil saturation in figure 7. 6 [6].

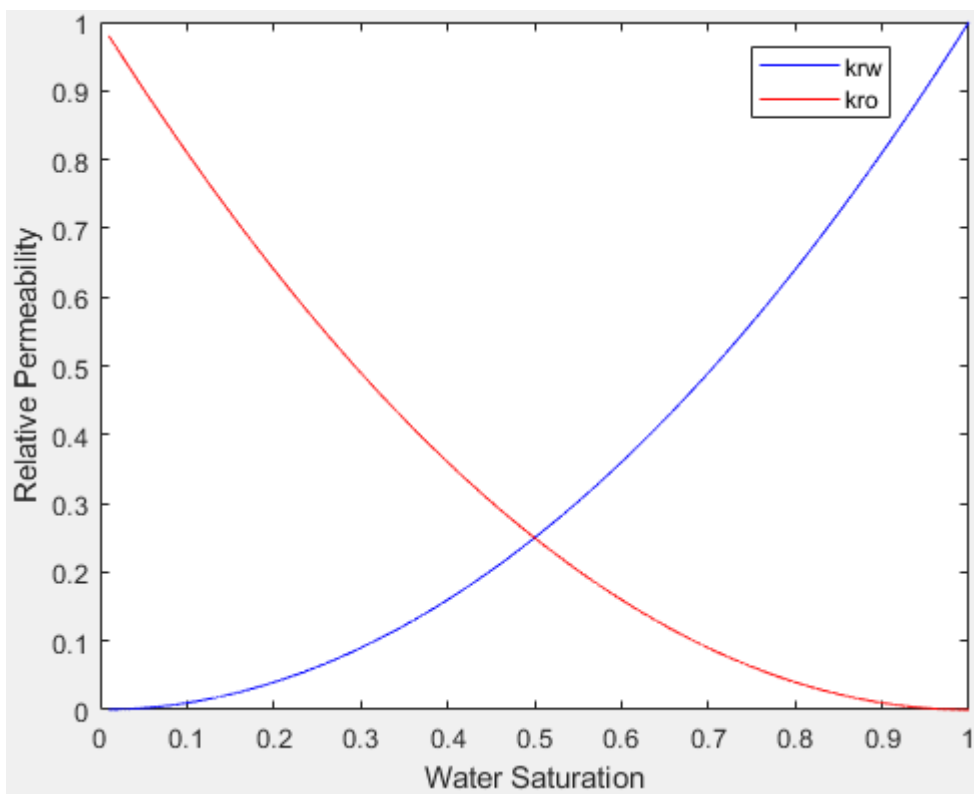


Figure 7.6: Relative permeability curves for intermediate wettability reservoir.

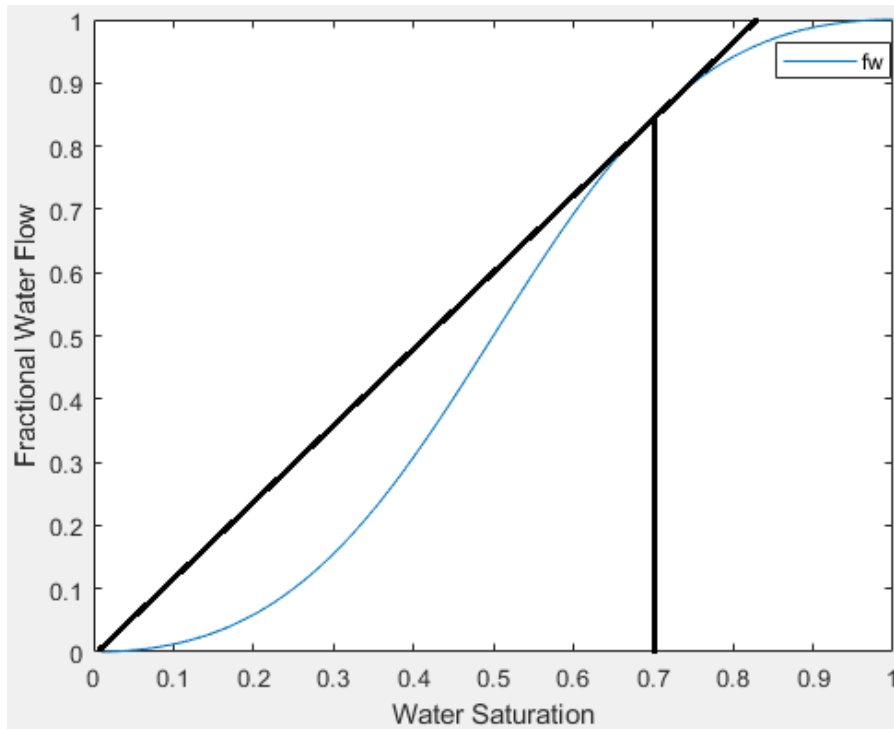


Figure 7.7: Fractional flow curves for intermediate wettability reservoir ($S_{wf}=0.7041$).

In order to obtain B-L analytical solution, we need to determine front water saturation. Using Matlab Code, front water saturation is obtained as 0.7041. Figure 7.7 shows determination of front water saturation as broadly.

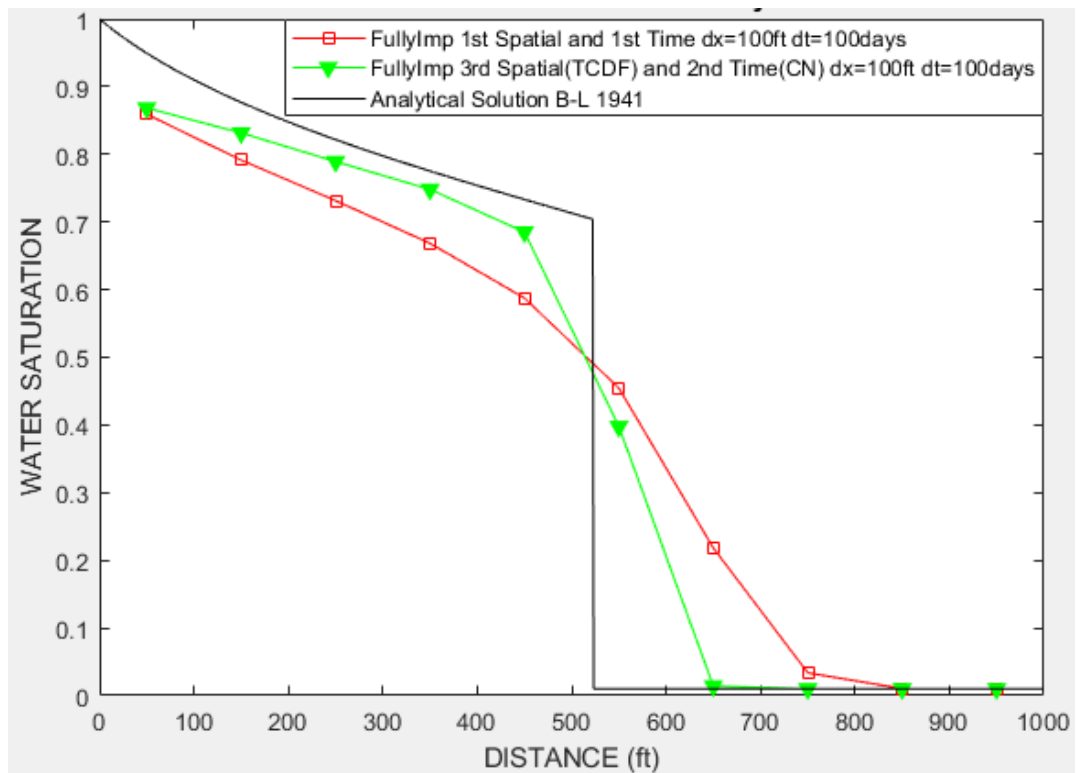


Figure 7.8: $dx=100ft$ and $dt=100days$ for case 3.

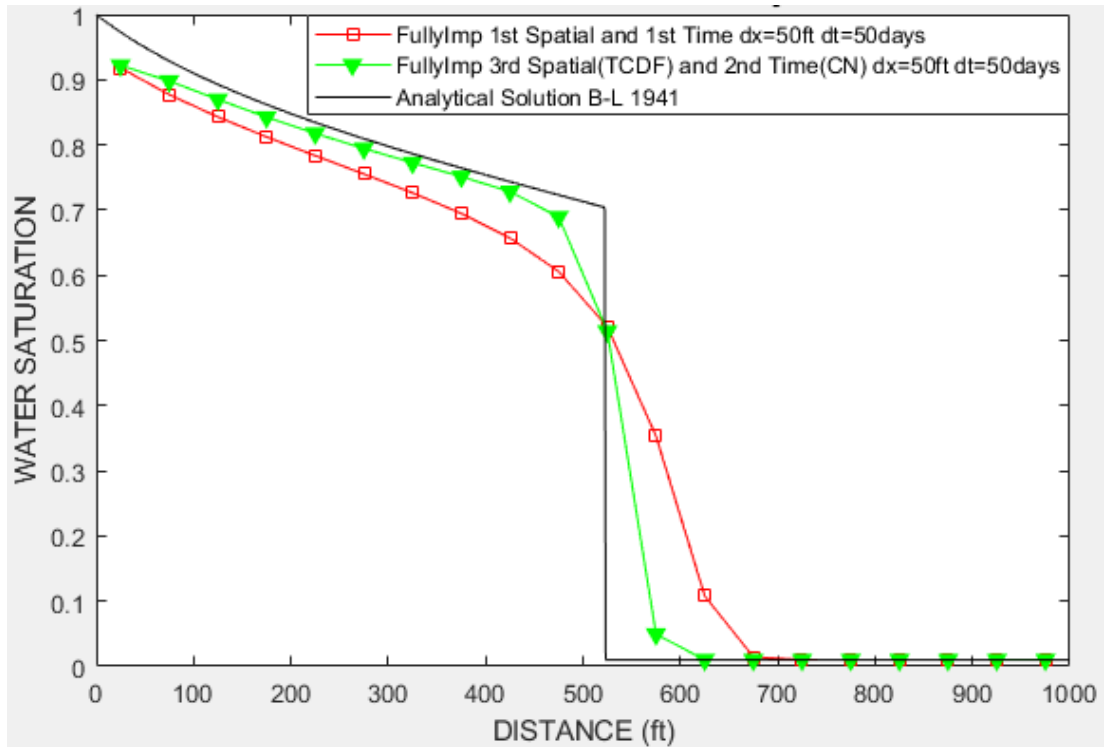


Figure 7.9: $dx=50\text{ft}$ and $dt=50\text{days}$ for intermediate wettability reservoir.

Figure 7.8-7.12 show comparison of fully implicit third order spatial (TCDF) second order time (CN) method and fully implicit first order spatial first order time method for different spatial and different time step intervals.

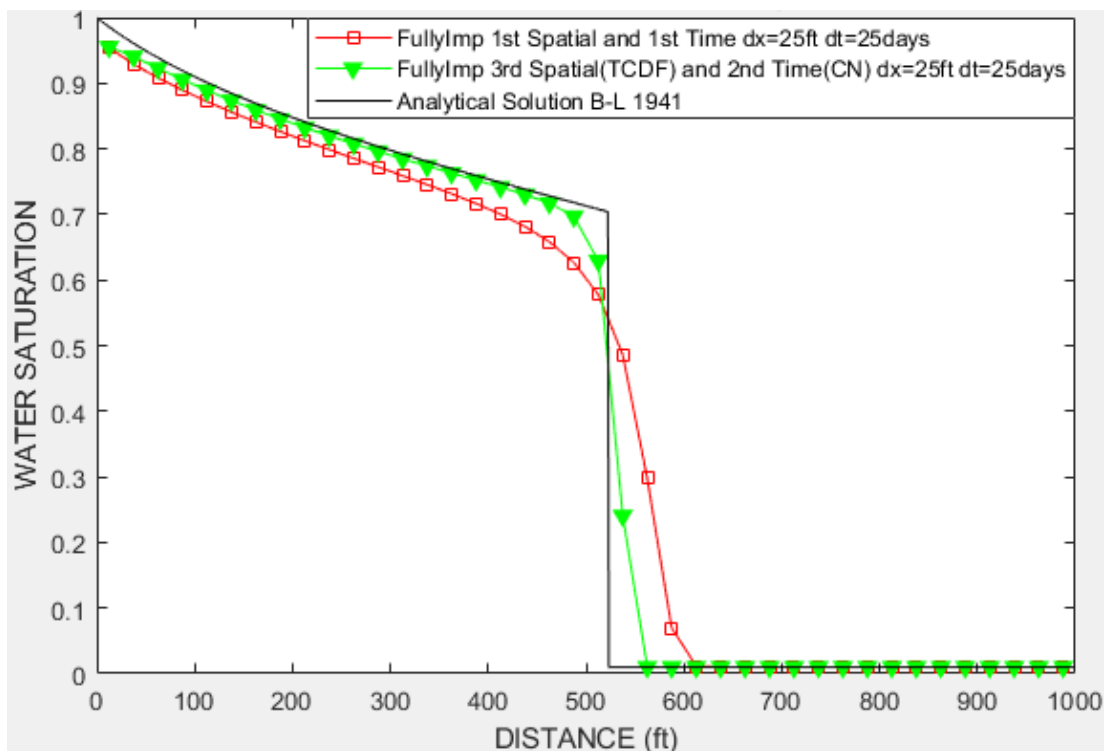


Figure 7.10: $dx=25\text{ft}$ and $dt=25\text{days}$ for intermediate wettability reservoir.

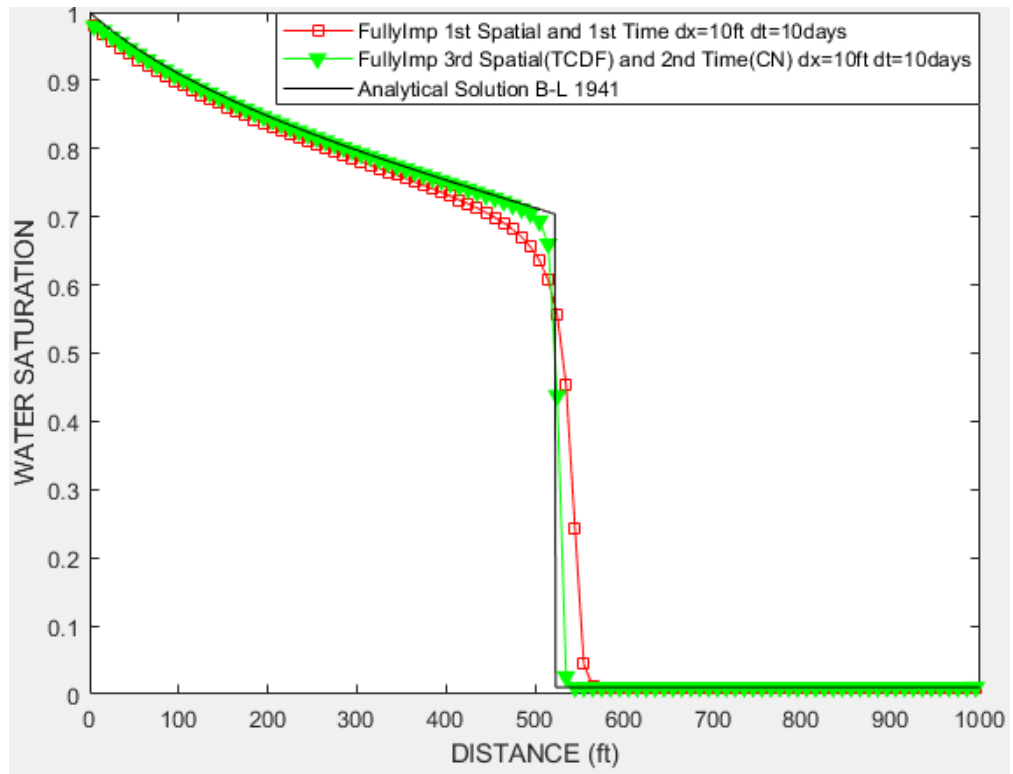


Figure 7.11: $dx=10\text{ft}$ and $dt=10\text{days}$ for intermediate wettability reservoir.

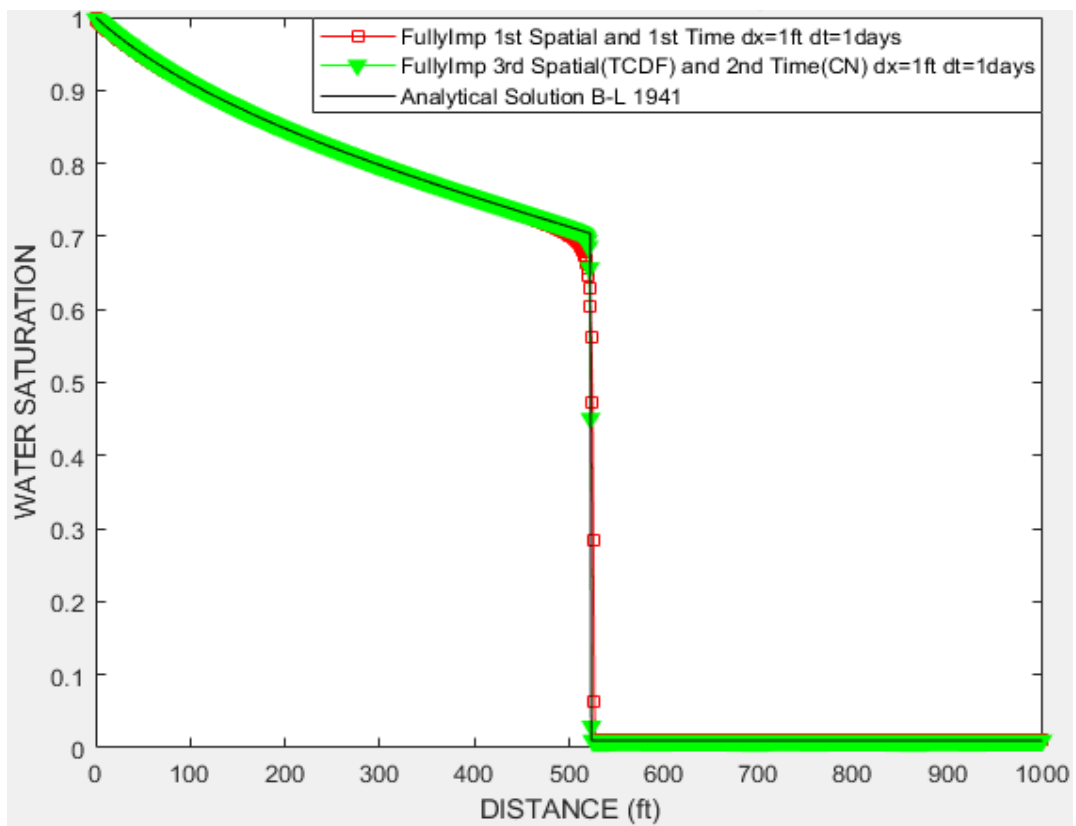


Figure 7.12: $dx=1\text{ft}$ and $dt=1\text{days}$ for intermediate wettability reservoir.

In 2D reservoir simulations, we will use water breakthrough time in order to compare different reservoir simulation models. During history matching of observed production data of brown fields, one of the key matching parameters in the water break-through time. Water break-through time is the time at which significant water production begins at a producing well [23].

For 2D simulation, it is assumed that total simulation time 4000 days, $dt=40$ days, $dx=100$ ft, $dy=100$ ft, $dz=10$ ft, i-direction block 10, j-direction block 10, $Swi=0.01$, $Sor=0$, $Pi=1000$ psia, $q_{inj}=75.96$ b/d. In addition to these data, relative permeability curves in figure 7.6 and front water saturation (0.7041) in figure 7.7 were used.

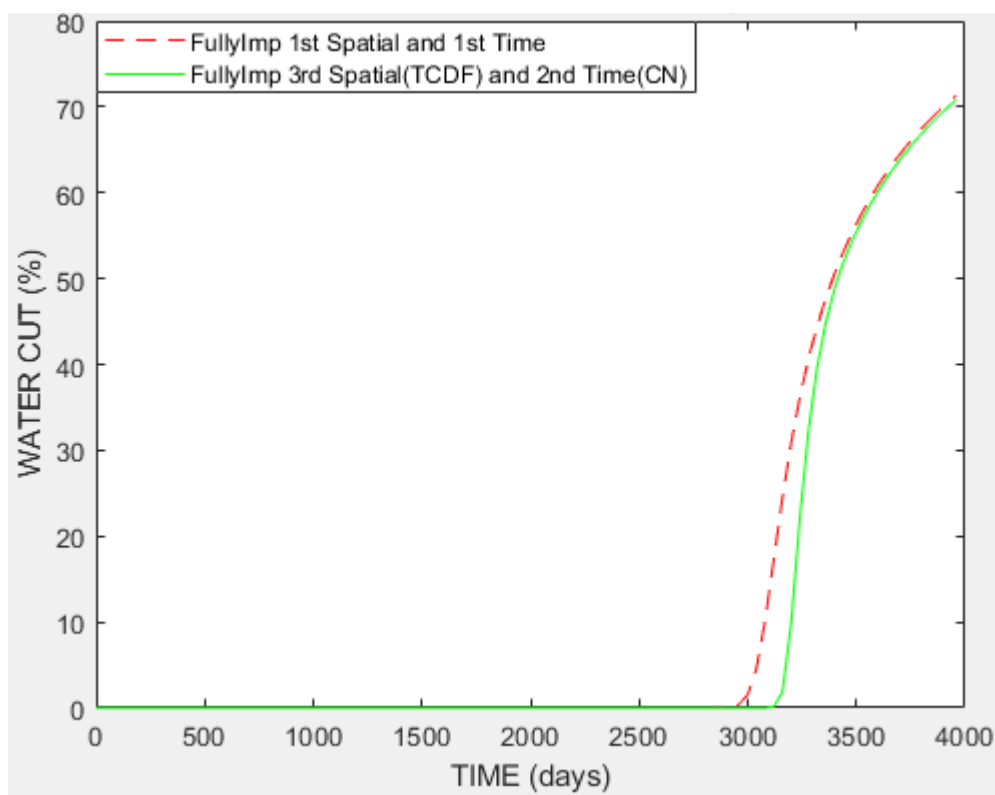


Figure 7.13: Water breakthrough time for intermediate wettability reservoir.

Figure 7.13 shows breakthrough times of fully implicit third order spatial (TCDF) second order time (CN) method and fully implicit first order spatial first order time method. According to figure 7.14, using fully implicit first order spatial first order time method cause 200 days earlier breakthrough time compared with fully implicit third order spatial (TCDF) second order time (CN) method. That situation adversely affects prediction of oil reservoir performance.

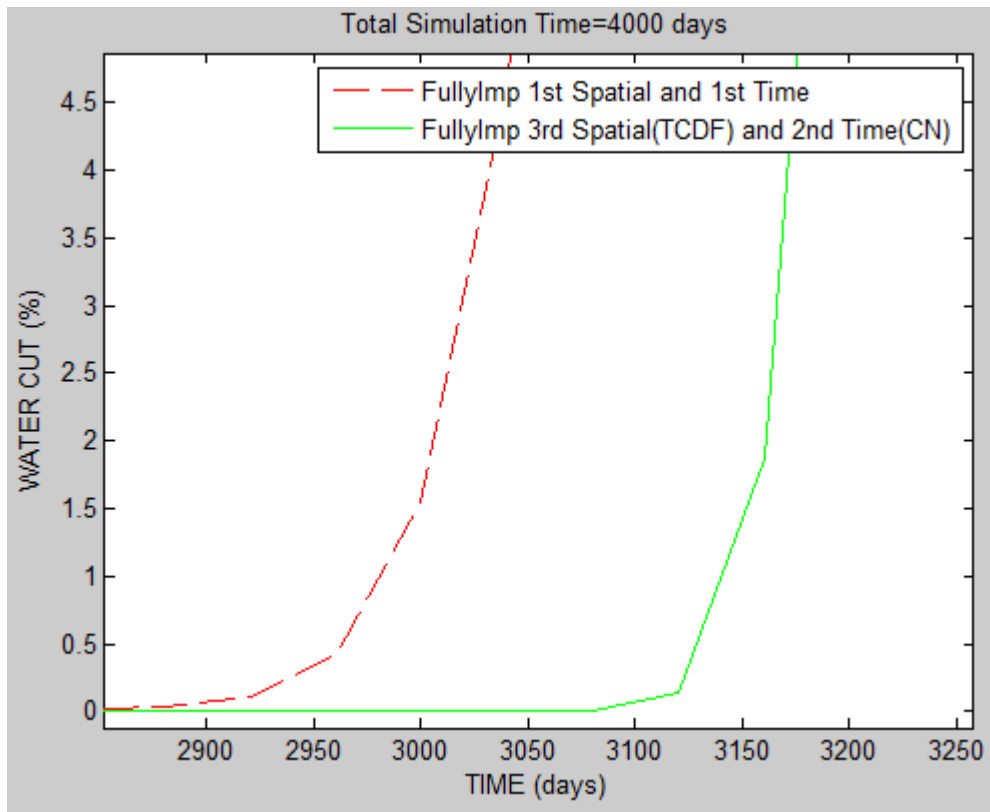


Figure 7.14: Water breakthrough time for intermediate wettability reservoir in detail.

8. CONCLUSION

Numerical reservoir simulations are indispensable tools of predicting the performance of the oil and gas reservoirs. The major problems encountered in reservoir simulations may be listed as numerical dispersion, unphysical oscillation and grid orientation effects.

In addition, specially in immiscible displacement of oil with water the estimation of grid blocks face saturations is of utmost importance. Since Buckley Leverett model dictates the accurate estimate of face saturations for correct calculation of influx and outflux values. The numerical simulators inherently and unavoidably calculate and use average grid block saturation. This enters as an inherent inaccuracy of block face estimations.

Detailed investigations of elementary and some high order space discretization methods of convection dominated flow and transport has revealed that the first order methods are highly dispersive but with an apparent advantage of negative feedback sensitivity to smooth out the oscillation. The even high order methods reduce the numerical dispersion but they are much more oscillatory. In 1979, The Leonard introduced his famous third order discretization which reduced the numerical dispersion and having a negative feedback sensitivity is less prone to oscillations. Nevertheless, even this method becomes oscillatory for some very small and very large Courant numbers.

In order to mitigate the numerical dispersion and reduce unphysical oscillations a method called as TVD has been introduced and implemented in elementary and some high order schemes. In 1984, Sweby introduced his classical work of framing the stability region for the flux limiters of TVD schemes.

We have noticed that Leonard method is in fact a special TVD scheme where its flux limiter falls on a straight line, may be called as straight-line flux limiter.

For simulations of miscible displacement, combining explicit Quick with Crank Nicholson method (Kocabas and Margoup) method reduces both the unphysical

oscillation of Quick-explicit and the numerical dispersion of Quick-implicit methods. Thus, it yields both stable and highly accurate profiles compared to all previous methods for a large range of Courant Numbers.

The following improvements have been achieved in order: higher order spatial discretization schemes using Quick (without limiter function Leonard), piecewise linear flux limiter (Pinto and Sweby), TCDF smooth flux limiter (Zhang) and Adaptive smooth flux limiter methods (Jiang).

Our contribution to this field is two folds. Implementing a flexible flux limiter which is specified as a function of Courant number thus avoiding the oscillation for all ranges of Courant Numbers. Then implementing all of these improvements including the flexible flux limiter to Leonard Crank Nicholson discretization.

These two improvements distinctly showed the superiority of the method in both better front capturing and oscillation avoiding features compared to the previously developed method. One other major advantage is that this new method has also reduced the number of iterations for high Courant number simulations especially in two phase flow simulations. In summary:

- 1) Third order space second order time (C-N) scheme give most accurate results for miscible displacement.
- 2) On the other hand, the third order space second order time (C-N) scheme exhibit a single large unphysical hump before the front for immiscible displacement.
- 3) All unphysical oscillations in all schemes can be attributed to violation of Sweby stability constraint. Therefore they require use of flux limiters.
- 4) The flux limiters are not needed in fully implicit upstream scheme as it contain only numerical dispersion and no unphysical oscillations.
- 5) Employing flux limiters in third order space second order time (C-N) scheme improves the solutions greatly. Making the schemes better than fully implicit first and second order upstream schemes.
- 6) The novel flexible flux limiter method presented in this work further improves the results of third order space second order time (C-N) scheme.

REFERENCES

- [1] Peng, Y., Liu, C., & Shi, L. (2013). *Soution of Convection-Diffusion Equations*. Paper presented at the International Conference on Information Computing and Applications.
- [2] Kurganov, A., & Tadmor, E. J. J. o. C. P. (2000). New high-resolution central schemes for nonlinear conservation laws and convection–diffusion equations. *160*(1), 241-282.
- [3] Kamalyar, K., Kharrat, R., Nikbakht, M. J. P. S., & Technology. (2014). Numerical Aspects of the Convection–Dispersion Equation. *32*(14), 1729-1762.
- [4] Peaceman, D. W. (2000). *Fundamentals of numerical reservoir simulation* (Vol. 6): Elsevier.
- [5] Kocabas, I., Margoub, A. J. E. F. P. R. I. s. t. E., & Production Division ADNOC, U. U., Al Ain, UAE. (2000). Improved numerical schemes for transport equations in oil reservoirs.
- [6] Jiang, J., & Younis, R. M. (2017). *An Efficient Fully-Implicit MFD-MUSCL Method Based on a Novel Multislope Limiting Procedure*. Paper presented at the SPE Reservoir Simulation Conference.
- [7] Ertekin, T., Abou-Kassem, J. H., & King, G. R. (2001). *Basic applied reservoir simulation*.
- [8] Hashan, M., Jahan, L. N., Zaman, T. U., Elhaj, M., Imtiaz, S., & Hossain, M. E. (2018). *Modelling of fluid flow in a petroleum reservoir using an engineering approach*. Paper presented at the SPE Trinidad and Tobago Section Energy Resources Conference.
- [9] Jamal, H., SM, F. A., & M Rafiq, I. (2006). Petroleum reservoir simulation: a Basic Approach. In: Gulf Publishing Company.
- [10] Datta Gupta, A., & JENNINGS JR, J. (1988). *Accurate resolution of physical dispersion in the multidimensional numerical modeling of miscible and chemical displacements*. Paper presented at the SPE/DOE symposium on enhanced oil recovery. 6.
- [11] Wolcott, D., Kazemi, H., & Dean, R. (1996). *A practical method for minimizing the grid orientation effect in reservoir simulation*. Paper presented at the SPE annual technical conference and exhibition.
- [12] Buckley, S. E., & Leverett, M. J. T. o. t. A. (1942). Mechanism of fluid displacement in sands. *146*(01), 107-116.
- [13] Al-Sofi, A. M., & Blunt, M. J. (2010). *Control of numerical dispersion in simulations of augmented waterflooding*. Paper presented at the SPE Improved Oil Recovery Symposium.
- [14] Carr, A., & Christie, M. (1983). *Controlling numerical diffusion in reservoir simulation using flux corrected transport*. Paper presented at the SPE Reservoir Simulation Symposium.
- [15] Goda, T., & Sato, K. J. J. o. t. J. P. I. (2009). Application of Constrained Interpolation Profile(CIP) Method for Numerical Simulation of Two-phase Flow in Porous Media. *52*(5), 257-264257.

- [16] Laprea-Bigott, M., & Morse, R. A. (1980). *Improved pressure response representation and reduction of numerical dispersion effects in reservoir simulation*. Paper presented at the SPE Annual Technical Conference and Exhibition.
- [17] Pinto, A., Correa, A., & Cunha, M. (1992). *High-resolution schemes for conservation laws: applications to reservoir engineering*. Paper presented at the European Petroleum Computer Conference.
- [18] Taggart, I., & Pinczewski, W. J. S. R. E. (1987). The use of higher-order differencing techniques in reservoir simulation. *2*(03), 360-372.
- [19] Todd, M., O'dell, P., & Hirasaki, G. J. S. o. P. E. J. (1972). Methods for increased accuracy in numerical reservoir simulators. *12*(06), 515-530.
- [20] Wheatley, M. J. (1979). *A Version of Two Point Upstream Weighting for Use in Implicit Numerical Reservoir Simulators*. Paper presented at the SPE Reservoir Simulation Symposium.
- [21] Young, M. S., Casinader, P. C., & Wilson, D. C. (1980). *The Use of Higher Order Finite Difference Methods in Reservoir Simulation*. Paper presented at the European Offshore Technology Conference and Exhibition.
- [22] Zhao, F., Shen, R., Gao, S. S., & Xu, G. J. J. o. t. J. P. I. (2014). Application and calculation method of waterflood front in low permeability reservoir. *57*(6), 271-275.
- [23] Kayode, B., Surdiman, S., Ghareeb, Z., & Salem, H. (2017). *A New Approach for Reducing Numerical Dispersion in Reservoir Simulation*. Paper presented at the SPE Kingdom of Saudi Arabia Annual Technical Symposium and Exhibition.
- [24] Chen, W., Durlofsky, L., Engquist, B., & Osher, S. J. S. A. T. S. (1993). Minimization of grid orientation effects through use of higher order finite difference methods. *1*(02), 43-52.
- [25] Leonard, B. J. A. m. m. (1994). Comparison of truncation error of finite-difference and finite-volume formulations of convection terms. *18*(1), 46-50.
- [26] Ahmed, T. (2018). *Reservoir engineering handbook*: Gulf Professional Publishing.
- [27] Crotti, M., & Cobeñas, R. (2001). *Scaling Up of Laboratory Relative Permeability Curves. An Advantageous Approach Based on Realistic Average Water Saturations*. Paper presented at the SPE Latin American and Caribbean Petroleum Engineering Conference.
- [28] Crotti, M., & Cobeñas, R. (2003). *Upscaling of relative permeability curves for reservoir simulation: an extension to areal simulations based on realistic average water saturations*. Paper presented at the SPE Latin American and Caribbean Petroleum Engineering Conference.
- [29] Moukalled, F., Mangani, L., Darwish, M. J. A. a. i. w. O., pdf, M. N. Y. S. R. d. h. w. g. n. r. M.-F.-O.-M., & et al. (2016). The finite volume method in computational fluid dynamics.
- [30] Sweby, P. K. J. S. j. o. n. a. (1984). High resolution schemes using flux limiters for hyperbolic conservation laws. *21*(5), 995-1011.
- [31] Harten, A. (1984). On a class of high resolution total-variation-stable finite-difference schemes. *SIAM Journal on Numerical Analysis*, *21*(1), 1-23.
- [32] Zhang, D., Jiang, C., Liang, D., & Cheng, L. J. J. o. C. P. (2015). A review on TVD schemes and a refined flux-limiter for steady-state calculations. *302*, 114-154.

- [33] Liu, J., Delshad, M., Pope, G. A., & Sepehrnoori, K. (1994). Application of higher-order flux-limited methods in compositional simulation. *Transport in Porous media*, 16(1), 1-29.
- [34] Liu, J., Pope, G. A., & Sepehrnoori, K. (1995). A high-resolution finite-difference scheme for nonuniform grids. *Applied mathematical modelling*, 19(3), 162-172.

APPENDICES

APPENDIX A

$$D \frac{\partial^2 C}{\partial x^2} - u \frac{\partial C}{\partial x} = \frac{\partial C}{\partial t} \quad (\text{A.1})$$

In order to understand the feedback sensitivity, let's assume that a numerical solution of equation A.1 has been carried out. The evolution of the central node value C_i :

$$\frac{\partial C_i}{\partial t} = RHS \quad (\text{A.2})$$

where RHS represents the numerically modeled terms on the right hand side. In general, RHS will involve some dependence on C_i ; thus the evolution of perturbations in C_i can be studied by taking the variation of equation A.2 with respect to C_i , giving

$$\frac{\partial \delta C_i}{\partial t} = \frac{\partial RHS}{\partial C_i} \delta C_i \quad (\text{A.3})$$

which has a closed form solution

$$\delta C_i = \exp\left(\int \sigma \, dt\right) \quad (\text{A.4})$$

where the feedback sensitivity is given by

$$\sigma = \frac{\partial RHS}{\partial C_i} \quad (\text{A.5})$$

For example, central differencing of the diffusion operator

$$D \frac{\partial^2 C_i}{\partial C_i^2} \cong D \frac{C_{i+1}^n - 2C_i^n + C_{i-1}^n}{\Delta X^2} \quad (\text{A.6})$$

$$\sigma = \frac{-2D}{\Delta x^2} \quad (\text{A.7})$$

APPENDIX B

2D Impes First Order Space and Time Solutions

FO pressure solution

$$\nabla \cdot (m_w + m_o) \nabla p + q = 0 \quad (\text{B.1})$$

$$\frac{m_{tw_{i,j}} \frac{p_{i,j} - p_{i-1,j}}{\Delta x} - m_{te_{i,j}} \frac{p_{i+1,j} - p_{i,j}}{\Delta x}}{\Delta x} + \frac{m_{tn_{i,j}} \frac{p_{i,j} - p_{i,j-1}}{\Delta y} - m_{ts_{i,j}} \frac{p_{i,j+1} - p_{i,j}}{\Delta y}}{\Delta y} + q_{i,j} = 0 \quad (\text{B.2})$$

$$m_{tw_{i,j}} = -0.001127 \left[\frac{k_x \times k_{rw}[S_{w_{i-1,j}}]}{\mu_w} + \frac{k_x \times k_{ro}[S_{w_{i-1,j}}]}{\mu_o} \right] \quad (\text{B.3})$$

$$m_{te_{i,j}} = -0.001127 \left[\frac{k_x \times k_{rw}[S_{w_{i,j}}]}{\mu_w} + \frac{k_x \times k_{ro}[S_{w_{i,j}}]}{\mu_o} \right] \quad (\text{B.4})$$

$$m_{tn_{i,j}} = -0.001127 \left[\frac{k_y \times k_{rw}[S_{w_{i,j-1}}]}{\mu_w} + \frac{k_y \times k_{ro}[S_{w_{i,j-1}}]}{\mu_o} \right] \quad (\text{B.5})$$

$$m_{ts_{i,j}} = -0.001127 \left[\frac{k_y \times k_{rw}[S_{w_{i,j}}]}{\mu_w} + \frac{k_y \times k_{ro}[S_{w_{i,j}}]}{\mu_o} \right] \quad (\text{B.6})$$

Suppose that there are five grid block x-direction and five grid block y-direction, first grid block is injection constant pressure grid block and fiftyth grid block is production grid block. In this case,

- ✓ Pressure equation for first grid block;

$$\frac{0 - m_{te_1} \frac{p_2 - p_1}{\Delta x}}{\Delta x} + \frac{0 - m_{ts_1} \frac{p_6 - p_1}{\Delta y}}{\Delta y} + q_1 = 0 \quad (\text{B.7})$$

- ✓ Pressure equation for second grid block;

$$\frac{m_{tw_2} \frac{p_2 - p_1}{\Delta x} - m_{te_2} \frac{p_3 - p_2}{\Delta x}}{\Delta x} + \frac{0 - m_{ts_2} \frac{p_7 - p_2}{\Delta y}}{\Delta y} + q_2 = 0 \quad (\text{B.8})$$

- ✓ Pressure equation for thirteenth grid block;

$$\frac{m_{tw_{13}} \frac{p_{13} - p_{12}}{\Delta x} - m_{te_{13}} \frac{p_{14} - p_{13}}{\Delta x}}{\Delta x} + \frac{m_{tn_{13}} \frac{p_{13} - p_8}{\Delta y} - m_{ts_{13}} \frac{p_{18} - p_{13}}{\Delta y}}{\Delta y} + q_{13} = 0 \quad (\text{B.9})$$

- ✓ Pressure equation for twenty-fourth grid block;

$$\frac{m_{tw_{24}} \frac{p_{24} - p_{23}}{\Delta x} - m_{te_{24}} \frac{p_{25} - p_{24}}{\Delta x}}{\Delta x} + \frac{m_{tn_{24}} \frac{p_{24} - p_{19}}{\Delta y} - 0}{\Delta y} + q_{24} = 0 \quad (\text{B.10})$$

- ✓ Pressure equation for twenty-five grid block;

$$\frac{m_{tw_{25}} \frac{p_{25} - p_{24}}{\Delta x} - 0}{\Delta x} + \frac{m_{tn_{25}} \frac{p_{25} - p_{20}}{\Delta y} - 0}{\Delta y} + q_{25} = 0 \quad (\text{B.11})$$

There are twenty-four unknown pressures and there are twenty-five equations, therefore unknown pressure values can be determined.

FO saturation solution

$$\nabla \cdot (v_t \times f_w) + q = \phi \frac{\partial S_w}{\partial t} \quad (\text{B.12})$$

$$v_t = (m_w + m_o) \nabla p \quad (\text{B.13})$$

$$f_w = \frac{m_w}{m_w + m_o} \quad (\text{B.14})$$

$$\nabla \cdot \left((m_w + m_o) \nabla p \times \frac{m_w}{m_w + m_o} \right) + q = \phi \frac{\partial S_w}{\partial t} \quad (\text{B.15})$$

$$\nabla \cdot (m_w \nabla p) + q = \phi \frac{\partial S_w}{\partial t} \quad (\text{B.16})$$

$$S_w^{t+1} = S_w^t + \left[\frac{v_w - v_e}{\Delta x} + \frac{v_n - v_s}{\Delta y} + q \right] \times \frac{5.614583 \times \Delta t}{\phi} \quad (\text{B.17})$$

$$v_w = -0.001127 \frac{k_x \times k_{rw}[S_{w_{i-1,j}}]}{\mu_w} \times \frac{P_{i,j} - P_{i-1,j}}{\Delta x} \quad (\text{B.18})$$

$$v_e = -0.001127 \frac{k_x \times k_{rw}[S_{w_{i,j}}]}{\mu_w} \times \frac{P_{i+1,j} - P_{i,j}}{\Delta x} \quad (\text{B.19})$$

$$v_n = -0.001127 \frac{k_y \times k_{rw}[S_{w_{i,j-1}}]}{\mu_w} \times \frac{P_{i,j} - P_{i,j-1}}{\Delta y} \quad (\text{B.20})$$

$$v_s = -0.001127 \frac{k_y \times k_{rw}[S_{w_{i,j}}]}{\mu_w} \times \frac{P_{i,j+1} - P_{i,j}}{\Delta y} \quad (\text{B.21})$$

APPENDIX C

2D Impes Third Order (Leonard-TVD) Space and Time Solutions

Leonard-TVD pressure solution

$$\nabla \cdot (m_w + m_o) \nabla p + q = 0 \quad (\text{C.1})$$

$$\frac{m_{tw_{i,j}} \frac{p_{i,j} - p_{i-1,j}}{\Delta x} - m_{te_{i,j}} \frac{p_{i+1,j} - p_{i,j}}{\Delta x}}{\Delta x} + \frac{m_{tn_{i,j}} \frac{p_{i,j} - p_{i,j-1}}{\Delta y} - m_{ts_{i,j}} \frac{p_{i,j+1} - p_{i,j}}{\Delta y}}{\Delta y} + q_{i,j} = 0 \quad (\text{C.2})$$

➤ Calculation for west side, $m_{tw_{i,j}}$

$$m(1) = -0.001127 \left[\frac{k_x \times k_{rw} [S_{w_{i-2,j}}]}{\mu_w} + \frac{k_x \times k_{ro} [S_{w_{i-2,j}}]}{\mu_o} \right] \quad (\text{C.3})$$

$$m(2) = -0.001127 \left[\frac{k_x \times k_{rw} [S_{w_{i-1,j}}]}{\mu_w} + \frac{k_x \times k_{ro} [S_{w_{i-1,j}}]}{\mu_o} \right] \quad (\text{C.4})$$

$$m(3) = -0.001127 \left[\frac{k_x \times k_{rw} [S_{w_{i,j}}]}{\mu_w} + \frac{k_x \times k_{ro} [S_{w_{i,j}}]}{\mu_o} \right] \quad (\text{C.5})$$

$$r = (m(2) - m(1)) / (m(3) - m(2)) \quad (\text{C.6})$$

$$Lf = \max[0, \min(2, 2r, (2 + r)/3)] \quad (\text{C.7})$$

$$m_{tw_{i,j}} = m(2) + 0.5 \times Lf \times (m(3) - m(2)) \quad (\text{C.8})$$

➤ Calculation for east side, $m_{te_{i,j}}$

$$m(1) = -0.001127 \left[\frac{k_x \times k_{rw} [S_{w_{i-1,j}}]}{\mu_w} + \frac{k_x \times k_{ro} [S_{w_{i-1,j}}]}{\mu_o} \right] \quad (\text{C.9})$$

$$m(2) = -0.001127 \left[\frac{k_x \times k_{rw} [S_{w_{i,j}}]}{\mu_w} + \frac{k_x \times k_{ro} [S_{w_{i,j}}]}{\mu_o} \right] \quad (\text{C.10})$$

$$m(3) = -0.001127 \left[\frac{k_x \times k_{rw} [S_{w_{i+1,j}}]}{\mu_w} + \frac{k_x \times k_{ro} [S_{w_{i+1,j}}]}{\mu_o} \right] \quad (\text{C.11})$$

$$r = (m(2) - m(1)) / (m(3) - m(2)) \quad (\text{C.12})$$

$$L_f = \max[0, \min(2, 2r, (2 + r)/3)] \quad (\text{C.13})$$

$$m_{te_{i,j}} = m(2) + 0.5 \times L_f \times (m(3) - m(2)) \quad (\text{C.14})$$

➤ Calculation for north side, $m_{tn_{i,j}}$

$$m(1) = -0.001127 \left[\frac{k_y \times k_{rw} [S_{w_{i,j-2}}]}{\mu_w} + \frac{k_y \times k_{ro} [S_{w_{i,j-2}}]}{\mu_o} \right] \quad (\text{C.15})$$

$$m(2) = -0.001127 \left[\frac{k_y \times k_{rw} [S_{w_{i,j-1}}]}{\mu_w} + \frac{k_y \times k_{ro} [S_{w_{i,j-1}}]}{\mu_o} \right] \quad (\text{C.16})$$

$$m(3) = -0.001127 \left[\frac{k_y \times k_{rw} [S_{w_{i,j}}]}{\mu_w} + \frac{k_y \times k_{ro} [S_{w_{i,j}}]}{\mu_o} \right] \quad (\text{C.17})$$

$$r = (m(2) - m(1)) / (m(3) - m(2)) \quad (\text{C.18})$$

$$L_f = \max[0, \min(2, 2r, (2 + r)/3)] \quad (\text{C.19})$$

$$m_{tn_{i,j}} = m(2) + 0.5 \times L_f \times (m(3) - m(2)) \quad (\text{C.20})$$

➤ Calculation for south side, $m_{ts_{i,j}}$

$$m(1) = -0.001127 \left[\frac{k_y \times k_{rw}[S_{w_{i,j-1}}]}{\mu_w} + \frac{k_y \times k_{ro}[S_{w_{i,j-1}}]}{\mu_o} \right] \quad (\text{C.21})$$

$$m(2) = -0.001127 \left[\frac{k_y \times k_{rw}[S_{w_{i,j}}]}{\mu_w} + \frac{k_y \times k_{ro}[S_{w_{i,j}}]}{\mu_o} \right] \quad (\text{C.22})$$

$$m(3) = -0.001127 \left[\frac{k_y \times k_{rw}[S_{w_{i,j+1}}]}{\mu_w} + \frac{k_y \times k_{ro}[S_{w_{i,j+1}}]}{\mu_o} \right] \quad (\text{C.23})$$

$$r = (m(2) - m(1))/(m(3) - m(2)) \quad (\text{C.24})$$

$$L_f = \max[0, \min(2, 2r, (2 + r)/3)] \quad (\text{C.25})$$

$$m_{ts_{i,j}} = m(2) + 0.5 \times L_f \times (m(3) - m(2)) \quad (\text{C.26})$$

After that point, pressure solution of Leonard-TVD is quite analogous to pressure solution of FO.

Leonard-TVD saturation solution

Using equation 2.6

$$S1_w^n = S_w^n + \left[\frac{v_w - v_e}{\Delta x} + \frac{v_n - v_s}{\Delta y} + q \right] \times \frac{5.614583 \times \Delta t}{\phi} \quad (\text{C.27})$$

➤ Calculation for west side, v_w

$$v(1) = -0.001127 \left[\frac{[k_x \times k_{rw} [S_{w_{i-2,j}}]]}{\mu_w} \right] \quad (\text{C.28})$$

$$v(2) = -0.001127 \left[\frac{[k_x \times k_{rw} [S_{w_{i-1,j}}]]}{\mu_w} \right] \quad (\text{C.29})$$

$$v(3) = -0.001127 \left[\frac{[k_x \times k_{rw} [S_{w_{i,j}}]]}{\mu_w} \right] \quad (\text{C.30})$$

$$r = (v(2) - v(1))/(v(3) - v(2)) \quad (\text{C.31})$$

$$L_f = \max[0, \min(2, 2r, (2 + r)/3)] \quad (\text{C.32})$$

$$v_w = [v(2) + 0.5 \times L_f \times (v(3) - v(2))] \times \frac{p_{i,j} - p_{i-1,j}}{\Delta x} \quad (\text{C.33})$$

➤ Calculation for east side, v_e

$$v(1) = -0.001127 \left[\frac{[k_x \times k_{rw} [S_{w_{i-1,j}}]]}{\mu_w} \right] \quad (\text{C.34})$$

$$v(2) = -0.001127 \left[\frac{[k_x \times k_{rw} [S_{w_{i,j}}]]}{\mu_w} \right] \quad (\text{C.35})$$

$$v(3) = -0.001127 \left[\frac{[k_x \times k_{rw} [S_{w_{i+1,j}}]]}{\mu_w} \right] \quad (\text{C.36})$$

$$r = (v(2) - v(1))/(v(3) - v(2)) \quad (\text{C.37})$$

$$L_f = \max[0, \min(2, 2r, (2 + r)/3)] \quad (\text{C.38})$$

$$v_e = [v(2) + 0.5 \times Lf \times (v(3) - v(2))] \times \frac{p_{i+1,j} - p_{i,j}}{\Delta x} \quad (\text{C.39})$$

➤ Calculation for north side, v_n

$$v(1) = -0.001127 \left[\frac{k_y \times k_{rw} [S_{w_{i,j-2}}]}{\mu_w} \right] \quad (\text{C.40})$$

$$v(2) = -0.001127 \left[\frac{k_y \times k_{rw} [S_{w_{i,j-1}}]}{\mu_w} \right] \quad (\text{C.41})$$

$$v(3) = -0.001127 \left[\frac{k_y \times k_{rw} [S_{w_{i,j}}]}{\mu_w} \right] \quad (\text{C.42})$$

$$r = (v(2) - v(1)) / (v(3) - v(2)) \quad (\text{C.43})$$

$$Lf = \max[0, \min(2, 2r, (2 + r)/3)] \quad (\text{C.44})$$

$$v_n = [v(2) + 0.5 \times Lf \times (v(3) - v(2))] \times \frac{p_{i,j} - p_{i,j-1}}{\Delta y} \quad (\text{C.45})$$

➤ Calculation for south side, v_s

$$v(1) = -0.001127 \left[\frac{k_y \times k_{rw} [S_{w_{i,j-1}}]}{\mu_w} \right] \quad (\text{C.46})$$

$$v(2) = -0.001127 \left[\frac{k_y \times k_{rw} [S_{w_{i,j}}]}{\mu_w} \right] \quad (\text{C.47})$$

$$v(3) = -0.001127 \left[\frac{k_y \times k_{rw} [S_{w_{i,j+1}}]}{\mu_w} \right] \quad (\text{C.48})$$

$$r = (v(2) - v(1))/(v(3) - v(2)) \quad (\text{C.49})$$

$$L_f = \max[0, \min(2, 2r, (2 + r)/3)] \quad (\text{C.50})$$

$$v_s = [v(2) + 0.5 \times L_f \times (v(3) - v(2))] \times \frac{p_{i,j+1} - p_{i,j}}{\Delta y} \quad (\text{C.51})$$

$$S_w^{n+1} = \frac{3}{4} S_w^n + \frac{1}{4} S1_w^n + \frac{1}{4} \times \left[\frac{v1_w - v1_e}{\Delta x} + \frac{v1_n - v1_s}{\Delta y} + q \right] \times \frac{5.614583 \times \Delta t}{\emptyset} \quad (\text{C.52})$$

Calculations of $v1_w, v1_e, v1_n$ and $v1_s$ are very same to calculation of v_w, v_e, v_n and v_s using $S1_w^n$ instead of using S_w^n .

$$S_w^{n+1} = \frac{1}{3} S_w^n + \frac{2}{3} S2_w^n + \frac{2}{3} \times \left[\frac{v2_w - v2_e}{\Delta x} + \frac{v2_n - v2_s}{\Delta y} + q \right] \times \frac{5.614583 \times \Delta t}{\emptyset} \quad (\text{C.53})$$

Calculations of $v2_w, v2_e, v2_n$ and $v2_s$ are very same to calculation of $v1_w, v1_e, v1_n$ and $v1_s$ using $S2_w^n$ instead of using $S1_w^n$.

APPENDIX D

2D Fully Implicit First Order Space and Time Solution

Suppose that there are twenty-five grid blocks through x-direction and there are twenty-five grid blocks through y-direction. In this case, water and oil equations for thirteenth grid block:

$$\begin{aligned}
 f_{w13} &= \left(-0.001127 \frac{A_{12,13} \times k_x \times k_{rw_{12,13}} \times (P_{13}^{n+1} - P_{12}^{n+1}) \times \rho}{\mu_w \times \Delta x} \right) \\
 &- \left(-0.001127 \frac{A_{13,14} \times k_x \times k_{rw_{13,14}} \times (P_{14}^{n+1} - P_{13}^{n+1}) \times \rho}{\mu_w \times \Delta x} \right) \\
 &+ \left(-0.001127 \frac{A_{8,13} \times k_y \times k_{rw_{8,13}} \times (P_{13}^{n+1} - P_8^{n+1}) \times \rho}{\mu_w \times \Delta y} \right) \\
 &- \left(-0.001127 \frac{A_{13,18} \times k_x \times k_{rw_{13,18}} \times (P_{18}^{n+1} - P_{13}^{n+1}) \times \rho}{\mu_w \times \Delta y} \right) \\
 &+ q_{w13,mass}^{n+1} - \frac{V_{13} \times \emptyset \times \rho \times (S_{w13}^{n+1} - S_{w13}^n)}{\Delta t} = 0
 \end{aligned} \tag{D.1}$$

$$\begin{aligned}
 f_{w13} &= \left(-0.001127 \frac{k_x \times k_{rw}[S_{w12}^{n+1}] \times (P_{13}^{n+1} - P_{12}^{n+1})}{\mu_w \times \Delta x^2} \right) \\
 &- \left(-0.001127 \frac{k_x \times k_{rw}[S_{w13}^{n+1}] \times (P_{14}^{n+1} - P_{13}^{n+1})}{\mu_w \times \Delta x^2} \right) \\
 &+ \left(-0.001127 \frac{k_y \times k_{rw}[S_{w8}^{n+1}] \times (P_{13}^{n+1} - P_8^{n+1})}{\mu_w \times \Delta y^2} \right) \\
 &- \left(-0.001127 \frac{k_x \times k_{rw}[S_{w13}^{n+1}] \times (P_{18}^{n+1} - P_{13}^{n+1})}{\mu_w \times \Delta y^2} \right) \\
 &+ \frac{q_{w13,volume}^{n+1}}{V_{13}} - \frac{\emptyset \times (S_{w13}^{n+1} - S_{w13}^n)}{\Delta t} = 0
 \end{aligned} \tag{D.2}$$

$$\begin{aligned}
& f_{o13} \\
& = \left(-0.001127 \frac{A_{12,13} \times k_x \times k_{ro_{12,13}} \times (P_{13}^{n+1} - P_{12}^{n+1}) \times \rho}{\mu_o \times \Delta x} \right) \\
& - \left(-0.001127 \frac{A_{13,14} \times k_x \times k_{ro_{13,14}} \times (P_{14}^{n+1} - P_{13}^{n+1}) \times \rho}{\mu_o \times \Delta x} \right) \\
& + \left(-0.001127 \frac{A_{8,13} \times k_y \times k_{ro_{8,13}} \times (P_{13}^{n+1} - P_8^{n+1}) \times \rho}{\mu_o \times \Delta y} \right) \\
& - \left(-0.001127 \frac{A_{13,18} \times k_x \times k_{ro_{13,18}} \times (P_{18}^{n+1} - P_{13}^{n+1}) \times \rho}{\mu_o \times \Delta y} \right) \\
& + q_{o13, mass}^{n+1} - \frac{V_{13} \times \emptyset \times \rho \times (-S_{w13}^{n+1} + S_{w13}^n)}{\Delta t} = 0
\end{aligned} \tag{D.3}$$

$$\begin{aligned}
f_{o13} & = \left(-0.001127 \frac{k_x \times k_{ro} [S_{w12}^{n+1}] \times (P_{13}^{n+1} - P_{12}^{n+1})}{\mu_o \times \Delta x^2} \right) \\
& - \left(-0.001127 \frac{k_x \times k_{ro} [S_{w13}^{n+1}] \times (P_{14}^{n+1} - P_{13}^{n+1})}{\mu_o \times \Delta x^2} \right) \\
& + \left(-0.001127 \frac{k_y \times k_{ro} [S_{w8}^{n+1}] \times (P_{13}^{n+1} - P_8^{n+1})}{\mu_o \times \Delta y^2} \right) \\
& - \left(-0.001127 \frac{k_x \times k_{ro} [S_{w13}^{n+1}] \times (P_{18}^{n+1} - P_{13}^{n+1})}{\mu_o \times \Delta y^2} \right) \\
& + \frac{q_{o13, volume}^{n+1}}{V_{13}} - \frac{\emptyset \times (-S_{w13}^{n+1} + S_{w13}^n)}{\Delta t} = 0
\end{aligned} \tag{D.4}$$

Total number of water and oil equations is equal to number of unknown pressure and saturation, so governing equations can be solved using Newton-Rapson iteration method.

$$\begin{bmatrix} P_1^{v+1} \\ P_2^{v+1} \\ \vdots \\ S_{w1}^{v+1} \\ S_{w2}^{v+1} \\ \vdots \end{bmatrix} = \begin{bmatrix} P_1^v \\ P_2^v \\ \vdots \\ S_{w1}^v \\ S_{w2}^v \\ \vdots \end{bmatrix} - \begin{bmatrix} \frac{df_{w1}^v}{dP_1^v} & \frac{df_{w1}^v}{dP_2^v} & \dots & \frac{df_{w1}^v}{dS_{w1}^v} & \frac{df_{w1}^v}{dS_{w2}^v} & \dots \\ \frac{df_{w2}^v}{dP_1^v} & \dots & \dots & \frac{df_{w2}^v}{dS_{w1}^v} & \dots & \dots \\ \vdots & \dots & \dots & \dots & \dots & \dots \\ \frac{df_{o1}^v}{dP_1^v} & \frac{df_{o1}^v}{dP_2^v} & \dots & \frac{df_{o1}^v}{dS_{w1}^v} & \frac{df_{o1}^v}{dS_{w2}^v} & \dots \\ \frac{df_{o2}^v}{dP_1^v} & \dots & \dots & \frac{df_{o2}^v}{dS_{w1}^v} & \dots & \dots \\ \vdots & \dots & \dots & \dots & \dots & \dots \end{bmatrix}^{-1} \times \begin{bmatrix} f_{w1}^v \\ f_{w2}^v \\ \vdots \\ f_{o1}^v \\ f_{o2}^v \\ \vdots \end{bmatrix} \quad (\text{D.5})$$

APPENDIX E

2D Fully Implicit Third Order Space (TVD-L) and First Order Time Solution

$$\begin{aligned}
 f_{w13} = & \left(-0.001127 \frac{k_x \times k_{rw_{12,13}} \times (P_{13}^{n+1} - P_{12}^{n+1})}{\mu_w \times \Delta x^2} \right) \\
 & - \left(-0.001127 \frac{k_x \times k_{rw_{13,14}} \times (P_{14}^{n+1} - P_{13}^{n+1})}{\mu_w \times \Delta x^2} \right) \\
 & + \left(-0.001127 \frac{k_y \times k_{rw_{8,13}} \times (P_{13}^{n+1} - P_8^{n+1})}{\mu_w \times \Delta y^2} \right) \\
 & - \left(-0.001127 \frac{k_x \times k_{rw_{13,18}} \times (P_{18}^{n+1} - P_{13}^{n+1})}{\mu_w \times \Delta y^2} \right) \\
 & + \frac{q_{w13,volume}^{n+1}}{V_{13}} - \frac{\phi \times (S_{w13}^{n+1} - S_{w13}^n)}{\Delta t} = 0
 \end{aligned} \tag{E.1}$$

➤ Calculation for west side, $k_{rw_{12,13}}$

$$k(1) = k_{rw}[S_{w_{i-2,j}}] \tag{E.2}$$

$$k(2) = k_{rw}[S_{w_{i-1,j}}] \tag{E.3}$$

$$k(3) = k_{rw}[S_{w_{i,j}}] \tag{E.4}$$

$$r = (k(2) - k(1))/(k(3) - k(2)) \tag{E.5}$$

$$Lf = \max[0, \min(2, 2r, (2 + r)/3)] \tag{E.6}$$

$$k_{rw_{12,13}} = k(2) + 0.5 \times Lf \times (k(3) - k(2)) \tag{E.7}$$

➤ Calculation for east side, $k_{rw_{13,14}}$

$$k(1) = k_{rw}[S_{w_{i-1,j}}] \quad (\text{E.8})$$

$$k(2) = k_{rw}[S_{w_{i,j}}] \quad (\text{E.9})$$

$$k(3) = k_{rw}[S_{w_{i+1,j}}] \quad (\text{E.10})$$

$$r = (k(2) - k(1))/(k(3) - k(2)) \quad (\text{E.11})$$

$$Lf = \max[0, \min(2, 2r, (2 + r)/3)] \quad (\text{E.12})$$

$$k_{rw_{13,14}} = k(2) + 0.5 \times Lf \times (k(3) - k(2)) \quad (\text{E.13})$$

➤ Calculation for north side, $k_{rw_{8,13}}$

$$k(1) = k_{rw}[S_{w_{i,j-2}}] \quad (\text{E.14})$$

$$k(2) = k_{rw}[S_{w_{i,j-1}}] \quad (\text{E.15})$$

$$k(3) = k_{rw}[S_{w_{i,j}}] \quad (\text{E.16})$$

$$r = (k(2) - k(1))/(k(3) - k(2)) \quad (\text{E.17})$$

$$Lf = \max[0, \min(2, 2r, (2 + r)/3)] \quad (\text{E.18})$$

$$k_{rw_{8,13}} = k(2) + 0.5 \times Lf \times (k(3) - k(2)) \quad (\text{E.19})$$

➤ Calculation for south side, $k_{rw_{13,18}}$

$$k(1) = k_{rw}[S_{w_{i,j-1}}] \quad (\text{E.20})$$

$$k(2) = k_{rw}[S_{w_{i,j}}] \quad (\text{E.21})$$

$$k(3) = k_{rw}[S_{w_{i,j+1}}] \quad (\text{E.22})$$

$$r = (k(2) - k(1))/(k(3) - k(2)) \quad (\text{E.23})$$

$$Lf = \max[0, \min(2, 2r, (2 + r)/3)] \quad (\text{E.24})$$

$$k_{rw_{13,18}} = k(2) + 0.5 \times Lf \times (k(3) - k(2)) \quad (\text{E.25})$$

The values of oil relative permeability is quite similar to the values of water relative permeability.

$$\begin{aligned} f_{o13} = & \left(-0.001127 \frac{k_x \times k_{ro_{12,13}} \times (P_{13}^{n+1} - P_{12}^{n+1})}{\mu_o \times \Delta x^2} \right) \\ & - \left(-0.001127 \frac{k_x \times k_{ro_{13,14}} \times (P_{14}^{n+1} - P_{13}^{n+1})}{\mu_o \times \Delta x^2} \right) \\ & + \left(-0.001127 \frac{k_y \times k_{ro_{8,13}} \times (P_{13}^{n+1} - P_8^{n+1})}{\mu_o \times \Delta y^2} \right) \\ & - \left(-0.001127 \frac{k_x \times k_{ro_{13,18}} \times (P_{18}^{n+1} - P_{13}^{n+1})}{\mu_o \times \Delta y^2} \right) \\ & + \frac{q_{o13,volume}^{n+1}}{V_{13}} - \frac{\phi \times (-S_{w13}^{n+1} + S_{w13}^n)}{\Delta t} = 0 \end{aligned} \quad (\text{E.26})$$

CURRICULUM VITAE

Name Surname: Osman ÜNAL

Place and Date of Birth: Eğirdir 12.03.1992

Address: İzmir Katip Çelebi Üniversitesi, Mühendislik ve Mimarlık Fakültesi, Petrol ve Doğal Gaz Mühendisliği Bölümü, Baltçık/Çiğli/İzmir, Turkey

E-Mail: osman.unal@ikc.edu.tr

B.Sc. (1st major): Marine Engineering

B.Sc. (2nd major): Petroleum and Natural Gas Engineering

Professional Experience:

Company/Institution	Duty	Year
Izmir Katip Celebi University	Research Assistant	2018 -